UNIVERSITÀ
DEGLI STUDI
DI PADOVA

Sede Amministrativa: Università degli Studi di Padova

Dipartimento di Ingegneria Elettrica

SCUOLA DI DOTTORATO DI RICERCA IN INGEGNERIA INDUSTRIALE

INDIRIZZO ENERGETICA

CICLO XXIII

ENERGY EFFICIENCY IMPROVEMENTS OF HOUSEHOLD HEAT PUMP SYSTEMS

Direttore della Scuola : Ch.mo Prof. Paolo Bariani

Coordinatore d'indirizzo: Ch.mo Prof. Alberto Mirandola

Supervisore :Ch.mo Prof. Luca Doretti

Correlatore: Ch.mo Prof. Ezio Fornasieri

Dottorando : Ferdinando Mancini

31 Gennaio 2011

Dedicated to my parents

INDEX

ABSTRACT

Sustainable development is one of the major challenges that humanity faces today. The rational use of energy resources and the increase of systems efficiency seems to be an important task for all contexts of modern life, from industry to transport and household appliances. The interest on this subject is justified not only by the price of energy, which can potentially increase, but also by the need to reduce emissions of gases, which are thought to be responsible for global warming.

This work wants to present innovative solutions for the energy efficiency improvement of household heat pump systems, with particular reference to heat pump dryers, domestic refrigerators and tap water heat pumps.

Since clothes drying is a very energy-intensive process, in recent years much attention has been paid to the development of energy efficient dryers. The heat pump has been recognised as a very attractive technology for this application. Actual interest is focused on finding good alternatives to halocarbon refrigerants. Because it's safe for domestic rooms, carbon dioxide is regarded as a possible substitute for the traditional synthetic compounds. In this research work, the CO_2 transcritical cycle is compared with the traditional R134a subcritical cycle. The comparison is carried out with a theoretical analysis and experimental tests, returning a positive assessment for CO_2 as working fluid.

Tap water heat pumps are considered a privileged application for the employment of CO_2 as refrigerant. This work presents an innovative upper cycle pressure control logic to face the optimisation problem, and also reports an experimental investigation of CO_2 heat pump prototype, using a double wall plate heat exchanger gas cooler. This solution was studied as a possibility to reduce the risk of tap water contamination with lubricant oil.

Here some innovative solutions for the energy efficiency improvements of household refrigerators are presented. An experimental study was carried out on a under-counter refrigerator to analyse the effect of the operating cycling frequency on the electric consumptions. The experimental results show a reduction in energy consumption when the frequency of the compressor start-up increases.

To better understand these issues it was developed a dynamic simulation model for evaporators, based on the “moving boundary” scheme. Temporal integration of core variables makes the mean void fraction to be time-variant. The use of this kind of variables improves the model accuracy and speed, with respect to boundary variables, when the compressor start-up is simulated. This choice was considered suitable to simulate household refrigerators, which typically work with continuous on/off cycles.

Finally it’s presented an innovative solution for the energy efficiency improvement of total no-frost combi refrigerators. In these systems the fresh food compartment is cooled by air streams coming from the freezer. Therefore, the refrigeration unit produces the cooling effect at a temperature which is suitable for the freezer, but considerably colder than what is needed for the fridge. Consequently the system works with the thermodynamic disadvantage of supplying the cooling power at the lowest level of temperature. It was studied a combined household refrigerator (fridge/freezer), which works with a single refrigeration unit, but with two different air-loops. The unit consists of a single evaporator, which is employed to cool both the compartments. The air flow, involving the heat exchanger, comes alternately from the fridge or from the freezer. In this way the system works at two different evaporating temperatures, improving the thermodynamic efficiency when the fresh food compartment requires the cooling supply.

SOMMARIO

Lo sviluppo sostenibile rappresenta una delle più importanti sfide che oggi l'umanità deve affrontare. L'uso razionale delle risorse energetiche e l'aumento dell'efficienza dei sistemi che le utilizzano, è un importante obiettivo per tutti i contesti della vita moderna, dal settore industriale, ai trasporti, agli elettrodomestici di uso quotidiano. L'interesse verso questo tema è giustificato, non solo dal prezzo dell'energia in potenziale aumento, ma anche dalla necessità di ridurre le emissioni dei gas che sono ritenuti responsabili del riscaldamento globale.

Questo lavoro si inquadra nello studio di soluzioni tecnologiche innovative volte al miglioramento dell'efficienza energetica di apparecchiature domestiche, più precisamente macchine che operano con un ciclo inverso a compressione di vapore. In particolare verrà fatto riferimento ad asciugabiancheria a pompa di calore, refrigeratori domestici e pompe di calore per il riscaldamento di acqua calda sanitaria.

Come è noto, le asciugatrici domestiche realizzano un processo termodinamico che richiede un elevato dispendio energetico. Per questo motivo negli ultimi anni si è dato molto spazio alla ricerca di soluzioni che ne possano ridurre i consumi elettrici, trovando nella tecnologia della pompa di calore una significativa possibilità di miglioramento. Oggi l'attenzione è rivolta a incrementarne ulteriormente l'efficienza energetica e a trovare dei sostituiti ai tradizionali fluidi refrigeranti alogenati per ridurne l'impatto sull'ambiente. Poiché non è né tossica né infiammabile, l'anidride carbonica è perfettamente compatibile con gli ambienti domestici, ed è vista come un possibile sostituto dei composti sintetici. In questo lavoro il ciclo transcritico ad anidride carbonica viene messo a confronto, sia su base teorica che sperimentale, con il ciclo subcritico a R134a. I risultati di questa indagine mostrano buone prospettive per l'impiego della CO_2 in questa applicazione.

Nella sezione successiva verranno approfonditi aspetti teorici e tecnologici delle pompe di calore dedicate al riscaldamento di acqua calda sanitaria, applicazione in cui il ciclo transcritico ad anidride carbonica risulta essere molto efficace. L'analisi prevede lo studio di logiche di controllo di tipo adattativo per l'ottimizzazione della pressione superiore di ciclo. Sarà inoltre presentato uno studio sperimentale di macchine operanti

con gas-cooler a piastre a doppia parete, impiegato per ridurre il rischio di contaminazione del circuito idraulico.

Verranno poi approfondite alcune tematiche legate al miglioramento dell'efficienza energetica dei refrigeratori domestici. Si riportano i risultati di un'indagine sperimentale condotta su un frigorifero domestico di tipo "sottotavolo", i cui consumi elettrici sono stati monitorati al variare della frequenza ciclica di accensione del compressore. Per questa apparecchiatura è stata registrata una significativa riduzione dei consumi ad elevati frequenze.

Per approfondire ulteriormente questi temi, mediante simulazione numerica, è stato sviluppato un modello per evaporatori in regime di funzionamento dinamico, seguendo uno schema di tipo "moving boundary". Un'opportuna scelta delle variabili di stato (nello specifico, variabili corrispondenti a proprietà medie e non a grandezze di confine del modello) ha permesso di tenere conto delle variazioni nel tempo del grado di vuoto medio della zona bifase e di conseguire una maggiore velocità di simulazione dei transitori di avviamento del compressore. Questo modello è stato quindi sviluppato appositamente per la simulazione di refrigeratori domestici che operano in regime ciclico di funzionamento.

Infine, nell'ottica del miglioramento dell'efficienza dei refrigeratori domestici combinati di tipo total-no-frost, viene presentata una soluzione innovativa per il ciclo termodinamico. In queste apparecchiature il vano dei prodotti freschi viene di solito raffreddato facendo circolare una piccola portata d'aria proveniente dal vano dei prodotti surgelati. Questo tipo di funzionamento è inefficiente, in quanto la potenza frigorifera viene erogata al più basso livello di temperatura. La soluzione studiata prevede, invece, di convogliare alternativamente verso l'evaporatore due flussi d'aria che raffreddano distintamente i due vani refrigerati. Così facendo è possibile differenziare due livelli di temperatura per la produzione della potenza frigorifera, conseguendo un aumento dell'efficienza energetica quando l'unità opera al raffreddamento del vano a temperatura positiva.

INTRODUCTION

I.1 The global energy issue

During the twentieth century, the scientific and technological progress has greatly accelerated, as had never happened in previous eras. In particular, during postwar, the industrial development, the widespread use of vehicles and the increase of the standard of the lifestyle, brought a consistent increase of the energy consumption. Even if we don't know the true limits of fossil resources, we continue to increase their consumptions, basing almost the entire energy chain on the exhaustible resources.The first evidence of the unsustainability of this development process it was seen during the energy crisis of 1973: the surge in oil prices (which more than tripled in just a few months) and the consequent awareness of the excessive dependence on this source, led to the first steps towards energy conservation and research for alternative ones.

The possible decrease of the fossil reserves and the increase of greenhouse gases and pollutants in the atmosphere (nitrogen oxides, sulfur oxides, particulate, etc..), requires to drastically reduce energy consumption, decreasing wastes and using energy-efficient equipments.This represents a major challenge for humanity in the third millennium, because it's become necessary to reorganize our lifestyle in order to limit energy consumption. Moreover, it is required to increase technological progress to obtain more efficient equipments.

With the Green Paper on energy efficiency [1], the European Commission identified the areas in which it is necessary to implement the energy conservation. The attention is focused on household appliances, because they are consuming a substantial share of the total European use of energy (fig. I.1).

I.2 The Energy Labeling of household appliances

European Union is facing the energy saving problem since 1992, when the Directive 92/75/EEC stated the need to assign the energy label to the major appliances. In 1994 the first directive was issued, and has been gradually implemented by member states.

CECED (European association of manufacturers of electrical appliances) represents the household appliance manufacturing industry in Europe. Its member companies employ over 200,000 people, they are mainly based in Europe, and they have a turnover of about EUR 40 billion. If upstream and downstream business is taken together, the sector employs over 500,000 people. Since 1997, the CECED has promoted a voluntary agreement, signed by the major manufacturers to promote energy efficiency in the use of appliances. In 2002, this voluntary agreement was reiterated with new and more ambitious goals.

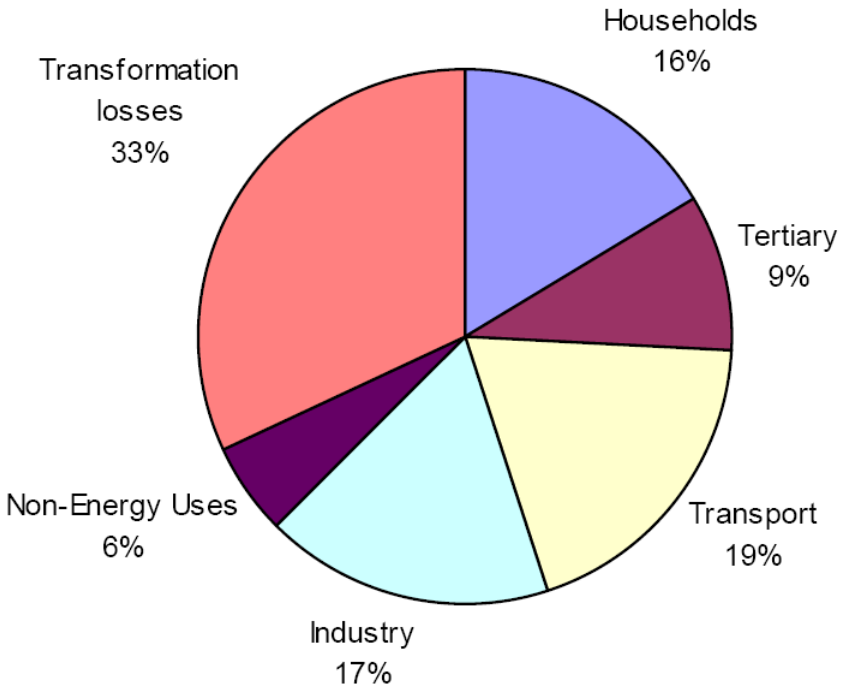

Figure I.1. Energy primary consumption in EU25 (2005) [2]

Soon the combined effects of the energy label introduction and these voluntary agreements were shown: the CECED estimated that in 10 years the introduction of more efficient household appliances has resulted in saving 17 million tons of CO_2.emission.

Recently, CECED has proposed a revision of the energy labels, giving up the alphabetic energy classes in order to introduce the numerical ones. The class numeration gets higher while the consumptions decrease. As previously, in the new layout there are colored arrows of different lengths, to help the consumer to understand the label (fig. I.3)

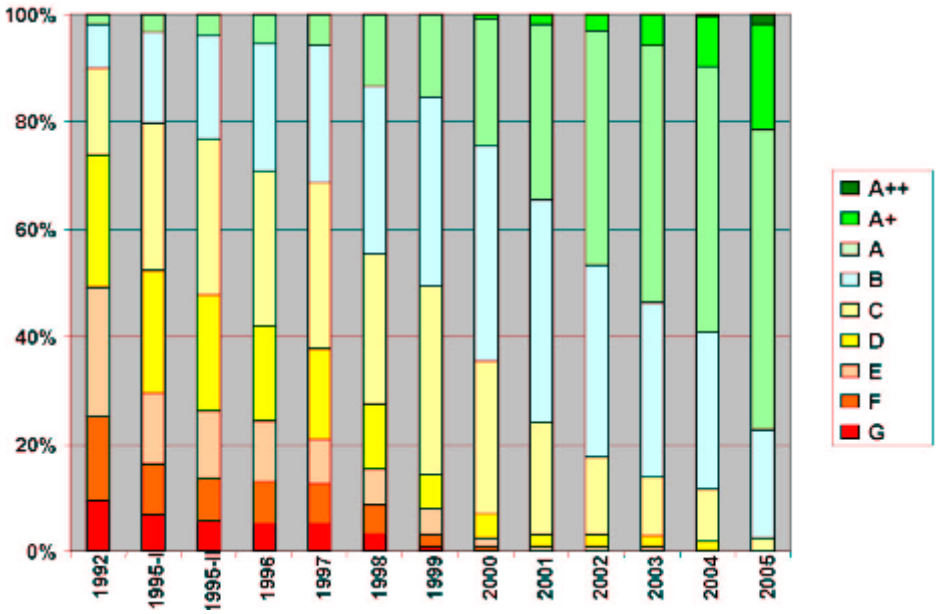

Figure I.2 – (Source CECED) Evolution energy classes 1992-2005

Figure I.3 – CECED proposal for the energy efficiency classes of household appliances [3]

With this new system, class 1 is the less efficient, while number 7 is the best one. Once a producer enters the market with an appliance which consumes less than the previous highest energy class, it is introduced another label class and the worst class gets eliminated. In this way there are no longer limits to the reduction of energy consumption, as it is now with the A class.

The advantages of this new system are represented by the clarity for consumers, maintaining conceptual and graphic continuity with the previous labelling. The absence of upper limits offers incentives to producers to continuously improve their appliances, and may induce users to replace obsolete equipments.

The CECED proposal is currently under review by the European Commission, and it is better accepted by producers and consumers groups, then the rescaling of the current consumption classes. In fact this could confuse final customers and reduce the incentive for producers to continuously improve their products.

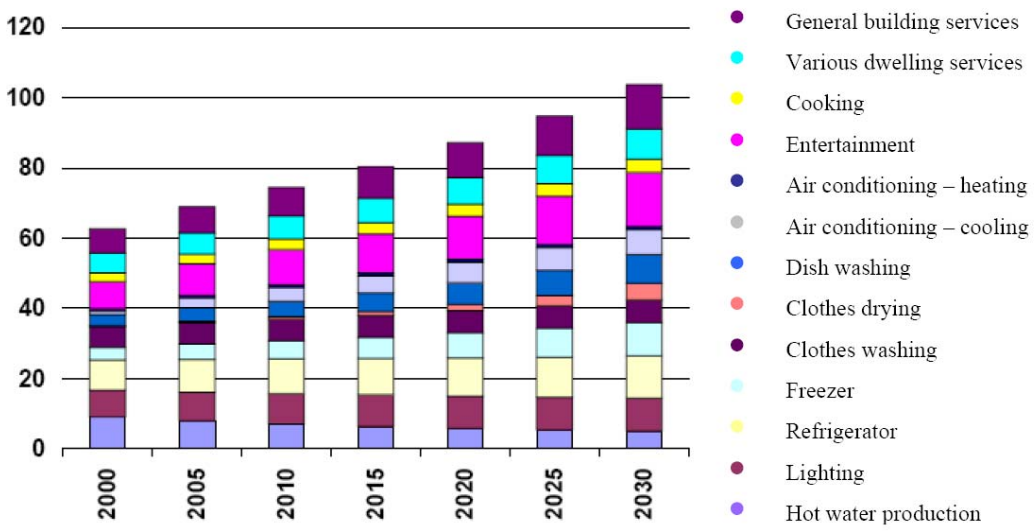

Figure I.4 Distribution of electricity consumption in the residential sector in Italy (CESI)

Vapour compression technology was historically applied first to domestic refrigerators and freezers. Nowadays heat pump dryers and tap water heat pumps are spreading on the market and, in some cases, they have started a partial phase-out of the traditional electrical appliances. Statistical forecasts show how the contribution of these appliances will be a consistent part of the dwelling energy consumptions.

I.3 Vapour compression units in household appliances

I.3.1 Household refrigerators

The first domestic refrigeration units entered the market in the late twenties with some historical brands products, as Isko, Mechanical Refrigerator Company, General Electric and Kelvinator. A very important development was the two-temperature

refrigerator, which was introduced around 1939 and which became popular in the post-war period. This was the first unit with two compartment at two different temperatures.

As shown in figures I.5 and I.6, from the early nineties, industrial manufactures pushed on the development of more efficient refrigeration systems, reaching in few years remarkable goals.

Today the vapour compression system is considered a mature technology for this application. The main options to improve the energy efficiency of these appliances can be summarized in four areas: improving the refrigerator cycle efficiency, reducing the cycle losses, decreasing the cabinet heat leakage and reducing the energy to defrost.

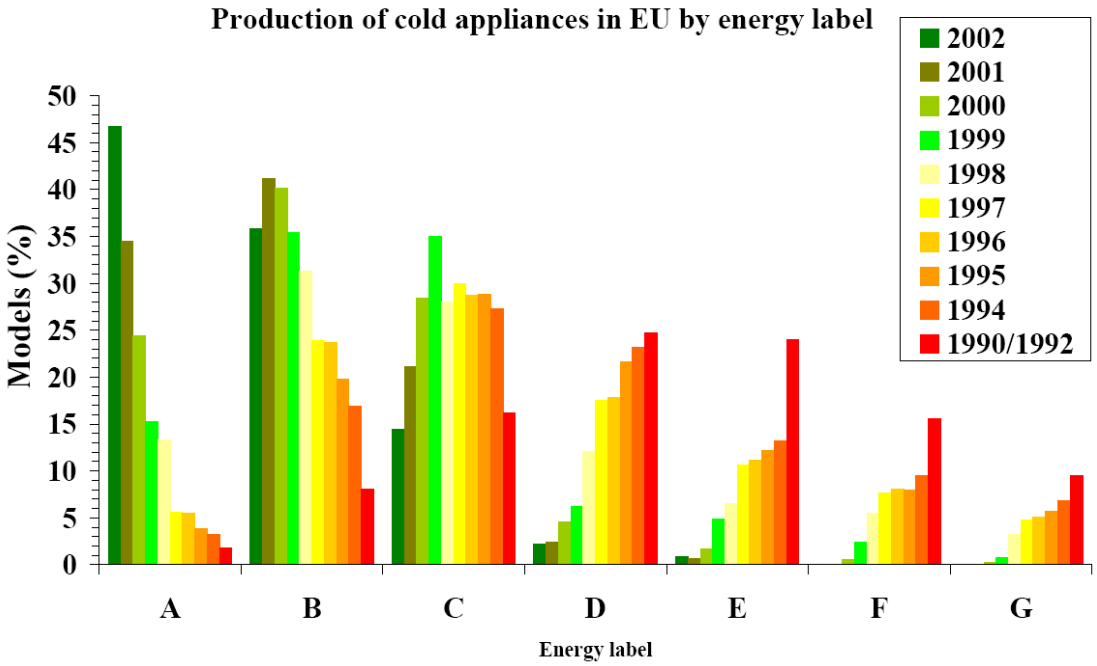

Figure I.5 Production of cold appliances in EU by energy label. CECED

I.3.2 Household clothes dryers

The Heat pump has been recognised as a very attractive technology for household clothes dryers. Clothes drying is a very energy-intensive process; for this reason in recent years much attention has been devoted to the development of energy efficient dryers, in order to decrease electrical costs and to face the global warming problem. In a closed-loop drying process, the necessity of dehumidifying the exhaust air and reheating it again suits the use of a vapour compression heat pump system, which contemporaneously provides a refrigerating and heating effect.

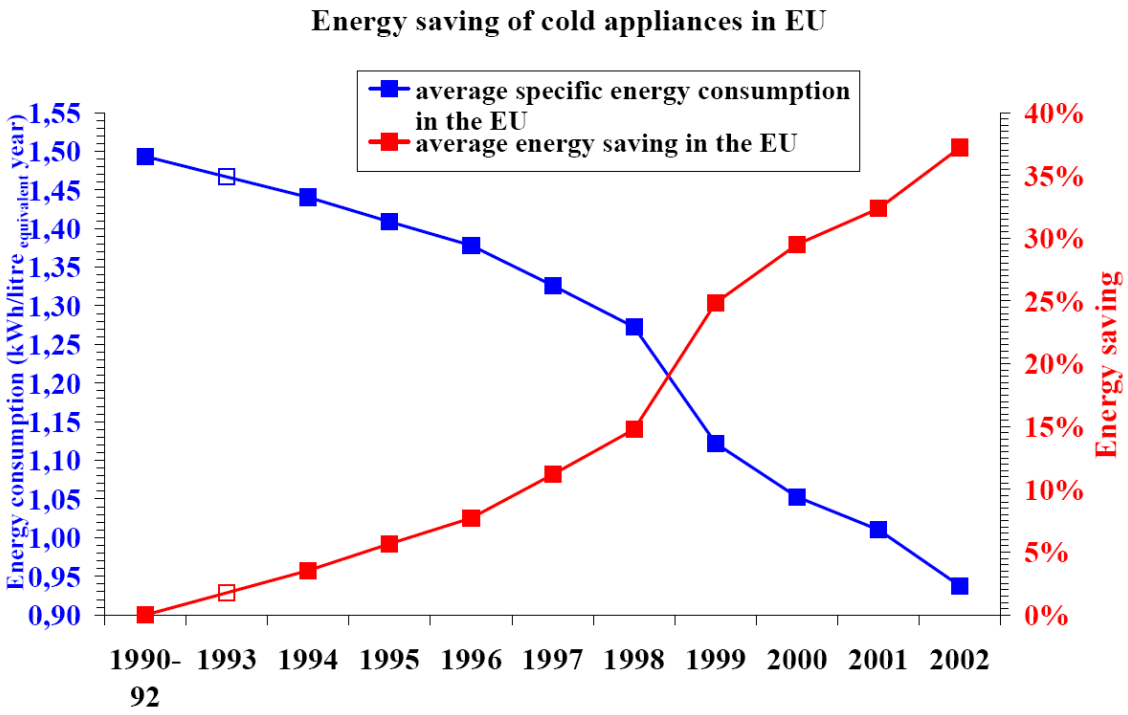

Figure I.6 Energy saving of cold appliances in EU. CECED

This allows significant energy saving, comparing this technology with traditional electrically heated tumble dryers. Today, the possible energy saving with heat pump dryers available on the market, which are mainly equipped with R134a compressors, is very conspicuous. Market investigations (Stiftung Warentest, 2006) have estimated the average energy saving achievable to be 46%, in comparison with the considered models of conventional electrically heated tumbler dryers.

I.3.3 Heat pumps for hot water production

Carbon dioxide, operating according to a transcritical cycle, is regarded as an energy efficient option for tap water heat pumps: the gas cooling process well fits the warming up of a finite stream of water, resulting in a quite large temperature lift in water, without significant penalisation in COP, as it was clearly demonstrated in the technical literature.

For heat pump dryers and tap water heat pumps, the CO_2 transcritical cycle was demonstrated to be an efficient option to achieve energy savings. Considerations

regarding the energy saving potential for these two applications will be presented and discussed later. Before introducing the main topics it is going to be presented the historical steps, which lead to the CO_2 revival as refrigerant.

I.4 Natural refrigerants: a solution to the environment concern

In recent years the concern about the environment and the climate change as a result of human activities is growing. The main concerns are related to the destruction of the stratospheric ozone layer and to the increase of the greenhouse effect.

The growing awareness of these problems in the scientific community, had important consequences in political and global economical trends. Evidences of this fact are the various conferences held in recent years.

Among these, it should be mentioned the conference in Buenos Aires (1998), in which it was decided to accelerate the measures laid down in the conference in Rio de Janeiro (1992) and codified in the Kyoto Protocol (1997). The Protocol sets out reductions of the emissions into the atmosphere from human activities that result in the greenhouse effect [6].

All industrialized countries are trying to adapt to the regulations imposed by the various protocols. However, it must be noted that some countries, in particular Sweden, Germany, Austria, Britain, Denmark, took more restrictive positions about the cessation of production and use of CFCs, HCFCs and HFCs [7-11].

The parameter ODP (Ozone Deplection Potential) indicates the potential for stratospheric ozone destruction and it is defined, for each refrigerant, respecting to the R-11 effect on the ozone [8] [9]. The GWP (Global Warming Potential) is the parameter that expresses the greenhouse potential of a substance. It is defined as the ratio, in a fixed time horizon, of the greenhouse effect produced by the emission of a unit mass of refrigerant and the greenhouse effect due to the emission of a unit mass of CO_2 at the same time.

There is also a second parameter: the TEWI (Total Equivalent Warming Impact). It takes into account:

- the direct effect of the fluid poured into the atmosphere during the operative life and in the end of the useful life of the system;
- the indirect effect, caused by the emission of carbon dioxide resulting in the production of energy consumed in the plant period of his life.

The index TEWI, unlike ODP (ozone depletion potential) and GWP (greenhouse potential), which depend only on the type of fluid, is greatly influenced by the particular equipment and also by the places where it is used.

Therefore it appears that the substitute should not implement energy efficiency of the cycle worse than those obtained with fluids replaced, especially when the direct part is greater than the indirect effect.

With regard to refrigeration systems, there are four types of possible interventions to reduce the greenhouse effect, some already made and others to be undertaken by the industry: reduction of charge leakages, reduction of the refrigerant amount inside the plant, improving the efficiency of refrigeration equipment and research of gas with little or no threat to the environment (GWP as low as possible) [10-14].

At present two classes of refrigerants are potential candidates to replace CFCs and HCFCs: hydrofluorocarbons HFCs, pure or mixed synthetic products [15], and natural fluids [16], [17].

HFCs, while they don't contain chlorine or bromine in its molecule,being harmless to the ozone layer, they have a high greenhouse potential. For this reason they were included in the Kyoto Protocol as fluids to be eliminated [18].

Natural fluids are safe for the ozone layer and almost innocuous toward the atmosphere. The principal fluids used as working fluids are Propane, Isobutan, Ammonia and Carbon Dioxide. The main problem arising from the use of hydrocarbons is related to their flammability and related safety issues. Propane is highly flammable and it is not suited for domestic environment. .For this reason, they can be used in applications that require extremely low refrigerant charge. Ammonia is toxic and is incompatible with copper.

The CO_2 is neither flammable nor toxic, is also compatible with the most common mineral oils, it does not attack metals or elastomers. It is cheap, widely available and has a very low environmental impact. Its greenhouse potential is unitary, but it may be

considered zero if the refrigerant is recovered as product of other industrial products. The result is that carbon dioxide is an excellent alternative of natural fluids, especially in household applications where the toxicity of ammonia and hydrocarbons e the flammability can be a problem.

I.5 References

[1] Green paper book on energy efficiency. European Commission. 2005

[2] Action Plan for Energy Efficiency: Realising the Potential (2006). Communication from the commission. Brussels. (COM545)

[3] Beyond A, CECED, 2007, http://www.beyonda.eu

[4] CESI Ciarniello U., D'Ermo V., Santi F., Curcio E., Rapporto CESI: "Previsione tendenziale della domanda elettrica 2010 – 2030 su base regionale ed elementi di variabilità per la costruzione di scenari alternativi", Milano, 2005, http://www.cesi.it

[5] Stiftung Warentest, October 2006, Customers German Magazine.

[6] http://www.unfccc.de/resource/convkp.html, testo del Protocollo di Kyoto.

[7] "Climate change. The UK programme presented to Parliament on Friday 17th November 2000"

[8] G. Gasparrini, G. Sgalambro, "La protezione dell'ozono stratosferico. Il protocollo di Montreal e le legislazioni nazionali. La legislazione italiana", Congress FREE '97 Verona, 1997.

[9] Ministry of Environment and Energy, Denmark, Danish Environmental Protection Agency, "Proposal for regulating the potent industrial greenhouse gasses (HFCs, PFCs and SF6)", January 2000.

[10] G. Malinverno, "The new European Regulation on substances that deplete the ozone layer", Congress FREE 2000 – Milano, 2000.

[11] C. Casale, "Restrizioni del nuovo regolamento europeo riguardanti i sistemi di condizionamento dell'aria", Congress FREE 2000 – Milano, 2000.

[12] F.S. Rowland, M.J. Molina, "Stratospheric sink for chlorofluoromethanes: chlorine atom-catalised destruction of ozone", Nature, 1974 (249; 810-2).

[13] A.Cavallini, "Impatto ambientale da fluidi frigorigeni alogenati", Il freddo 4/91.

[14] C. Casale, G. Pellegrini, "Impieghi dei nuovi refrigeranti: il punto di vista dell'industria costruttrice di componenti", Congress FREE '98 – Milano, 1998.

[15] A. Cavallini, “Recenti sviluppi nelle applicazioni dei refrigeranti sintetici”, FREE ’97 – Verona, 1997.

[16] V. Casson, L. Cecchinato, E. Fornasieri, “Quale fluido per quale impianto”, Il freddo, year LV, sptember 2001, n°4.

[17] V. Casson, L. Cecchinato, E. Fornasieri “Costi di impianto e affidabilità di funzionamento con i nuovi fluidi” Il freddo – year LV – september 2001, n°5.

[18] J. T. McMullan, “Refrigeration and the environment – issues and strategies for the future”, International Journal of Refrigeration, 25 2002, 89-99.

[19] C. Casale, G. Pellegrini, “Ricaduta della normativa italiana conseguente al nuovo regolamento europeo sulle tecnologie della climatizzazione e confronto con la situazione internazionale”, Congress FREE ’99 – Milano, 1999.

PART 1:
ENERGY EFFICIENCY IMPROVEMENTS OF HEAT PUMP DRYERS

1.1 Summary

Carbon dioxide is accounted as an optimal working fluid for heat pump dryers. The transcritical cycle suits the closed-loop drying process, which requires dehumidification and re-heating according to high temperature lift of the air stream. In this section, the transcritical CO_2 cycle is compared with the sub-critical R134a cycle. The theoretical analysis is based on fixed temperature approach values at the heat exchangers. The study considers optimal high pressure for the transcritical cycle and optimal refrigerant subcooling for the sub-critical cycle. The theoretical analysis investigates the energy performance of the thermodynamic cycle as a function of the temperature and mass flow rate of the drying air. The optimisation of the operating conditions for CO_2 involves lower air temperature than in the case of R134a; these conditions can be satisfied by a suitable design of the appliance, whose thermal balance is achieved when the dissipated heat corresponds to the work spent by the compressor and the fan; the air temperature is a floating variable that adjusts its value to comply with the thermal balance. Experimental results, conducted on a prototype, give a positive assessment for CO_2 as working fluid for heat pump dryers: a negligible decrease in the electric power consumption, with a limited (+9%) increase in the cycle time, is shown in comparison with the reference R134a heat pump dryer.

1.2. Household clothes dryers: models on the market

The drying process consists essentially in heating an air stream to increase its potential of humidity transport, and then forcing it inside a tumbler drum for absorbing moisture from clothes. In traditional dryers, heating is provided by electrical power or gas combustion. Although there are several technological solutions and system designs, household tumbler dryers are mainly divided into two categories: air vented dryers and condensing dryers

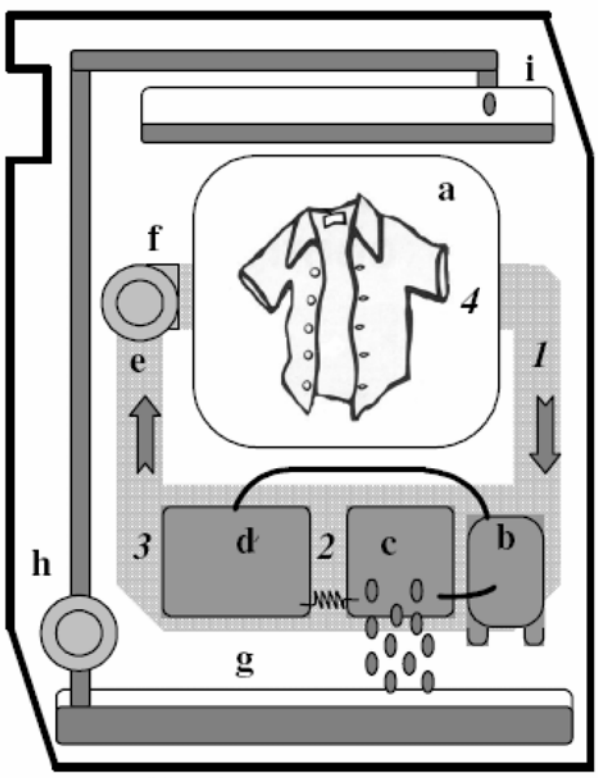

a. *Tumbler drum*
b. *Compressor*
c. *Evaporator*
d. *Condenser/Gas cooler*
e. *Air ducts*
f. *Fan*
g. *Collector tray*
h. *Pump*
i. *Condensation canister*

Figure 1.1 Heat pump dryer

.In air vented dryers, the air stream is drawn from outside, heated to the suitable temperature before passing through the clothes inside the drum, and then rejected into the laundry room or outdoors, if a wall break-through is available. In an open-cycle condensing dryer, the air flow coming from the drum is cooled and dehumidified inside an air-to-air heat exchanger where the external air is pre-heated. If external ducting is not provided, this solution makes it possible to add less moisture to the room than a conventional air vented dryer.

Close-cycle condensing dryers are very common on the market; they work according to a closed-loop air cycle, in which an air stream is previously heated inside a first heat exchanger, mainly by means of electric heaters, removes the moisture from the clothes and then is cooled and dehumidified inside a second heat exchanger, where the cooling fluid can be external air or tap water. In this case, the heat and mass transfer between the humid air and the tap water occurs by exposing the air stream to direct contact with water.

The vapour compression heat pump system appears to be the ideal technology for more efficient dryers. A heat pump assisted dryer involves a closed-loop air circulation, as depicted in Fig. 1, where the fan extracts the moistened air from the tumbler drum and forces it through the evaporator, removing the moisture; then the air stream is driven through the condenser/gas-cooler, before re-entering into the drum again. Thus, the heat pump refrigerating capacity is used to dehumidify the moistened air, whereas the heating capacity is used for warming up the cold air.

1.3 CO_2 as working fluid for heat pump dryers

1.3.1 Introduction

Clothes drying is a very energy-intensive process. In the last years much effort has been devoted to developing energy efficient dryers, in order to decrease electricity cost and to contribute to the environment preservation. Traditional technology involves the use of electric heaters to warm up the air, which operates the clothes drying process. In a theoretical analysis Bansal *et al.* [1] have discussed the relative advantages and disadvantages of four different household electrically heated dryers, to assess the effects of different variables on energy efficiency and on the specific moisture extraction rate.

Bansal *et al.* [2] and Bansal *et al.* [3] have recently proposed to replace electrical heaters with a heat exchanger where hot water from the domestic supply system is used. The energy efficiency of the modified dryers show to depend on water temperature, although the Authors do not introduce any efficiency in hot water production.

The Heat pump has been recognised as a very attractive technology for household clothes dryers.

Nomenclature

COP	coefficient of performance	*Subscripts*	
H	enthalpy [kJ·kg-1]	*Air*	air
$\dot{m}$	mass flow rate [$kg \cdot s^{-1}$]	*Cond*	condensation
P	pressure [bar]	*E*	evaporator
Q	thermal load [W]	*I*	inlet condition
SH	superheat [K]	*is*	isentropic
SMER	specific moisture extracting rate [$kg_w \cdot kWh^{-1}$]	*L*	latent
T	temperature [°C]	*O*	outlet condition
X	Specific humidity [$kg \cdot kg^{-1}$]	*R*	refrigerant
		S	saturated
Greek symbols		*W*	water
π	Specific exergy losses [$kW \cdot kg^{-1}$]	*Air*	air
Δ	Approach		
η_{ic}	compressor overall isentropic efficiency [-]		
φ	relative humidity [-]		

In a closed-loop drying process, the dehumidification and re-heating of the exhaust air suits the use of a vapour compression heat pump system, which contemporaneously provides refrigerating and heating effects.Heat pump technology can lead to significant energy saving when compared with traditional electrically heated tumbler dryers.

Nowadays, the possible energy saving with heat pump dryers available on the market, which are mainly equipped with R134a compressors, is very conspicuous. Market investigations [10] have estimated that state-of-the-art heat pump dryers can save up to 46% in comparison with conventional electrically heated tumbler dryers.

At present, interest is focused on finding good alternatives to halocarbon refrigerants. Because of their innocuousness to the environment, natural working fluids, as air,

propane and carbon dioxide, are studied as possible substitutes for the traditional synthetic compounds.

In a recent work, Braun *et al.*[4] have investigated the feasibility of a heat pump clothes dryer, working according to a reverse Brayton air cycle: the theoretical analysis has demonstrated that this dryer, with 5 kg load of clothes, can offer up to 40% improvement in energy efficiency versus the traditional electrically heated dryer. As the air pressure level is rather low, this solution allows using two air-to-air heat exchangers that can be easily removed from the unit for regular cleaning purposes.

Propane is a possible substitute for HFCs. As it was experimentally verified by Valero *et al.*[11], the performance of propane heat pump dryers is close to that of traditional R134a dryers. A prototype, derived from a R134a unit by changing the compressor, was tested in the different conditions with 6 kg of standard cotton clothes load; an average energy saving around 5% was achieved, with respect to the original unit. However, flammability might pose technical problems for large scale implementation.

Carbon dioxide is regarded as an interesting solution for heat pump clothes dryer (Nekså, 2002 [9]): it is neither flammable nor toxic and it is harmless to the environment (GWP=0). Moreover, the gas cooling process in a transcritical cycle well fits the warming up of a finite stream of air, resulting in a quite large temperature lift in air. However, the global energy performance and the cost increasing related to rather high operating pressures need to be carefully evaluated.

In a comparative study, Schmidt *et al.* (1998) [10] have analysed the thermodynamic losses of the heat pump drying process using R134a and CO_2 as refrigerants. The simulation shows that the two cycles are equivalent in terms of energy efficiency, having the same compression efficiency. However, with CO_2 better compression efficiency is expected and therefore higher energy efficiency might result.

Klöcker *et al.* (2010) [7] present experimental results achieved after a first optimisation of two CO_2 heat pump prototypes, with respectively 12 kW and 16 kW heating capacity, and compare their energy performance with a 12 kW conventional electrically-heated dryer. The Authors state that, if the drying time is not the main requirement, energy saving of about 65% can be realised. If high water extraction rate is the goal, lower energy savings of up to 53% can be realised, including fan power, but

with considerable shorter drying time than that of the conventional system.

In a recent work, Honma *et al.* (2008) [6] present an experimental study on a compact heat pump dryer using CO_2 as refrigerant, for a 4.5 kg dry clothes load. Tests reveal that the prototype system was able to reduce electric energy consumption by 59.2% in comparison with a conventional dryer.

In an experimental work, Valero *et al.* (2009) [11] tested a CO_2 heat pump dryer prototype, measuring 7% less energy consumption with respect to a typical R134a dryer. The only purpose of the Authors was to verify the feasibility of the CO_2 technology and to assess the potential of increasing energy efficiency over that of R134a systems, but the system tested was not optimised, so it is possible that further improvements still can be reached.

The present work offers a comparison between the transcritical CO_2 process and the sub-critical R134a cycle in terms of energy efficiency, drawn from a theoretical cycle analysis; experimental results achieved after a first optimisation of the CO_2 prototype confirm the theoretical analysis.

1.3.2 Theoretical analysis

In the following, a theoretical comparison between the R134a traditional heat pump cycle and the transcritical CO_2 cycle is presented. The performance of both cycles is analysed as a function of two independent variables: i) the air temperature at the heat pump inlet and ii) the mass flow rate of the air stream.

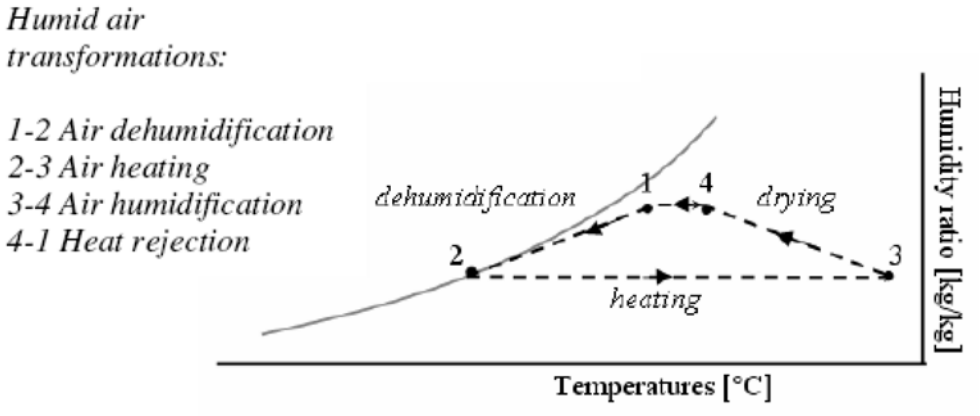

Figure 1. 2 Diagram of a closed cycle drying process

Along the closed loop the air stream is subjected to temperature variations as shown in Figure 1.2. Humid air enters the evaporator and is cooled down and dehumidified (1-2), it then enters the condenser/gas-cooler and is heated (2-3); finally enters the drum where a nearly isenthalpic process occurs (3-4) (clothes water evaporates and increases the air humidity ratio, while its temperature decreases as an effect of latent heat of vaporisation). The subsequent transformation (4-1) that closes the loop represents a further cooling due to heat dissipation: thermal balance is achieved when the dissipated heat corresponds to the work spent by the compressor and the fan. This transformation is represented by line 4-1 for the sake of simplification, but actually can occur by thermal losses, for example through the apparatus walls, or by air leakage.

The temperature level of the closed profile, qualitatively represented in Figure 1.2, depends on the thermal balance between compression and fan work and heat dissipation; the better the overall insulation of the dryer, the higher the temperature level will be.

The air flow rate is a design choice; the optimal value involves the search for the best trade-off between conflicting requirements, such as the heat transfer coefficient, the electrical power spent in the fan and the noise level.

This analysis investigates the thermodynamic behaviour of the subcritical and the transcritical cycle, in a wide range of the two independent variables (air mass flow rate and air temperature), offering further elements of evaluation for the choice between CO_2 and R134a as working fluids.

The traditional inverse cycle performed by R134a and the transcritical cycle performed by R744 are represented on the thermodynamic diagrams *T-h* of Figures 1.3 and 1.4, respectively. On the same diagram, the temperature profiles of the humid air circulating in the closed loop of the dryer are presented as well; here the air enthalpy variations are multiplied by a correction factor given by the ratio of the air mass flow rate to the refrigerant mass flow rate.

The COP optimisation problem of the transcritical cycle has to be solved by finding the optimal upper cycle pressure, under the constraint of an assigned temperature approach.

For the optimisation problem, a conventional COP value needs to be defined. Considering the single stage vapour compression cycles shown in Figures 1.3 and 1.4,

the processes undergone by the refrigerant inside the compressor are described by an adiabatic compression (a-b). The thermodynamic properties associated to point b depend on the compression efficiency η_{ic}. An isobaric heat rejection process has been considered both for the condenser or the gas cooler (b-c), both of them taking place in the high pressure side. The adiabatic expansion processes (c-d) and isobaric evaporation processes (d-a) are further shown.

The conventional coefficient of performance (*COP*), which considers only heating as the useful effect of the process, is defined as:

$$COP = \frac{h_b - h_c}{h_b - h_a} = h_{ic} \frac{h_b - h_c}{h_{b_{is}} - h_a}, \tag{1}$$

where (a-b_{is}) represent the adiabatic reversible compression processes. For the specific simulation, at extreme air temperature conditions (mainly at 50°C), the lower pressure of the transcritical cycle might be supercritical; in this case is not determined by the approach value as in the evaporation and is therefore subjected to a further optimisation process.

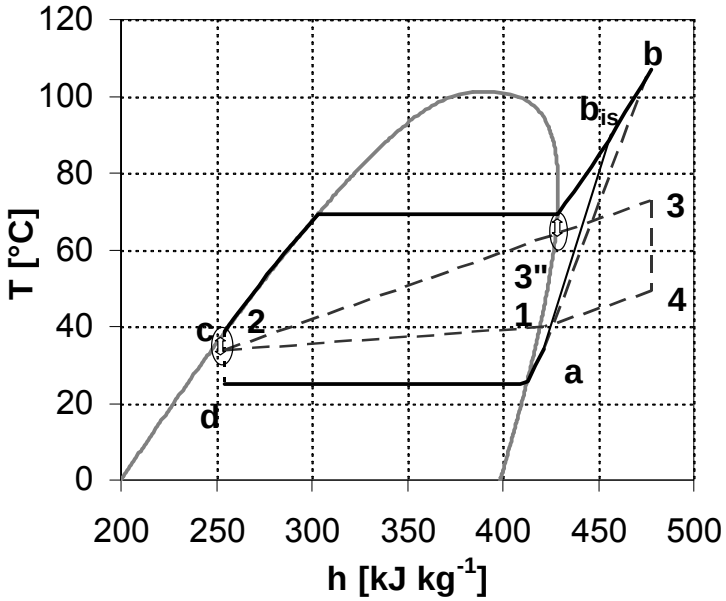

Figure 1.3 Sub-critical R134a drying cycle

Besides optimal pressures for the transcritical process, this study considers optimal liquid subcooling for the R134a subcritical cycle. The last condition is reached when the two pinch points result at the same value (corresponding to the minimum set approach of 5°C); they are respectively placed at the condenser outlet (T_c-T_2) and at the starting point of the refrigerant condensation (T_{cond}-$T_{3"}$), being Tcond the condensation temperature, as represented in Figure 3.

The performance comparison between R134a and CO_2 heat pump assisted dryers was carried out with a simplified method, based only on the thermodynamic cycles, where the energy transfers at the evaporator and the condenser/gas-cooler were assumed to occur at assigned approaches of the relevant driving potentials between the refrigerant and the air.

For the sensible heat transfer at the condenser/gas-cooler the temperature approach was set at 5°C. For the combined mass and heat transfer at the evaporator the driving potential is the humid air enthalpy (for the refrigerant the saturated humid air enthalpy at the refrigerant temperature) and the approach was set at 30 [kJ kg^{-1}], corresponding, for example, at the difference between the enthalpy of air at 40°C and 90% of relative humidity and the enthalpy of saturated air at 34°C (see Figures 1.3 and 1.4).

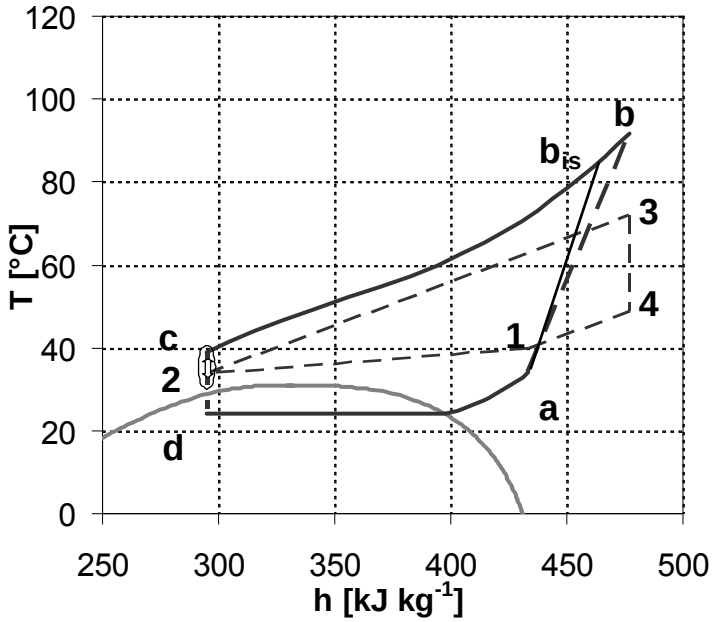

Figure 1.4 transcritical CO_2 drying cycle

The analysis was performed under the assumption that the latent heat flow exchanged at the evaporator ($q_{e,l}$) was constant and equal to 1 kW. That is to say that, assuming a constant value of the latent heat of water, the actual moisture removal rate ($\dot{m}_w$) is fixed roughly at 1.4 [kg·h^{-1}]. The superheat *SH* at the evaporator outlet was set at 10°C, for the compressor safety.

The evaporation temperature was calculated to satisfy the following boundary conditions, where the lower terms of air enthalpy in the approach expression are to be intended as the saturated air enthalpy at the refrigerant temperature:

$$\begin{cases} \varphi_{air,e,o} = 100\% \\ \Delta h_{air,e} = min\left\{(h_{air,e,i} - h_{air,T_{r,e,o}}), (h_{air,o} - h_{air,T_{r,e,i}})\right\} = 30 \quad [\text{kJ}\cdot\text{kg}^{-1}] \end{cases} \tag{2}$$

The assumption of the saturation condition for the air exiting the evaporator, together with the energy balance for the heat exchanged fully identifies the air status at the evaporator exit, being known its inlet condition, while the enthalpy approach ($\Delta h_{air,e}$) was assumed equal to 30 [kJ kg^{-1}] as previously mentioned. The approach might indifferently occur either at the warmer or the colder end of the evaporator; this is the meaning of the relevant expression in (2).

Under the mentioned assumptions, the only independent variables are the air mass flow and the a reference value for the temperature (in this case, for example, the air temperature at the evaporator inlet), which depends on the thermal level at which the heat pump operates, basically related to the thermal balance between the energy consumption of the compressor and the fan, which circulates the air in the heat pump, and the heat dissipation.

As the pinch-point position cannot be assessed *a priori*, the gas cooler was modelled according to perfect counter-flow and the temperature profiles of the two fluids were accordingly determined.

Since the theoretical analysis considers the air temperature and the air mass flow rate as independent variables, the most efficient working condition might result in the pinch point at the evaporator cold or hot end.

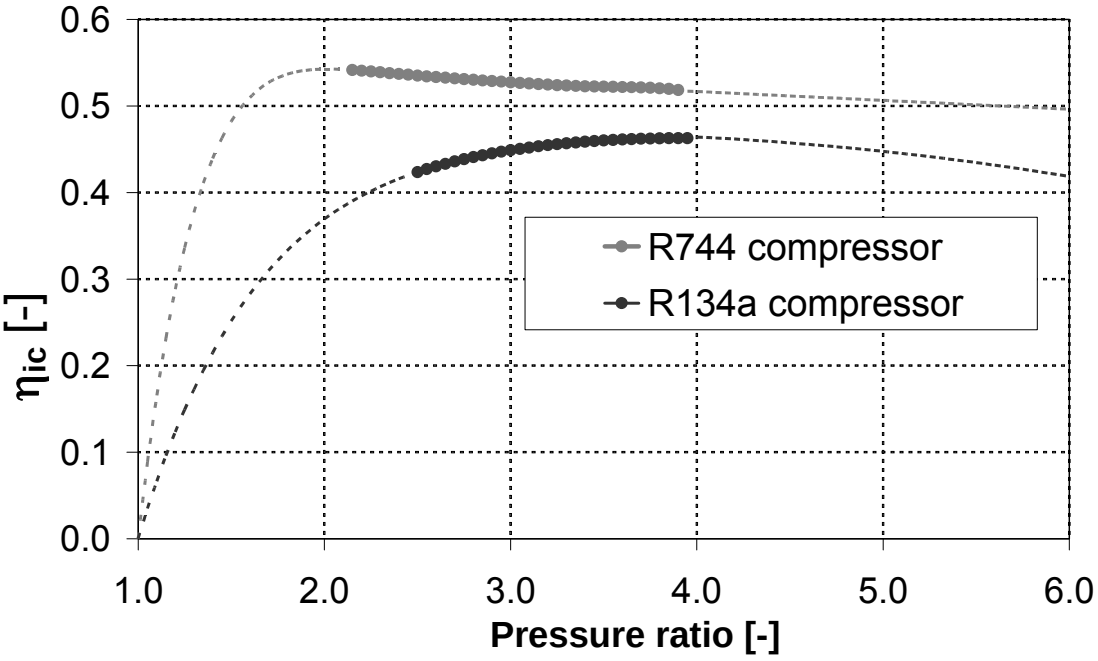

Figure 1.5 Compression efficiencies as a function of the pressure ratio

Table 1.1. Simulation parameters

Independent parameters			
Air mass flow rate $\dot{m}_{air}$	Variable	100 - 200	[kg·h^{-1}]
Air temperature at heat pump evaporator inlet $T_{air,e,i}$	Variable	30-50	[°C]
Power rate of latent heat transfer $q_{e,l}$	Fixed	1.0	[kW]
Condenser/gas-cooler: temperature approach $\Delta T_{air,c}$	Fixed	5	[°C]
Evaporator: enthalpy approach $\Delta h_{air,e}$	Fixed	30	[kJ·kg^{-1}]
Relative humidity of air at evaporator inlet $\varphi_{air,e,i}$	Fixed	90	[%]
Relative humidity of air at evaporator outlet $\varphi_{air,e,o}$	Fixed	100	[%]
Refrigerant superheating at compressor inlet *SH*	Fixed	10	[°C]

1.3.2.1 Exergy losses of the drying process

The drying process is characterized by specific thermodynamic losses in air and refrigerant transformations:

- *Compression*
- *Air heating*
- *Throttling*
- *Dehumidification*
- *Heat rejection*
- *Drying*

Here in the following the analytic development of exergy losses of the thermodynamic processes are presented.

$R_a = 287$ [J·kg^{-1}·K^{-1}] Characteristic constant of air; (3)

$R_w = 461$ [J·kg^{-1}·K^{-1}] Characteristic constant of water; (4)

The specific entropy of humid air was calculated with the following correlation

$$s_{air} = c_{p.air} \ln \frac{T}{T_0} - R_a \ln \frac{p_a}{p_0} - x \cdot c_{pw} \ln \frac{T}{T_0} - xR_w \frac{\varphi \cdot p_{vs}}{p_0} \quad (5)$$

Compression

The exergy losses of the compression process are calculated from the difference between the power input and the increment of the refrigerant co-enthalpy.

$$\pi_{comp} = e_{h3} - e_{h4} + L \quad (6)$$

$$\pi_{comp} = h_3 - h_4 - T_a(s_3 - s_4) + h_4 - h_3 \quad (7)$$

$$\pi_{comp} = T_a(s_4 - s_3) \quad (8)$$

Air heating

The exergy losses of the air heating process were calculated from the difference between the exergy decrement of the refrigerant fluid and the increment of the air exergy.

$$\Pi_{air.heating} = \dot{m}_r \cdot (e_{r4} - e_{r1}) - \dot{m}_{air} \cdot (e_{air.A4} - e_{air.A1}) \tag{9}$$

$$\begin{aligned} \Pi_{air.heating} &= \dot{m}_r \cdot \left[(h_{r4} - h_{r1}) - T_a (s_{r4} - s_{r1}) \right] ... \\ &... - \dot{m}_{air} \cdot \left[(h_{air.A3} - h_{air.A2}) - T_a (s_{air.A3} - s_{air.A2}) \right] \end{aligned} \tag{10}$$

$$\begin{aligned} \pi_{air.heating} &= \cdot (h_{r4} - h_{r1}) - T_a (s_{r4} - s_{r1}) ... \\ &... - \frac{\dot{m}_{air}}{\dot{m}_r} \cdot \left[(h_{air.A3} - h_{air.A2}) - T_a (s_{air.A3} - s_{air.A2}) \right] \end{aligned} \tag{11}$$

From the Gas-cooler/condenser thermal balance

$$\frac{\dot{m}_{air}}{\dot{m}_r} = \frac{h_{r4} - h_{r1}}{h_{air.A3} - h_{air.A2}} \tag{12}$$

$$\pi_{air.heating} = T_a \left[\frac{\dot{m}_{air}}{\dot{m}_r} (s_{air.A3} - s_{air.A2}) + (s_{r1} - s_{r4}) \right] \tag{13}$$

Throttling

The exergy losses are refrigerant co-enthalpy decrease. The process presents is adiabatic and with no power input/output.

$$\pi_{trotthling} = e_{r1} - e_{r2} \tag{14}$$

$$\pi_{trotthling} = h_{r1} - h_{r2} - T_a (s_{r1} - s_{r2}) \tag{15}$$

$$\pi_{trotthling} = T_a (s_{r2} - s_{r1}) \tag{16}$$

Dehumidification

The exergy losses of the dehumidification process were calculated from the difference between the exergy decrement of air and the increment of the refrigerant exergy.

$$\Pi_{air.dehumid} = \dot{m}_{air}(e_{air.A1} - e_{air.A2}) - \dot{m}_c(e_{r3} - e_{r2}) \tag{17}$$

$$\Pi_{air.dehumid} = \dot{m}_{air}[(h_{air.A1} - h_{air.A2}) - T_a(s_{air.A1} - s_{air.A2})]... \\ ... - \dot{m}_c[(h_{r3} - h_{r2}) - T_a(s_{r3} - s_{r2})] \tag{18}$$

$$\pi_{air.dehumid} = \frac{\dot{m}_{air}}{\dot{m}_c}[(h_{air.A1} - h_{air.A2}) - T_a(s_{air.A1} - s_{air.A2})]... \\ ... - [(h_{r3} - h_{r2}) - T_a(s_{r3} - s_{r2})] \tag{19}$$

From the evaporator thermal balance

$$\frac{\dot{m}_a}{\dot{m}_c} = \frac{h_{r3} - h_{r2}}{h_{air.A1} - h_{air.A2}} \tag{20}$$

$$\pi_{air.dehumid} = T_a\left[\frac{\dot{m}_a}{\dot{m}_r}(s_{air.A2} - s_{air.A1}) + (s_1 - s_4)\right] \tag{21}$$

Heat rejection

The thermodynamic irreversibilities results from the heat transfer between the system and the ambient.

$$\Pi_{heat.rejection} = \dot{m}_{air}[h_{air.A4} - h_{air.A1} - T_a(s_{air.A4} - s_{air.A1})] \tag{22}$$

$$\pi_{heat.rejection} = \frac{\dot{m}_{air}}{\dot{m}_r}[h_{air.A4} - h_{air.A1} - T_a(s_{air.A4} - s_{air.A1})] \tag{23}$$

Drying

Assuming the tumbler drum to be adiabatic, The exergy losses is related to the change of the air thermodynamic conditions.

$$\Pi_{drying} = \dot{m}_{air}(e_{air.A3} - e_{air.A4}) \tag{24}$$

$$\pi_{drying} = \frac{\dot{m}_{air}}{\dot{m}_r}\left[T_a(s_{air.A4} - s_{air.A3})\right] \tag{25}$$

1.3.2.2 Simulations results

Figure 1.6 reports curves of the specific moisture extracting rate SMER [$kg_w \cdot kWh^{-1}$] with reference to the air temperature at the evaporator inlet; each curve refers to a different air mass flow rate. SMER was here defined as the ratio between the moisture removal rate and the compressor power input; fan power and drum motor electrical consumption were neglected.

The analysis shows that, according to the assumptions made, it is not possible to define uniquely an optimal solution. The CO_2 transcritical cycle is more efficient than R134a traditional cycle at low temperature levels. It can be stated that the sub-critical R134a cycle always appears to have a benefit when the air temperature is increasing, while for the CO_2 cycle the SMER presents a maximum for an intermediate temperature value.

The evaporation temperature and the cooling capacity resulting from the simulation are listed in table 1.2. In Figure 1.7 the exergy losses of the two thermodynamic cycles are reported. The histogram shows the exergy losses of each transformation in the drying process. A general remark concerns the fact that the CO_2 cycle presents in most cases better compression and heating efficiencies; this arises from the peculiar characteristics of CO_2 concerning the compression process, mainly the fact that it operates at high values of mean effective pressure but with pressure ratios which are significantly smaller than in equivalent machines operated with traditional refrigerants, and the temperature profiles of the two fluids during the gas cooling that well fit together. This makes the transcritical cycle more suitable to applications dealing with high temperature lift of the heated fluid.

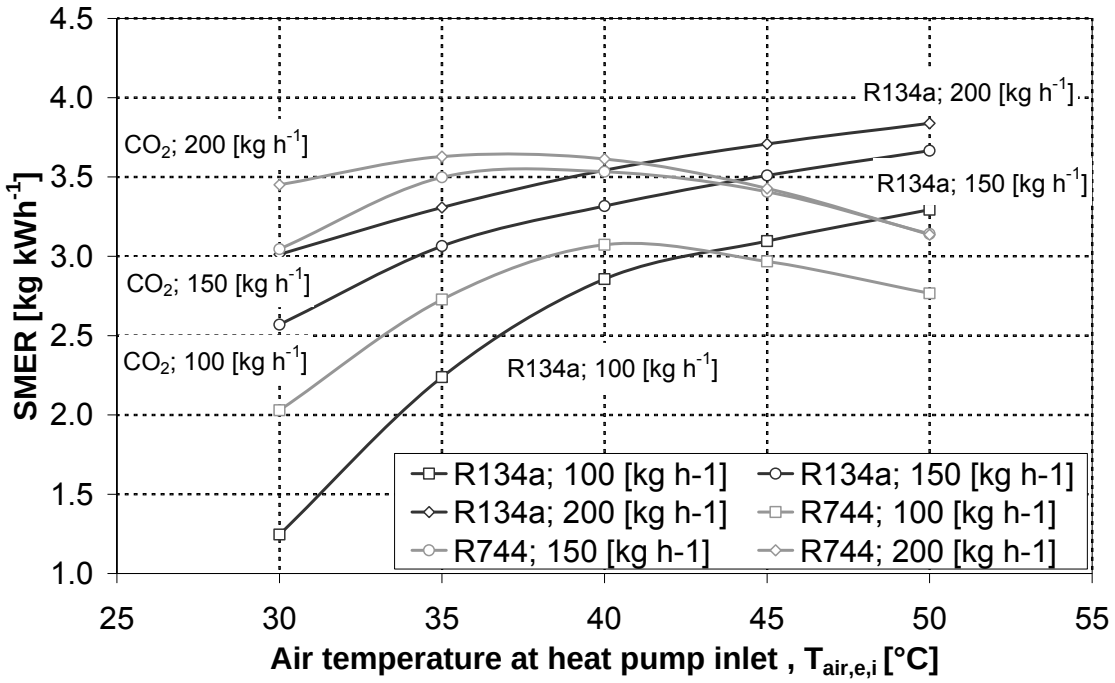

Figure 1.6 SMER [kg_w kWh^{-1}] trends as function of air mass flow rate and air temperature at evaporator inlet.

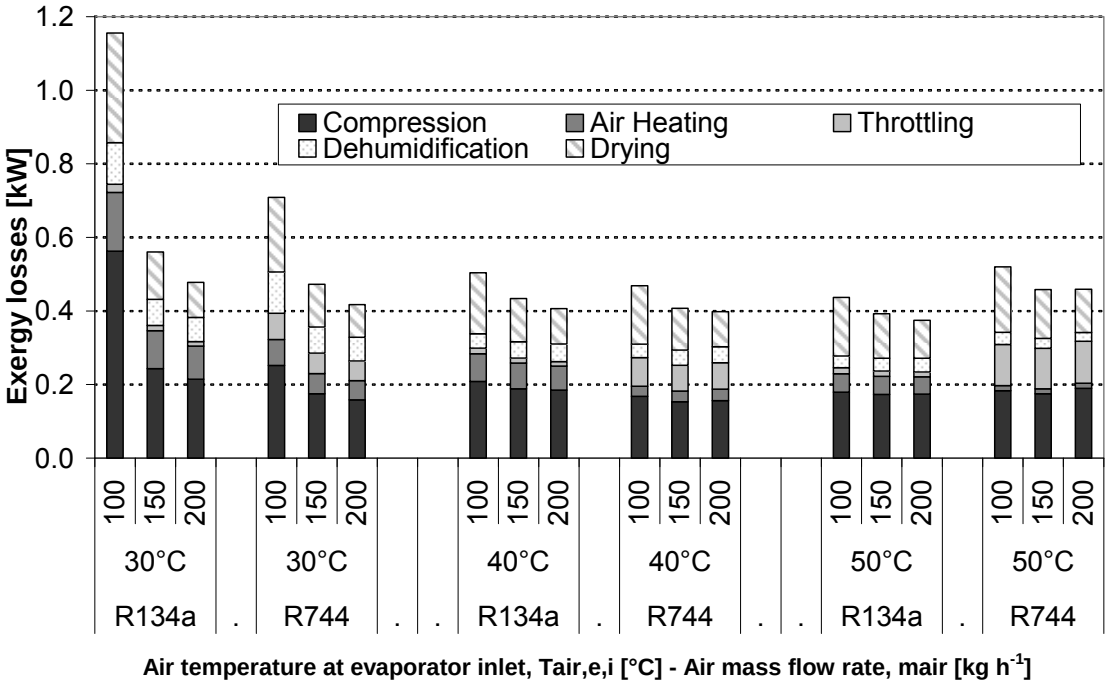

Figure 1.7 Exergy losses of CO_2 and R134a thermodynamic cycles

Table 1.2 Simulation results: evaporating temperature and cooling capacity (n.a. not applicable - supercritical pressure)

		30		35		40		45		50	
m_{air} [kg h^{-1}]	$T_{air,e,i}$ [°C]	T_e [°C]	q_e [kW]	T_e [°C]	q_e [kW]	T_e [°C]	q_e [kW]	T_e [°C]	q_e [kW]	T_e [°C]	q_e [kW]
100	R134a	-0.2	1.47	14.3	1.36	24.0	1.29	29.9	1.24	35.5	1.22
	CO_2							n.a.		n.a.	
150	R134a	9.3	1.45	17.8	1.36	24.0	1.30	29.9	1.27	35.5	1.24
	CO_2									n.a.	
200	R134a	11.4	1.45	17.8	1.38	24.0	1.33	29.9	1.30	35.5	1.28
	CO_2									n.a.	

1.3.3. Experimental analysis

To verify the performance of a CO_2 heat pump dryer, an experimental prototype was built and tested in laboratory. The CO_2 heat pump was designed for 7 kg of clothes load (dry weight). A performance comparison with an equivalent R134a heat pump dryer on the market is presented, which was tested with the same procedure as the prototype, thus allowing direct comparison between the CO_2 dryer, working according to a transcritical cycle and the traditional R134a subcritical heat pump dryer. The reference standard for the test is IEC 61121 (2002) [8]

1.3.3.1 Heat pump prototypes description

Two identical 7 kg clothes load dryers working with R134a available on the market were acquired. One of the dryers was simply equipped with pressure, temperature and power sensors, as it will be described in section 1.3.3.2.

The other one was modified, to operate with CO_2 as the refrigerant, assembling the heat exchangers and all other components inside the dryer machine basement, so as to replace the existing R134a unit. Thus, no functional components are outside the machine body. Figure 1.8 presents the lay-out of the heat pump components and air ducts. The compressor (1), which is a hermetic single stage piston compressor with

0.428 [$m^3 \cdot h^{-1}$] swept volume per unit time, was chosen to meet as closely as possible the design capacity of the R134a original one. The overall compression efficiency, already presented in Figure 1.5, has been derived from compressor data declared by the manufacturer.

The gas cooler (2) and the evaporator (3) are finned tube heat exchangers with smooth copper tube. They fit exactly in the original heat pump air ducts. The air duct circuit (4) is equipped with a lint filter (5) and it is fully integrated inside the machine framework.

1.3.3.2 The measuring system

Both the heat pumps and the air circuit were equipped with temperature and pressure sensors located as shown in Figure 1.8. Temperature and pressure measurements were acquired with an Agilent 34970A data logger equipped with two 34901A-20-channel modules. Eight copper-constantan thermocouples (T type) were used as temperature sensors.

The estimated accuracy of the entire temperature measurement system was ± 1.5 °C. Pressures were measured at the suction and discharge sides of the compressor. Two pressure sensors (Huba Control OEM relative pressure transmitters) were used, with the following measuring ranges: 0-25 bar (discharge pressure) and 0-16 bar (suction pressure) for R134a and 0-250 bar (discharge pressure) and 0-100 bar (suction pressure) for CO_2.

The accuracy of the pressure transducers was ±0.5% Full Scale. The overall dryer prototype electrical consumption, compressor and auxiliary motors, was measured with a wattmeter with 0.1% accuracy (Yokogawa Digital Power Meter model WT210). The test load weight was measured with a precision balance (Radwag precision balance model 25/C) with a repeatability of 0.1 g.

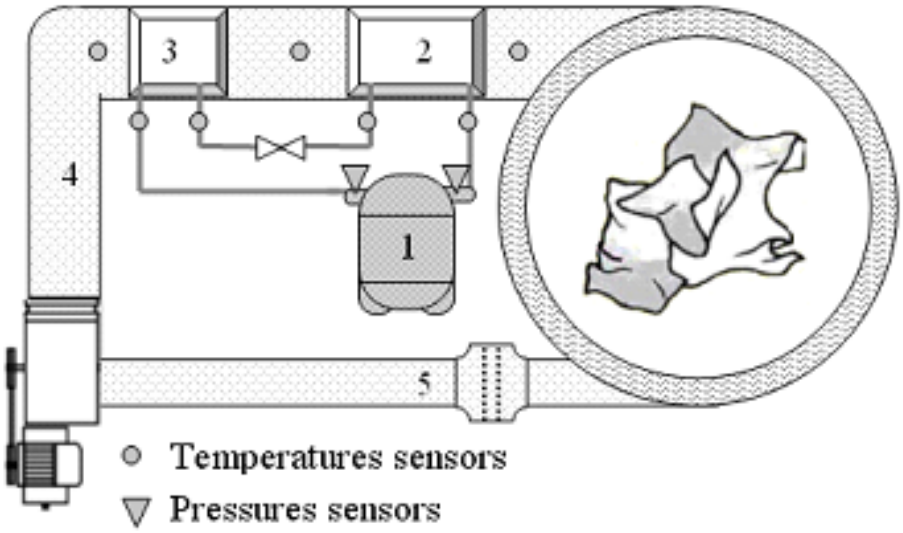

Figure 1.8 Scheme of the experimental prototype

1.3.3.3 Testing procedure

An Experimental test was performed with 7 kg of standard dry cotton clothes, subjected to preliminary wetting and spinning, according to the standard test procedure, thus assuring repeatability of the initial conditions of each test. The weight of the test load was measured immediately before and after the drying cycle; the mass of moisture condensed and accumulated inside the collecting canister is determined as well. The drying time and the total energy consumption measured are evaluated and corrected as stated by international standards IEC 61121 (2002) [8]; IEC 61121 (2002) gives the rules to normalise the performance (energy consumption) to the nominal conditions of moisture content content, i.e. 60% of initial moisture content and 0% of final moisture content for cotton textile.

1.3.3.4 Analysis of the experimental results

Figure 1.9 reports the total electrical power against time during the drying process, in terms of normalised values; normalised power is referred to the maximum power consumption of the R134a dryer, while normalised time is referred to the maximum drying time of CO_2 dryer. Total electrical consumption includes the contributions of compressor, fan and drum motors.

With reference to the corrected value of the total energy consumption, which considers the total cycle time, i.e. the drying time and the cooling time, when the heat pump is

switched off and the clothes cool down for safety reasons before door opening, the CO_2 prototype presents a negligible energy saving (less than 1%), with 9% increase in the cycle time.

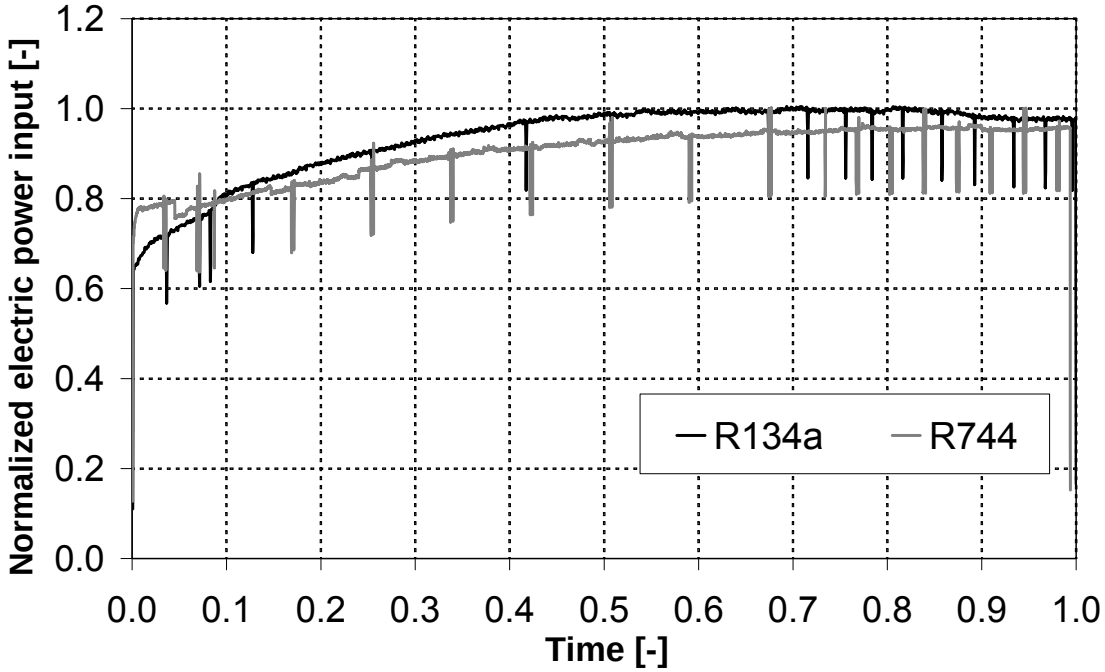

Figure 1.9 Normalized electrical power consumption

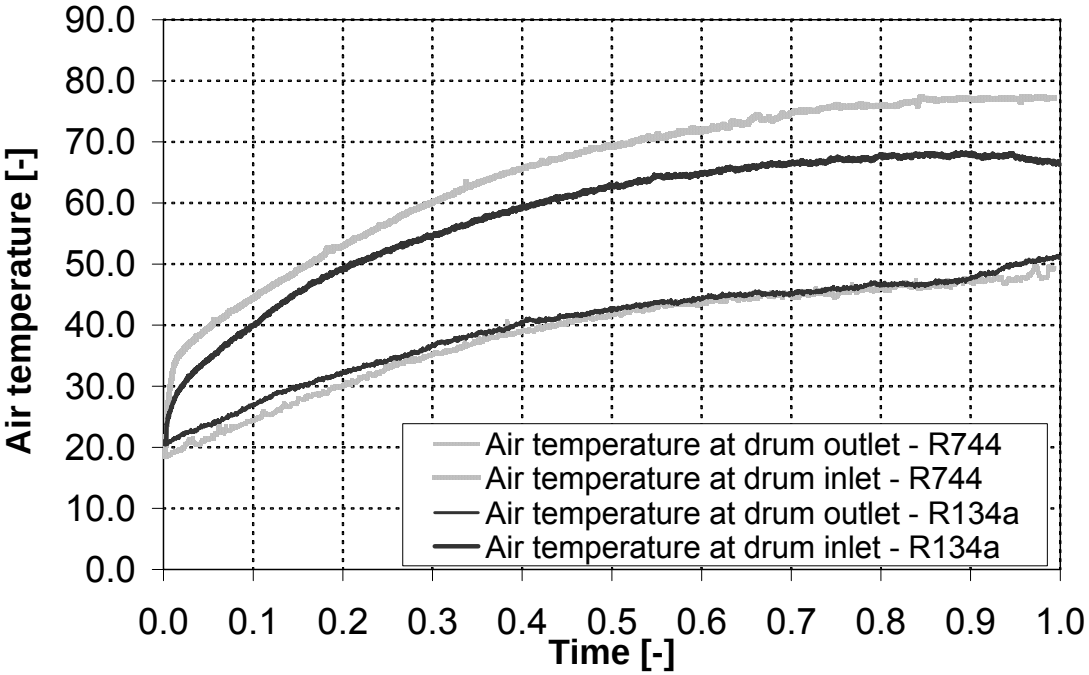

Figure 1.10 Temperature levels of the processed air

In Figure 1.10 the air temperature curves, at the drum inlet and outlet, are shown against the normalised drying time. As it can be seen, temperature levels rise continuously through time; according to the theoretical analysis, high temperature lift of air during heating suits the transcritical cycle characteristics which results in a higher air temperature lift. However, the ambient temperature was 18.2°C during the CO_2 dryer test and 21.6°C during the R134a one, being no possibilities of controlling the test room temperature better.

The experimental results (Fig.10) show that roughly for 60% of the drying time the temperature of the air at the evaporator inlet stays above 40°C, both for R134a and CO_2 heat pump dryers.

According to the results of the theoretical analysis presented in fig. 1.6, the expected performance of the CO_2 heat pump should be worse than the corresponding R134a one. However, the experimental results show about the same energy consumption.

The basic reason lies on the fact that the two units are basically different for the heat exchangers performance and moreover the conventional appliance was tested as got from the market and it does not seem to be tuned for optimal operating conditions. As a consequence, although in the simulation the effective performance of the two real compressors was considered, it is hard to draw a real confirmation of the theoretical analysis from the experimental results, but the analysis is adequate to enlighten the pros and cons of the two technologies and to give a general evaluation of the expected performance.

To explain the partial disagreement between the theoretical analysis and the experimental results we can observe that the gas cooler approach (CO_2) resulted much closer than the condenser approach (R134a) and there was no significant subcooling in the R134a unit.

According to the theoretical analysis (Fig.1.6), at the same air mass flow and heat pump component design, a possible improvement for the CO_2 unit should be found in the reduction of the air temperature, provided that the same capability of moisture extraction from the textile is maintained. As previously clarified, the thermal balance temperature depends, for the same heat pump, om the heat dissipation of the dryer structure. Of course, an increase in the overall thermal conductance of heat exchangers

can improve performances of both CO_2 and R134a heat pump, but it brings about cost increase and possibly higher noise level. On the other hand, the subcooling optimisation could significantly improve the R134a heat pump performance.

For complexity and cost reasons, no modifications to the simple transcritical cycle, such as multi-stage throttling or compression, were considered, though it is well known that they can widely improve energy performances especially at high values of air temperature (Cecchinato *et al.*, 2009 [5]).

1.3.4. Conclusions

The theoretical thermodynamic analysis shows that CO_2 operating in transcritical conditions is a viable alternative to the traditional technology in heat pump dryers. The optimisation of the operating conditions for CO_2 involves lower air temperature than in the case of R134a; these conditions can be satisfied by a suitable design of the appliance, whose thermal balance is achieved when the dissipated heat corresponds to the work spent by the compressor and the fan.

Tests performed on a prototype of a CO_2 heat pump dryer have shown negligible decrease in the electric power consumption, with a limited (+9%) increase in the cycle time, in comparison with a traditional R134a heat pump dryer. These results return a positive assessment for CO_2 as the working fluid for heat pump dryers.

1.4. References

[1] Bansal P. K., Braun J. E., Groll E. A., 2001, Improving the energy efficiency of conventional tumbler clothes drying systems, Int. J. Energy Research, Vol 25:1315-1332.

[2] Bansal P., Sharma K., Islam S., 2010a, A novel design of a household clothes tumbler dryer, Applied Thermal Engineering 30: 277–285.

[3] Bansal P., Sharma K., Islam S., 2010b, Thermal analysis of a new concept in a household clothes tumbler dryer, Applied Energy 87:1562–1571.

[4] Braun J.E., Bansal P.K., Groll E.A., 2002, Energy efficiency analysis of air cycle heat pump dryers, Int. J. Refrigeration 25: 954-965.

[5] Cecchinato L., Chiarello M., Corradi M.,Fornasieri E., Minetto S., Stringari P., Zilio C., 2009, Thermodynamic analysis of different two-stage transcritical carbon dioxide cycles, Int. J. Refrigeration. 32 : 1041-1048.

[6] Honma M., Tamura T., Yakumaru Y., Nishiwaki F., 2008, Experimental Study on Compact Heat Pump System for Clothes Drying Using CO2 as a Refrigerant., Proc: 7th IIR Gustav Lorentzen Conference on Natural Working Fluid, IIR.

[7] Klöcker K., Schmidt S.L., Steimle F., 2001, Carbon dioxide as working fluid in drying heat pumps. Int. J. Refrigeration 24: 100-107

[8] International Standard IEC 61121: Tumble dryers for household use, Method for measuring the performance, Third edition, IEC, 07/2002

[9] Nekså P, 2002, CO_2 heat pump systems, Int. J. Refrigeration, vol. 25(4): 421-427.

[10]Schmidt S.L., Klöcker K., Flacke N., Steimle F., 1998, Applying the CO2 transcitical process to a drying heat pump. Int. J. Refrigeration 21: 202-211.

[11] Stiftung Warentest, October 2006, Customers German Magazine.

[12] Valero P., Zigliczynski M., Casamassima R., 2009, Heat pump laundry dryer R134a and environment friendly alternatives, Proc. XIII European Congress, The latest technologies in air conditioning and refrigeration industry, Milano (Italy).

PART 2
ENERGY EFFICIENCY IMPROVEMENTS OF TAP WATER HEAT PUMPS

2.1 Summary

Increased concern about the environmental impact of the refrigeration technology is encouraging design solutions aimed at improving the energy efficiency of the related applications, using eco-friendly refrigerants, i.e. ozone-friendly and with the least possible global warming potential (GWP). In this respect, carbon dioxide (R744) is seen today as one of the most promising refrigerants and is raising great interest in industrial and scientific fields.

This work presents recent developments of tap water heat pumps, using CO_2 as refrigerant. In particular, the COP optimization of the transcritical cycle was investigated, developing a new upper cycle pressure control logic. An experimental air-to-water heat pump prototype was factory tested in order to test and validate the high pressure control system.

The task of the control logic is to find out the couple of variables, water flow rate and gas cooler pressure, that result in the best COP, under the constraint of fixed water temperature at the gas cooler outlet. The heat pump is to be coupled with stratification tank and a variable speed pump which forces the cold water from the stratification tank to the gas cooler. The water mass flow rate is modulated by a PID controller so as to reach and maintain the outlet water temperature at the set-point value.

To meet the regulations of some Countries and to reduce the risk of gas cooler leakages and the consequent tap water contamination with the lubricant oil, different solutions were investigated and presented in the technical literature. This section presents the performance of a CO_2 water/water heat. The peculiarity of the heat pump lies in the use of a double wall plate heat exchanger as the gas cooler, which creates a failure-proof barrier between the domestic water and the refrigerant. The basic design includes a back pressure valve and a low pressure receiver; plate heat exchangers were adopted both as evaporator and gas cooler. The heat pump was laboratory tested and

performances were recorded at different delivery temperatures of the tap water. Finally, an integrated plant of air conditioning and tap water heating is presented.

2.2 CO_2 as working fluids for tap water heat pump.

Since 1994, when G. Lorentzen [1] first revived carbon dioxide as a refrigerant and proposed it as a possible working fluid for heat pumps, tap water heat pumps have been considered a privileged application for CO_2.

The transcritical cycle is regarded as an energy efficient option for this application: the gas cooling process suits the warming up of a finite stream of water (fig.2.1), resulting in a quite large temperature lift in water without significant penalisations in COP, as it was clearly demonstrated in the technical literature [1, 2,3].

The peculiarities of the transcritical cycle require the use of once-through gas coolers in association with storage tanks where water keeps stratification, without mixing between the entering cold water from the town waterworks and the hot water delivered to users; only by this way the lowest refrigerant temperature can be achieved at the gas cooler outlet, leading this system to work in the best working conditions [3-5].

In a subcritical cycle the water maximum temperature that can be achieved is strongly linked to the condensation temperature, which involves a penalisation in COP whenever high temperature is required; in a transcritical cycle energy efficiency is linked more to the water inlet temperature, as it was clearly demonstrated by Nekså, 2002 [3] and Rieberer *et al.*, 1997. [6] As a consequence, the combination of CO_2 heat pumps with stratification tanks is almost mandatory, as was demonstrated by Cecchinato *et al.* [5] (2005).

2.3 The upper cycle pressure control logic

The task of the heat pump is to provide the storage tank with tap water at the required temperature in the most energy efficient way. As it is well known, unlike the common subcritical cycle, the transcritical cycle needs to find the optimal value of the cycle upper pressure, that is the one which leads to the maximum COP.

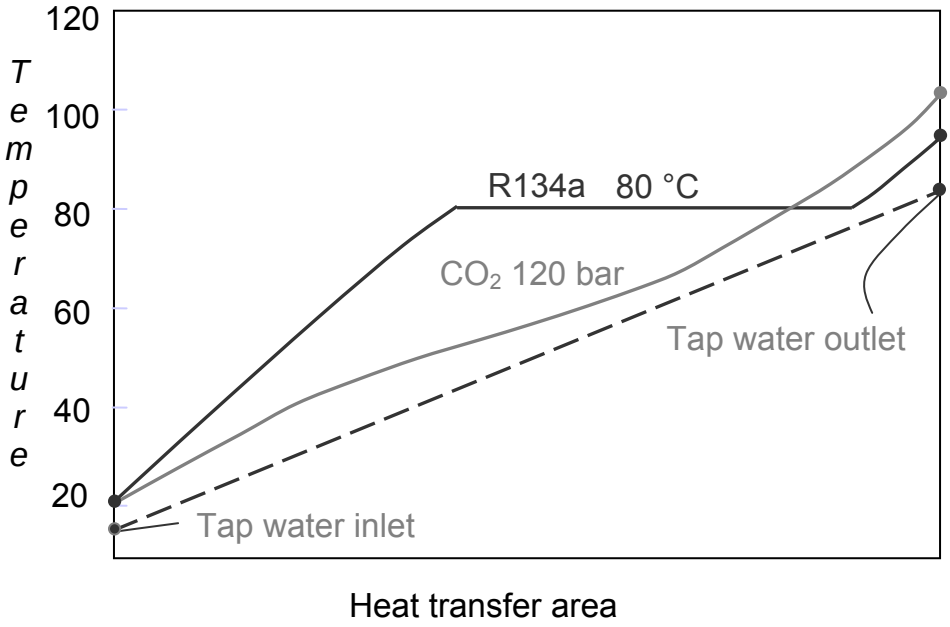

Figure 2.1 Temperature profile in tap water heat pump gas cooler/condenser

This system must be endowed with an on board unit control which operates on the flow factor of the expansion valve leading the machine to work at the optimal gas cooler pressure.

As previously mentioned, neither recirculation nor water mixing is planned in the water storage tank; as a consequence the gas cooler outlet water temperature must be carefully controlled. For this reason, the water mass flow rate is modulated by a PID controller so as to reach and maintain the outlet water temperature at the set-point value; therefore, the mass flow rate is intrinsically variable and linked to the heat flow rejected at the gas cooler.

The task of the control logic is to find out the couple of variables, water flow rate and gas cooler pressure, that result in the best COP, under the constraint of fixed water temperature at the gas cooler outlet.

2.3.1 The CO_2 trascritical cycle optimisation: related works

Several Authors [7-9] faced up the optimization problem of a transcritical system upper pressure. They analysed a single-stage refrigerating cycle working with an internal heat exchanger. By means of different simplifying assumption, the same

Authors theoretically worked out expressions to define the optimal cycle upper pressure as a function of the refrigerating cycle variables, which are mainly the gas cooler refrigerant outlet temperature and the evaporating temperature.

In a recent work, Cecchinato *at al.* [10] (2010) investigate the optimal energy efficiency and upper cycle pressure problem in single stage refrigerating carbon dioxide vapour compressor units operating in transcritical conditions. The Authors presented and critically discussed the literature approximated solutions to the optimisation problem. A numerical model for CO_2 heat exchangers and refrigerant systems was developed and a tap water heat pump unit was simulated to verify the energy performances of literature approximated solutions in presence of supply water temperature control. As shown in figure 2.2 the simulations results clearly point out large energy penalisation of all the literature solutions, up to -30%. It can be concluded that an approximated correlation must be critically evaluated before implementing it in a real controller.

As a consequence of a fixed outlet temperature, the system works in a wide range of water mass flow rate and may need to include this variable in the correlations for the optimal cycle upper pressure. This method leads to a very heavy experimental campaign in order to define the system performance in different working conditions. Otherwise, a very accurate numerical study is needed to predict the performance of each component of the heat pump, to find out the performance of a virtual prototype.

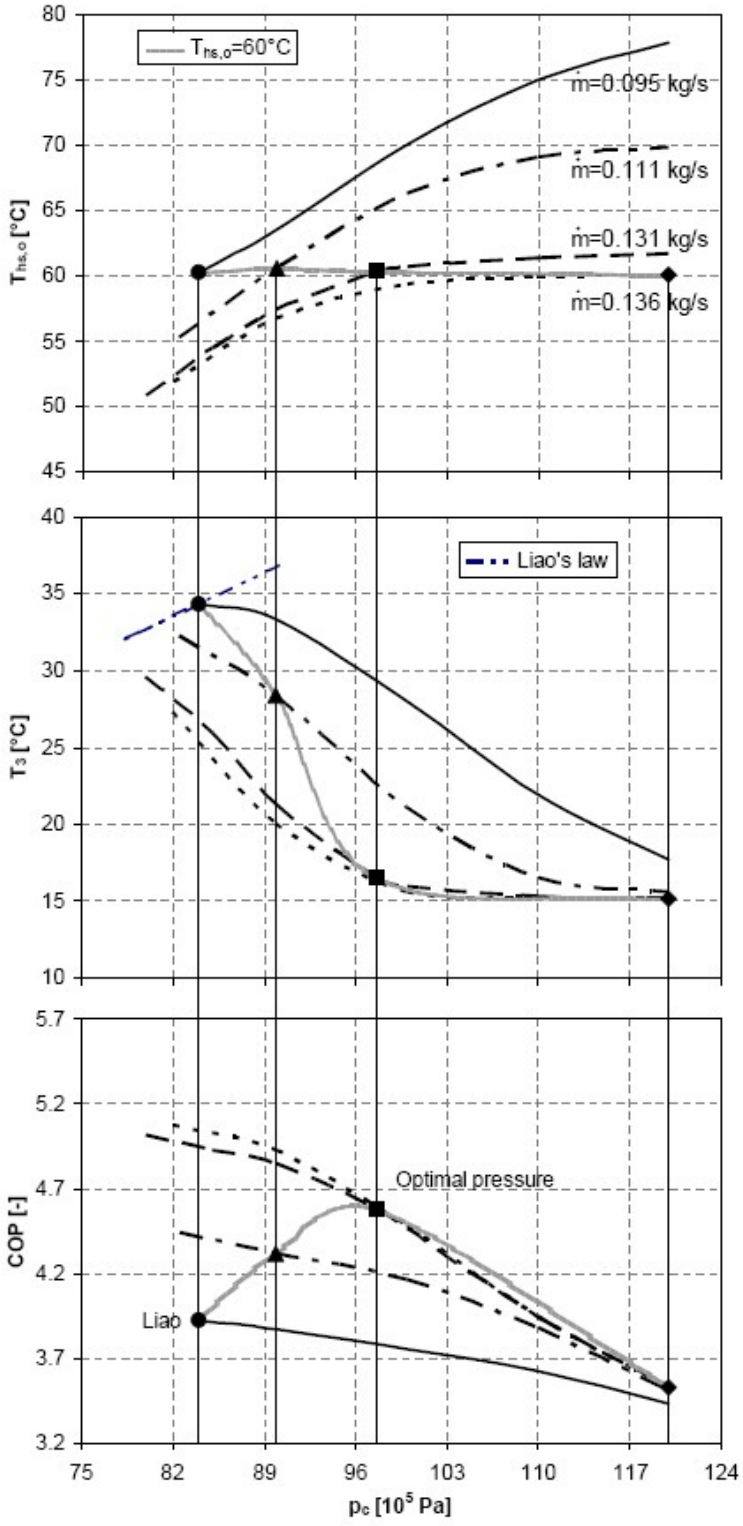

Figure 2.2 (Cecchinato et al. [10] *2010)*

Water and refrigerant gas cooler outlet temperature (T_3) and COP as a function of upper cycle pressure and water mass flow rate for the tap water heat pump at 20°C external air temperature and 15°C water inlet temperature

2.3.2 The mathematical model

A new method, presented in this work, is related to the use of a mathematical model of the thermodynamic cycle to estimate the heat pump COP and to find out the optimal heat rejection pressure, on the basis of few inputs: discharge pressures, gas cooler outlet temperature and evaporation temperature. This allows saving in time development, because it doesn't require the experimental based polynomials of the optimal upper cycle pressure.

As it was previously pointed out, the water temperature lift at the gas cooler depends, for a certain evaporating temperature and suction conditions, on the water mass flow rates as well as on the gas cooler pressure. The required water temperature value at the gas cooler outlet can be obtained with different couples of water flow rates and gas pressure, but each working condition involves different COP. The control logic which was developed manages simultaneously the water flow rate and the gas cooler pressure by acting on the pump and on expansion valve.

The water mass flow is modulated by a PID controller so as to reach and maintain the outlet water temperature at the set-point value; the controlled variable is compared with the set-point value and the pump speed is varied in order to minimise the error. At the same time, the control logic uses a mathematical model of the heat pump thermodynamic cycle to estimate the heat pump COP on the basis of few inputs: discharge pressures, gas cooler outlet temperature and evaporation temperature. To obtain the maximum COP, the upper cycle pressure is controlled using an adaptive logic; periodically this pressure is slightly modified and the effect on COP is evaluated by the thermodynamic model; then the upper pressure is further adjusted according to the COP trend.

The mathematical model is obtained through thermodynamic simulation of a single-stage compression cycle with set values of pressure and vapour superheating at the compressor inlet, for different pressures and temperatures of the refrigerant at the gas cooler outlet. A constant value of 0.7 was assumed for the overall isentropic compression efficiency, and superheating was fixed at 20°C. A ten coefficient polynomial expressing the COP as a function of gas cooler pressure (P_{gc}) and gas cooler outlet temperature (T_{gc}) was used. Simulations were performed at several evaporating temperatures (T_{ev}), so that each coefficient of the polynomials was

expressed as a function of the evaporating temperature. Each of these coefficients was expressed as a polynomial of variable order (from second to fourth). The polynomial's shape is given below:

$$COP = a(T_{ev}) + b(T_{ev}) \cdot T_{gc} + \frac{c(T_{ev})}{P_{gc}} + d(T_{ev}) \cdot T_{gc}^2 + \frac{e(T_{ev})}{P_{gc}^2} + \ldots$$
$$\ldots + f(T_{ev}) \frac{T_{gc}}{P_{gc}} + g(T_{ev}) \cdot T_{gc}^3 + \frac{h(T_{ev})}{P_{gc}^3} + i(T_{ev}) \frac{T_{gc}}{P_{gc}^2} + j(T_{ev}) \frac{T_{gc}^2}{P_{gc}} \quad (1)$$

2.3.3 System design and test procedure

An air-source heat pump unit has been factory tested to evaluate the energy performance and to fine-tune the control logic which was specifically developed for this system.

The system is designed to satisfy the domestic hot water requirements of a residential building. The estimated hot water consumption of the building is 6 [$m^3 \cdot day^{-1}$] of water at 60°C. The gas cooler of the heat pump is a once-through heat exchanger; water is warmed up in the gas cooler and stored in a tank where stratification is preserved.

The basic circuit of the heat pump and the water circuit which was set up in the factory for testing purpose are represented in Figure 2.3a. The main characteristics of the heat pump are summarised in Table1.The compressor (1) is a single-stage semi-hermetic piston compressor, whose swept volume is 3.5 [$m^3 \cdot h^{-1}$] The compressor performance was derived from the supplier's catalogue data and the overall compression efficiency η_c (1) and volumetric efficiency η_v (2) are expressed as functions of the compression ratio R_p The compression efficiencies are represented in fig. 4, for pressure ratios Rp ranging from 1.5 to 4.

The gas cooler (2) is a tube-in-tube heat exchanger operating with once-through flow of water. Two fin and tube evaporators (4) are connected in parallel; two evaporators were needed to fit them in the heat pump frame. A low pressure receiver (5) is located at the evaporators exit. Evaporator overfeeding, as well as lubricant recovery to the compressor, are provided by continuous liquid and oil removal from the

bottom of the low pressure receiver (5); the liquid exiting from the receiver (5) is completely evaporated in the suction gas heat exchanger (6), which is a coaxial type heat exchanger.

The water circuit, as it was designed for the utilisation, includes three storage water tanks, as represented in Figure 2.3b, connected in series (bottom to top, going from hottest to coldest) to avoid mixing between cold and hot water. The gas cooler is fed with cold water drawn from the bottom of the colder tank and the hot water exiting from the gas cooler is introduced inside the hottest tank, at its top from where it is drawn for consumption.

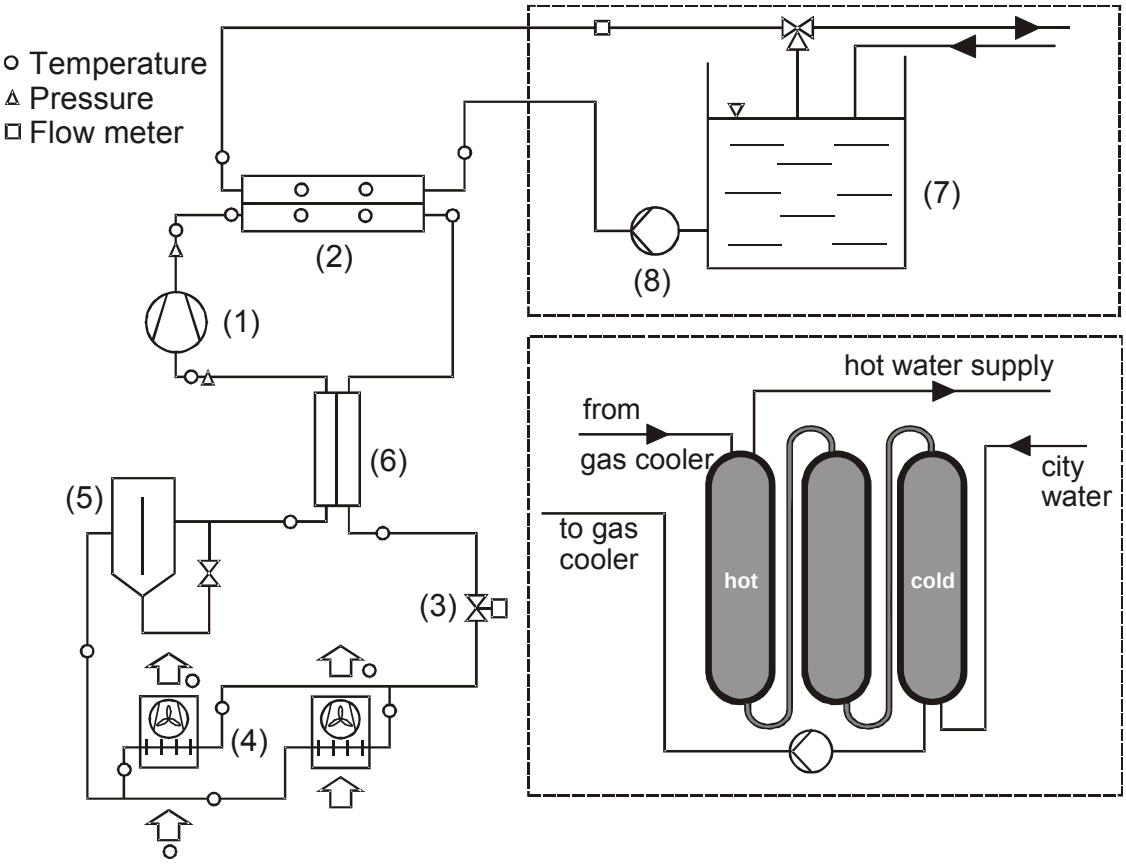

Figure 2.3a.
Heat pump and water circuit

Figure 2.3b.
Water circuit for the final plant

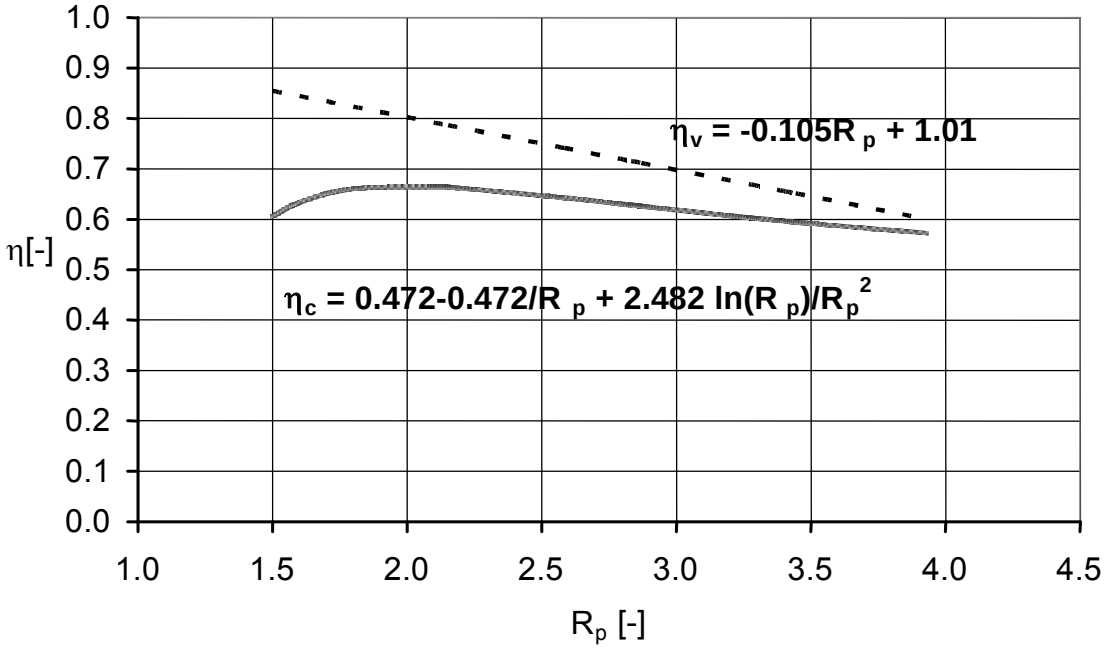

Figure 2.4 Compression efficiency as function of the pressure ratio

Table 2.1 Characteristics of the heat pump prototype

Compressor (1)	Reciprocating, semi-hermetic, single-stage. Swept volume 3.5 [$m^3 \cdot h^{-1}$]PAG oil.
Gas Cooler (2)	Counter flow, tube-in-tube heat exchanger. Stainless steel outer tube (CO_2 shell side), and inner tube (water tube side). Smooth tubes. Heat transfer area (CO_2 side) 0.68 m^2.
Expansion valve (3)	Electrically operated step motor valve.
Evaporators (4)	Fin and tube heat exchangers. Heat transfer area: external 41.1 m^2, internal 3.2 m^2
Low pressure receiver (5)	Carbon steel receiver. Inner volume 0.04 [m^3].
Suction gas heat exchanger (6)	Counter flow, tube-in-tube type heat exchanger. Carbon steel shell (low pressure side) and copper tubes (high pressure side). Heat transfer area (low pressure side) 0.5 m^2.
Water tank (7)	1 m^3 plastic water tank.
Water pump (8)	Centrifugal pump. Motor speed control. Max water flow 325 [$kg \cdot h^{-1}$]

This system was planned for nightly operation with thermal storage; during the loading period, the surface separation between hot and cold water moves toward the bottom of the tank and then moves inside the next colder tank, whereas in the unloading period this surface moves in the opposite way.

2.3.4 Experimental set-up

The water circuit arranged for the tests was initially filled with water from the public system. Cold water, drawn from the bottom of the tank enters the gas cooler. The hot water can be either discharged into the drain or partly mixed inside the tank if an higher water temperature is needed at the gas cooler inlet for testing purposes. The circulation pump (8), located at the water inlet to the gas cooler, is a centrifugal pump equipped with continuous speed regulation. The maximum water mass flow measured in the circuit is 325 $[\mathrm{kg \cdot h^{-1}}]$. The heat pump and the water circuit were equipped with temperature and pressure sensors located as shown in Figure 1a. Temperature and pressure measurements were acquired with an Agilent 34970A data logger equipped with two 34901A-20-channel modules.

20 copper-constantan thermocouples (T type) were used as temperature sensors. The estimated accuracy of the entire temperature measurement system is ±□1.5 °C.

Pressures were measured at the suction and discharge sides of the compressor. Two pressure sensors (Huba Control OEM relative pressure transmitters) were used, with the following measuring ranges: 0-160 bar (discharge pressure) and 0-60 bar (suction pressure). The accuracy of the pressure transducers is ±0.5% FS. The water flow rate was manually measured by means of a domestic water meter for ten minutes with an average accuracy of ±0.02 $[\mathrm{m^3 \cdot h^{-1}}]$.

2.3.5 Experimental results

The mathematical model used to estimate the COP, is based on two different polynomials developed to interpolate the thermodynamic cycle data in a wide range of values. The validity limits of the interpolation relations are reported in Table 2.2. The resulting polynomials were able to predict the COP within ±25%. Nevertheless, is not

important the real deviation between the predicted and the real COP, but it is essential to have similar shape curves concerning the location of the maximum COP. The largest errors occur when the system is operating close to the operative limits of the inverse cycle, i.e. low values in gas cooler pressure and high values in gas cooler outlet temperature. Tests were performed, being nearly constant the air ambient temperature and the inlet temperature of water, respectively at about 22°C and at about 20°C; the set-point of the water temperature at gas cooler outlet was varied from 60°C to 70°C by repeated steps of 5°C.

Table 2.2 Validity limits of the mathematical model

Ranges	Evaporating Temperature [°C]		Refrigerant temperature at Gas cooler outlet [°C]		Gas cooler pressure [bar]	
	Min	Max	Min	Max	Min	Max
1st	-10	10	10	30	80	120
2nd	8	14	28	48	80	110

Table 2.3 Experimental results to verify the operation of the logic of the controller

Water temperature			Gas cooler				
Set point	inlet	outlet	Pressure	Power	Evap. Temp.	Water mass flow	COP
[°C]	[°C]	[°C]	[bar]	[kW]	[°C]	[kg h^{-1}]	[-]
60	19.8	60.2	82.8	17.3	10.6	276.8	4.89
65	20.0	65.6	86.0	16.7	10.7	255.6	4.50
70	20.6	71.3	87.8	15.6	13.4	237.4	4.18

As shown by the data reported in Table 2.3, the response of the system was always satisfactory; at the same time the water flow rate forced by the pump was properly modulated to reach the new value of the set-point and the upper pressure of the cycle was modified in order to maximise the COP.

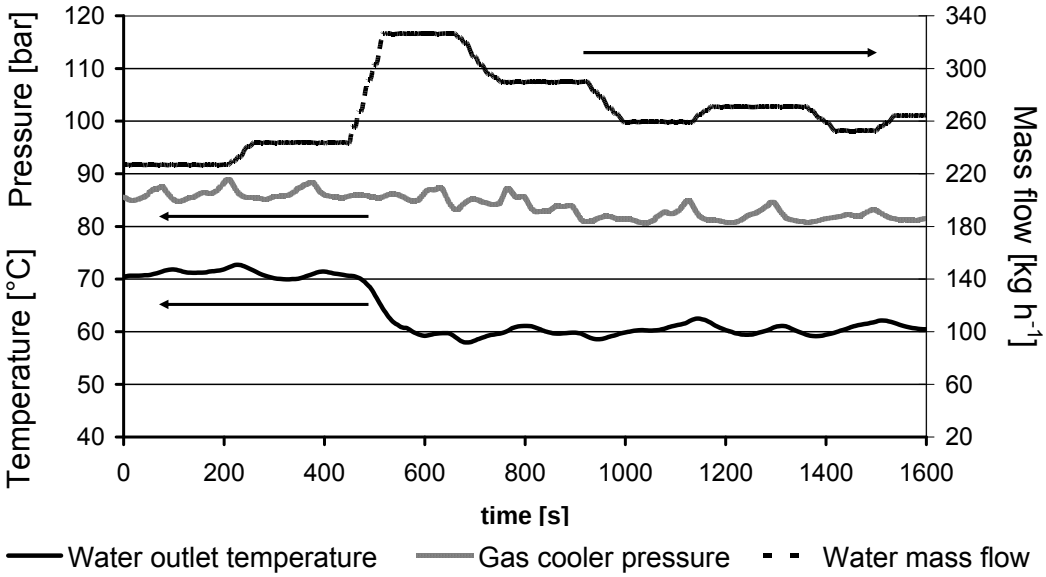

Figure 2.5 Response of the system to a variation in the water set point from 70°C to 60°C

The variation in terms of gas cooler power is reflected in the evaporating temperature, being also affected by the air temperature. The transition from the old to the new operating conditions was rather fast and only a very moderate hunting in the controlled variables can be observed during the stabilised period following the initial instability; as an example, in the diagram of fig. 2.5 a typical response of the system to a variation of the set-point is shown.

The ability of the system in promoting the maximum COP of the cycle was not definitely verified, but the value reported in Table 2.3 are consistent with the search for the optimisation of the operating conditions.

The values of the experimental COP are defined as the ones calculated from the performance of the compressor in correspondence of the actual operating conditions.

2.3.6 Conclusions

Energy efficient operation of a tap water heat pump requires the use of once-through gas coolers in association with storage tanks where water keeps stratification, without

mixing between the entering cold water from the town waterworks and hot water delivered to users. As consequence, the gas cooler outlet water temperature must be carefully controlled.

In order to optimise the heat pump performance an adaptive control logic can be utilised, which must be able to evaluate the effect on COP of a change in the upper pressure and of the correlated variations in the other variables, under the constraint of constant value of water at the utilisation.

A working unit was built, that performs at the same time the control of the temperature of the tap water and search for the optimal operation in terms of energy efficiency. Tests carried out at the factory prove that the goal was achieved.

2.4 CO_2 heat pump with the double wall plate gas cooler

2.4.1 Introduction

In the case of gas cooler leakage, tap water could be contaminated by the lubricant oil; to solve this problem and to meet the regulations of some Countries, heat pump manufacturer have proposed different solutions, that involve either the use of double wall heat exchangers (Hashimoto, 2006 [11]; Taira, 2007 [12]) or the possibility of separating the refrigerant and water circuit with an additional water loop (Hihara, 2003 [13]). Both solutions result in a penalisation in energy efficiency.

A CO_2 water/water heat pump for domestic hot water was built. The basic design includes a back pressure valve and a low pressure receiver; plate heat exchangers were adopted both as evaporator and gas cooler.

The peculiarity of the heat pump lies in the use of a double wall plate heat exchanger as the gas cooler, which creates a failure-proof barrier between the domestic water and the refrigerant. The heat pump was laboratory tested and performances were recorded at different delivery temperatures of the tap water.

2.4.2 System design

The layout of the system is represented in Figure 2.6. A piston semi-hermetic compressor (1) with swept volume of 4.3 [$m^3 \cdot h^{-1}$] was used. The gas cooler (2) is a double-wall plate heat exchanger, which will be described in details in sub-section 2.4.3.1. An electronic valve (3) driven by a step motor was used as the expansion valve. The valve is controlled by a dedicated logic, which was described in the previous section; the valve opening degree determines the high pressure value.

The evaporator (4) is a plate heat exchanger specifically designed for CO_2; the use of two reinforced end-plates assures working pressure up to 64 bar. For the specific circuit design with a back-pressure expansion valve arrangement, the evaporator operates in flooded conditions.

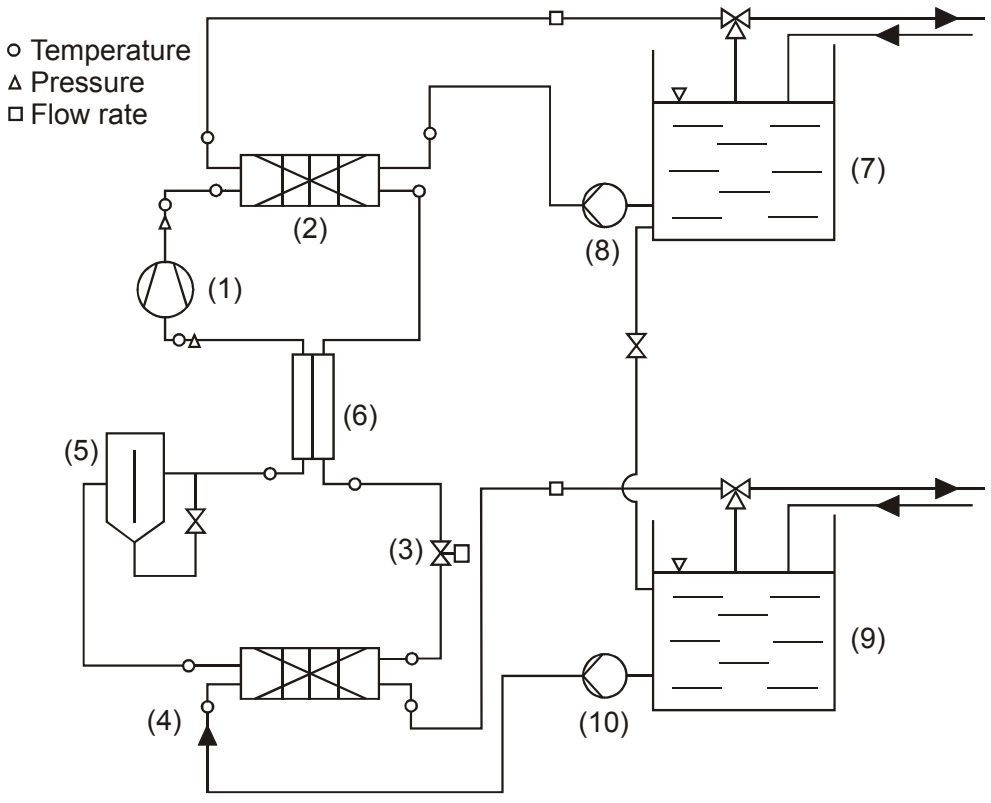

Figure 2.6 System layout

A liquid receiver (5) is located after the evaporator, to manage the liquid and oil flowing out of the evaporator. Liquid and oil are continuously removed from the bottom of the receiver and liquid is evaporated in the internal heat exchanger (6) before flowing back

to the compressor. The internal heat exchanger is an in-house built shell and tube heat exchanger.

For testing purpose, a water circuit was assembled. A water tank (7) was dedicated to the gas cooler: a variable speed pump (8) forced the water through the gas cooler; water coming from the gas cooler can be either poured back into the tank or drained off.

A second tank (9) was installed to provide water to the evaporator; the pump (10) has no capacity control. Cold water coming from the evaporator can come back to the tank; water from tank (7) can be transferred to tank (9) when necessary.

In the final installation the hot water would be stored in a stratification tank where mixing is minimized; the evaporator would be connected to the heat source, like the geothermal probe circuit or well water.

A brazed plate heat exchanger (2), which is represented in figure 2.7, was used as the gas cooler. In order to improve its mechanical resistance, the gas cooler was supplied with reinforced end-plates, so that operating pressure of 140 [bar] can be accepted.

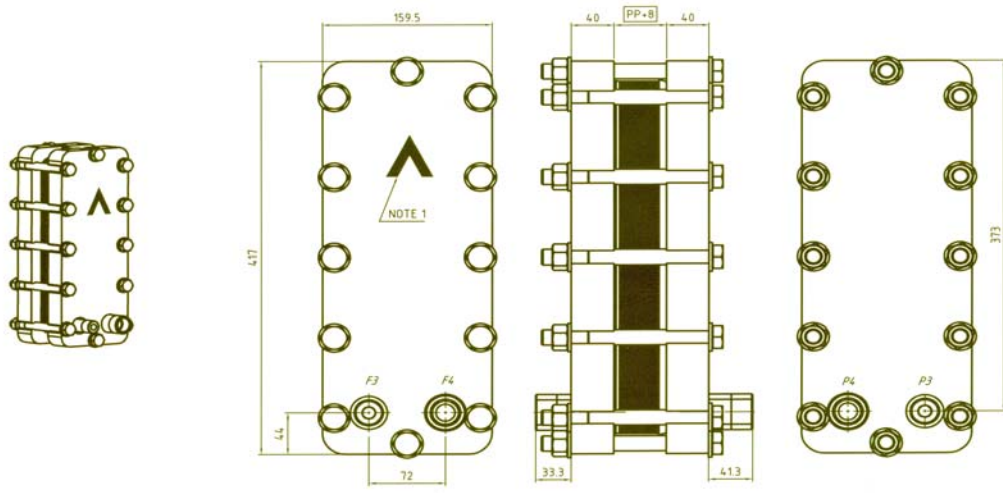

Figure 2.7 The double-wall plate heat exchanger gas cooler

The gas cooler has 33 plates and the overall dimensions are deducible from Figure 2.7 The circuit arrangement consists of two passes both for water and CO_2.

The peculiarity of the gas cooler lies in separating the CO_2 and water with double-plates including open-to-atmosphere gaps, so that, in the case of leakage, CO_2 and lubricant will not contaminate tap water and the leakage will be easily detected.

In order to evaluate the performance of the gas cooler, some tests were carried out and the results will be presented in section 3.

The evaporator (4) is a plate heat exchanger which has an overall external dimension of 121.7 mm (depth), 566 mm (height) , 159 mm (width). There are 22 plates and two passes both for CO_2 and water. The design pressure is 64 bar.

2.4.3 Experimental results

The heat pump and the water circuit were equipped with copper-constantan thermocouples (T type) and two pressure sensors located as shown in Figure 2.6. Temperature and pressure measurements were acquired with an Agilent 34970A data logger equipped with two 34901A-20-channel modules.

The estimated accuracy of the entire temperature measurement system is ± 1.5 °C. Pressure sensors have a range of 0-160 bar (discharge pressure) and 0-60 bar (suction pressure), and their accuracy is ±0.5% FS.

The water flow rate to the gas cooler and to the evaporator was measured with domestic water meter; the accuracy is estimated at ±0.02 [$m^3 \cdot h^{-1}$]. The first set of tests aimed at the evaluation of the gas cooler performance. For this purpose, gas cooler pressure and water flow rate were controlled manually. These tests were performed in the winter time, when the water net temperature was quite low (about 8°C). Also the evaporator performance was assessed during these preliminary tests.

Once that the performance of the gas cooler was mapped, the heat pump control logic was activated and the global performance was evaluated at different values of the water delivery temperature.

2.4.3.1 The gas cooler performance

The gas cooler performance was measured on board of the heat pump. The water inlet temperature was kept constant, while the water mass flow was varied in the range 0.23÷0.37 [$m^3 \cdot h^{-1}$] acting on the variable speed pump. For each value of water flow rate, gas cooler pressure was varied in the range 80-112 bar, acting on the expansion valve.

The water flow rate and inlet temperature to the evaporator were kept constant; therefore, the evaporation pressure varied as a consequence of the change in gas cooler performance. The performance of the internal heat exchanger was mainly influenced by the variation in the gas cooler outlet temperature. The evaporation temperature and the suction temperature influence the CO_2 mass flow rate, together with the compressor volumetric efficiency, which is a function of the pressure ratio.

Figure 2.7a shows evaporation temperature and CO_2 mass flow rate as functions of gas cooler pressure for different water flow rates at the gas cooler. Evaporator water mass flow rate was constantly equal to 1.64 [$m^3 \cdot h^{-1}$], while its temperature ranged between 5.5°C and 7.2°C, as there was partial water recirculation in the evaporator water tank.

As the gas cooler pressure increases, the evaporation temperature decreases, due to the higher cooling power of the system. The CO_2 mass flow rate decreases and the high pressure increases, in relation to the lower suction density of CO_2.

At the above mentioned conditions, the performance of the gas cooler was mapped; relevant parameters, like the gas cooler power, the temperature approach between the water inlet temperature and the CO_2 outlet temperature and the water delivery temperature are represented in Figure 2.4 as functions of the gas cooler pressure.

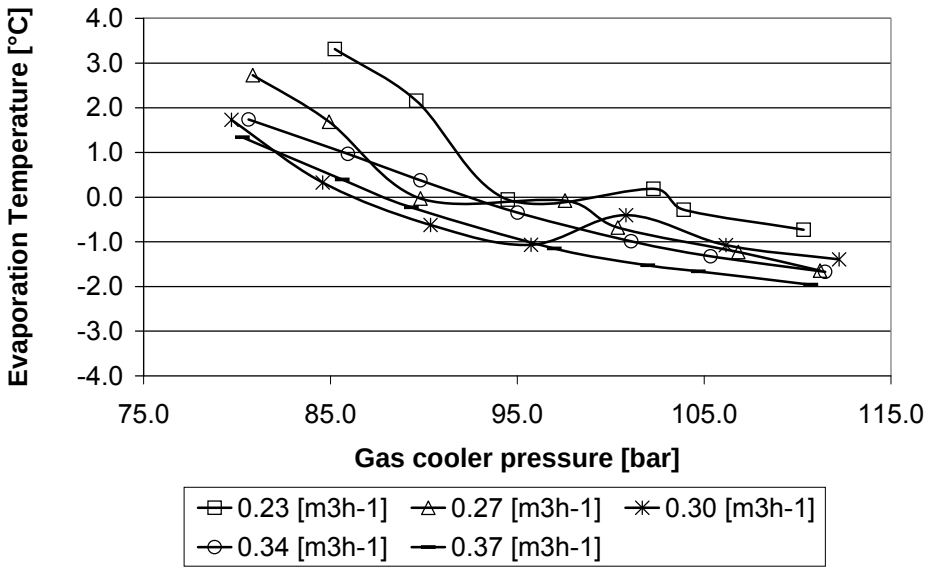

Figure 7a. Measured evaporation temperature as functions of gas cooler pressure.

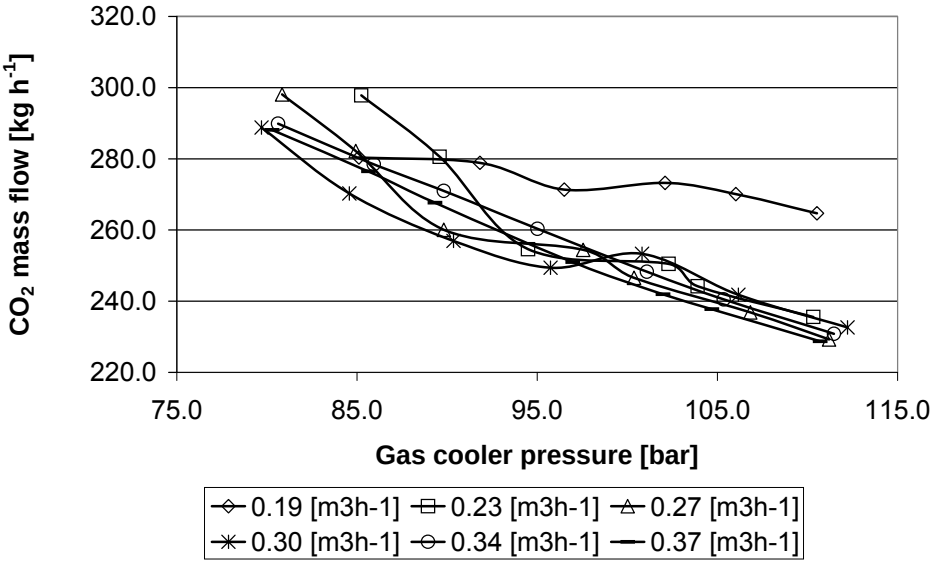

Figure 7b. CO_2 mass flow rate as functions of gas cooler pressure

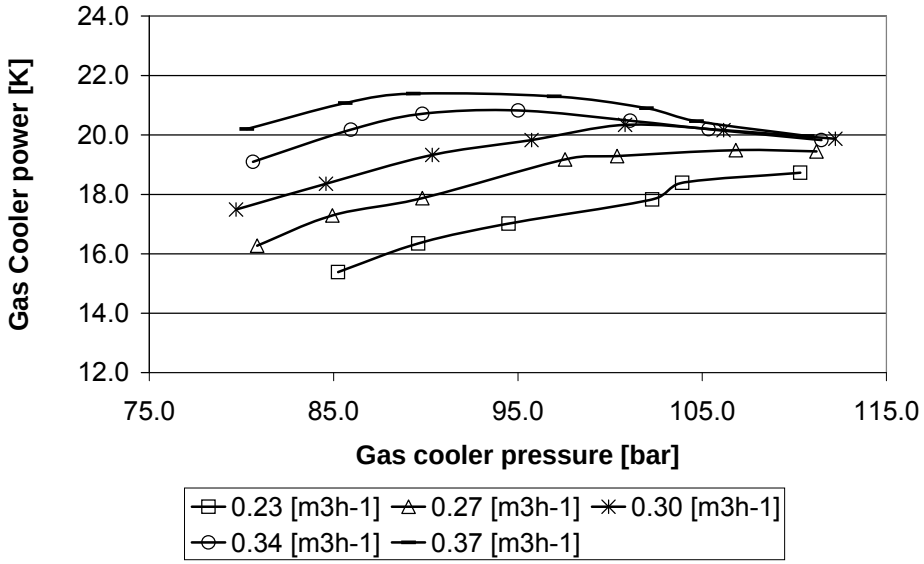

Figure 7c. Measured gas cooler power as functions of gas cooler pressure

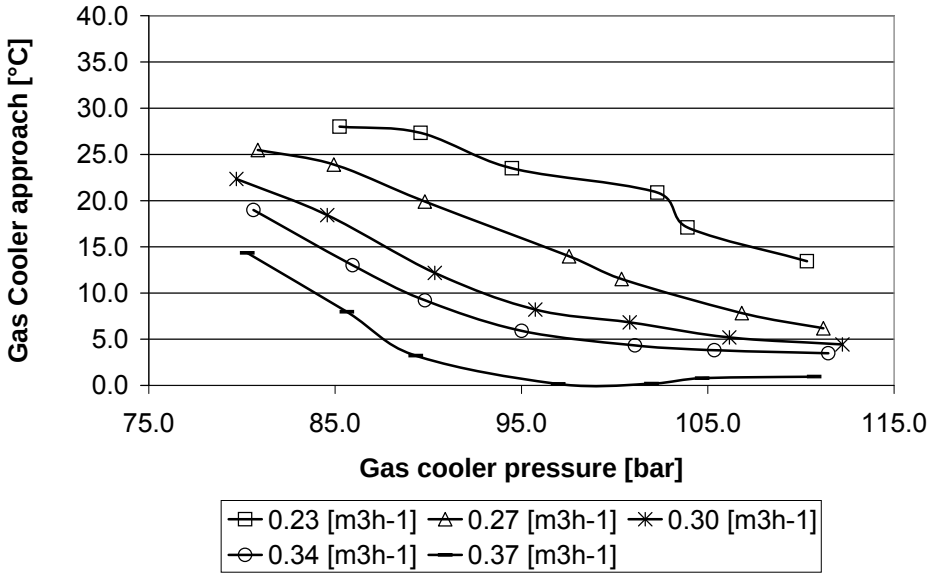

Figure 7d. Measured temperature approach at gas cooler outlet as functions of gas cooler pressure

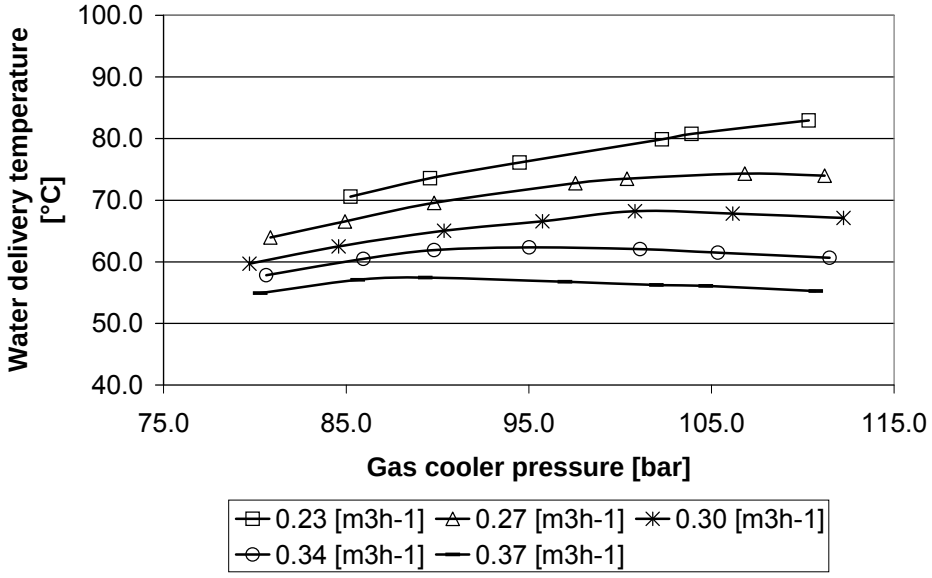

Figure 7e. Measured and water delivery temperature as functions of gas cooler pressure

As it clearly emerges from Figure 2.4, the same water delivery temperature can be obtained with different water mass flow rates at different values of gas cooler pressure. The control logic must be able to sort out the couple of variables that assures the maximum COP.

2.4.3.2 The evaporator performance

The performance of the evaporator was mapped varying the CO_2 mass flow rate. Controlling the amount of liquid drained from the low pressure receiver (5), the vapour quality at the evaporator exit was maintained close to one. As it was mentioned before, the water mass flow rate was constantly equal to 1.64 [$m^3 \cdot h^{-1}$] and its inlet temperature ranged between 5.5°C and 7.2°C.

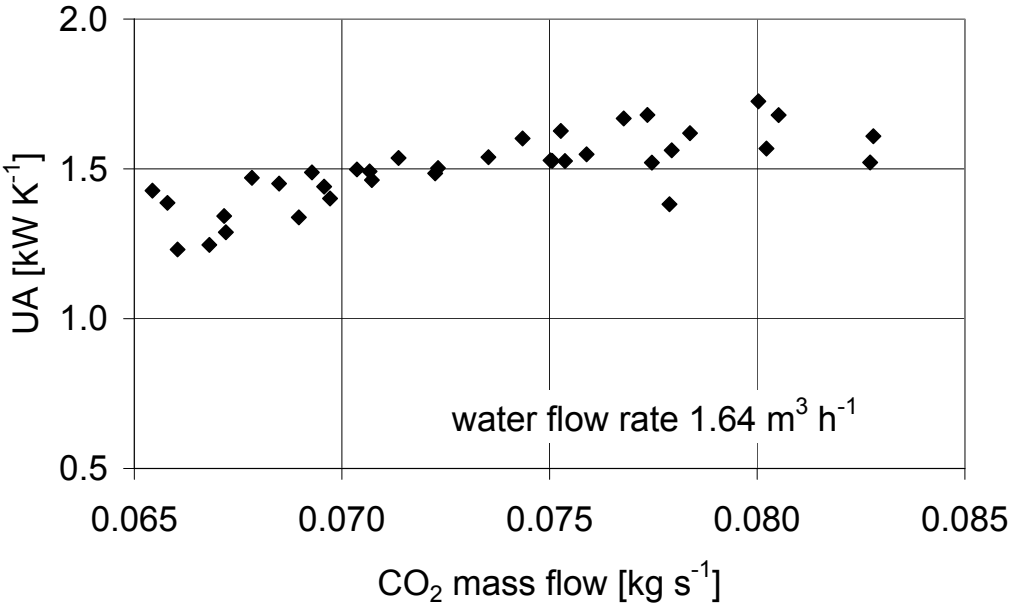

Figure 2.8 Evaporator overall thermal conductance UA.
Water mass flow rate 1.64 [m^3 h^{-1}]. Saturated vapour at evaporator exit

The overall thermal conductance (UA) of the evaporator was calculated as:

$$UA = \frac{Q}{\Delta t_{ml}} \quad [kW \cdot K^{-1}] \tag{2}$$

where Q is the cooling power and Δt_{ml} is the logarithmic mean temperature difference between the evaporator and the water. The *UA* value as function of CO_2 mass flow rate is represented in Figure 2.8.

2.4.3.3 The heat pump performance

After having evaluated the heat exchanger performance, the heat pump was tested with its own control logic set active; the aim of the test was to verify the ability of the system to find out the couple of variables, gas cooler pressure and water flow rate, that maximise the COP under the constrain of fixed water delivery temperature.

Two sets of measurements were performed: the first one was characterized by water inlet temperature close to 14.5 °C , the second one by water inlet temperature close to 20.0°C.

Figure 2.9 displays the water delivery temperature during the first test for three different set points of the heat pump, 60°C, 70°C and 80°C with water inlet temperature 14.5°C. The heat pump was able to maintain the set point within a very narrow interval; the maximum deviation from the set point was 2.1 °C, during the COP optimization procedure.

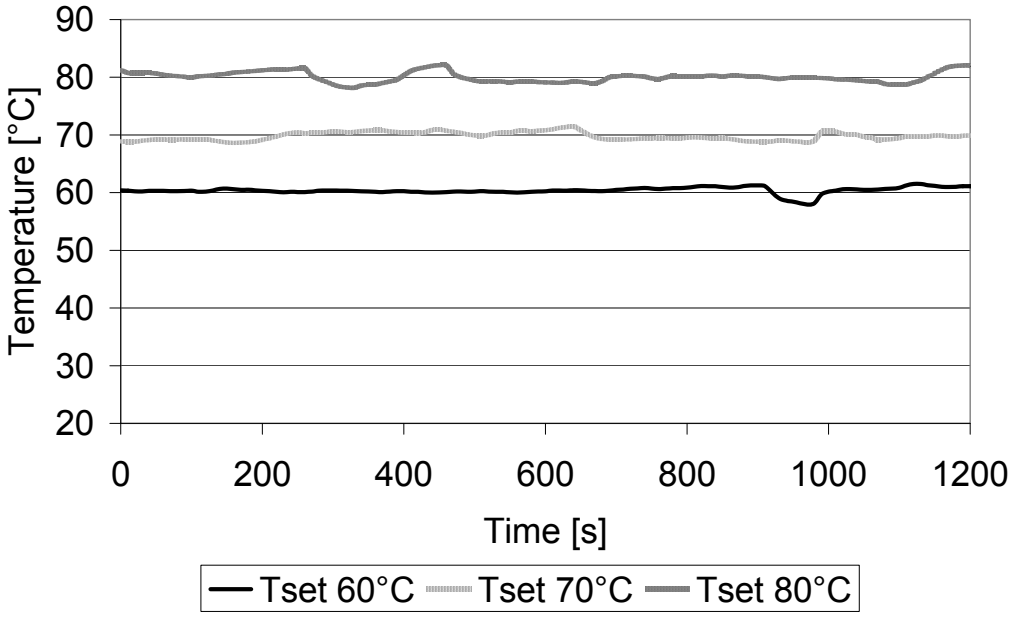

Figure 2.9 Water delivery temperature at different set points.
Water inlet temperature 14.5÷14.7°C.

Table 2.4 summarizes the main results of the two tests: for a given water inlet temperature, as the water delivery temperature set point temperature was increased, the heat pump reduced the water mass flow rate to meet higher value of delivery water

temperature. Then, the reduced heat transfer led the control logic to set higher value for the optimal high pressure.

The control logic proved to be effective in finding out to keep the upper pressure at the optimal value for COP.

Table 2.4 Heat pump test results

Set point	[°C]	60	70	80	60	70
Gas cooler water inlet temperature	[°C]	14.7	14.5	14.5	20.3	20.1
Water delivery temperature	[°C]	60.2	69.8	80.0	59.6	69.3
Gas cooler water mass flow rate	[kg h^{-1}]	416.9	313.7	264.6	457.0	356.1
Gas cooler pressure	[bar]	96.7	98.2	109.8	91.0	104.1
Gas cooler outlet temperature	[°C]	22.4	33.5	34.5	34.5	33.0
Evaporator water inlet temperature	[°C]	15.1	15.4	15.5	22.2	21.4
Evaporation temperature	[°C]	1.8	3.9	4.2	8.3	8.7
Gas cooler power	[kW]	20.6	18.6	18.9	19.5	21.5
COP	[-]	3.8	3.4	3.1	3.9	3.7

2.4.4 Conclusions

A water/water CO_2 heat pump for domestic hot water was built. The gas cooler is a double plate heat exchangers, which guarantees no water contamination by lubricant in the case of wall breakage. The evaporator is a plate heat exchanger.

The water delivery temperature is managed by a variable speed pump, while an adaptative control keeps the upper pressure value to the one that maximises the COP.

The heat pump was tested in order to assess the heat exchangers performance and to validate the control logic. At the testing conditions, the temperature approach at the gas cooler outlet ranged from near zero to 30°C, depending on the high pressure value and

on the water mass flow rate; the evaporator showed a quite strong dependence f the thermal performance on the CO_2 mass flow rate.

The tests performed in laboratory proved the system was able to steadily maintain the water delivery temperature up to 80°C and to find and keep the optimal value of the upper pressure for energy efficiency. The transcritical cycle with CO_2 confirmed to be an energy effective and reliable technology for tap water heating up to 80°C, performing better with the traditional cycle with HFCs.

2.5 An integrated system for air conditioning and hot water production.

2.5.1 Introduction

This section presents a CO_2 tap water heat pump working on an integrated plant on the field.

The design idea of using renewable energy sources has been realized with the installation of photovoltaic panels to meet the needs of electricity and heat pumps for space conditioning and hot water, using the ground as a source of heat through geothermal probes.

The air conditioning plant employs reversible machines, so during summer operation, heat is rejected to the ground through the circuit of geothermal.

2.5.2 The system

The building complex consists of 26 residential units. An estimated hot water requirement of 7.4 m^3day^{-1} at 50 °C was considered, the design heat load is approximately 120 kW, with the outside temperature of -10 ° C. the hot water is supplied with the maximum temperature of 45°C. The summer peak cooling load is estimated at about 100 kW with the outside air temperature of 32°C and the water temperature of 7° C.

The reversible heat pump for air conditioning operates with the synthetic fluid R134a: the high temperature of the return water (35°C to 40°C) would make the CO_2 heat pump less efficient than R134a for air conditioning of the buildings.

In Figure 2.10 shows the general scheme of the hydraulic connections between the R134a heat pump and the carbon dioxide heat pump (1). The water is heated up in the gas cooler with a single pass through. The design choice was on a system with three tanks (2) connected in series, as capable of promoting stratification easily. The water at the maximum storage temperature is sent to a mixing/distribution tank (3) and maintained in circulation in the ring distribution. The desuperheating power of the two R134a machines (5) is transferred to tap water to balance the heat leakage of the tank and of the distribution ring.

The tap water heat pump is continually active during the night charging the stratified tank when the R134a machine is turned off,. The ignition during the day occurs only when the removal of water from the tanks exceeds a preset threshold level.

The R134a heat pump is equipped with two semi-hermetic reciprocating compressors (1) with swept volume of 71 [$m^3 \cdot h^{-1}$]. The two compressors work in parallel. The plate heat exchanger (2), which operates in any mode of operation, recovers most of the heat desuperheating, compensating the heat leakages of the recirculation circuit and of the storage tank.

In summer operation, the heat of condensation is transfered to the ground through the heat exchanger (4). The throttling valve (7), which feeds the evaporator (5), is a reversible flow type and it is controlled by a signal of liquid level high pressure (6a). The heat exchanger works with direct crossing of the fluid, as the traditional dry-expansion evaporators. Downstream of the evaporator, the suction line of the compressor is therefore provided a receiver-liquid separator (10), which act as storage tank for the charge transfer arising from changes in retention refrigerant that occur in different parts of the circuit. The liquid along with the lubricant is drawn off from the bottom of the receiver and it is sent to the regenerative heat exchanger (8th) through the valve (9a), where the supercooled liquid evaporates before the expansion valve (7).
The lubricant is distributed equally on both compressors, with an appropriate design of the intake manifold.

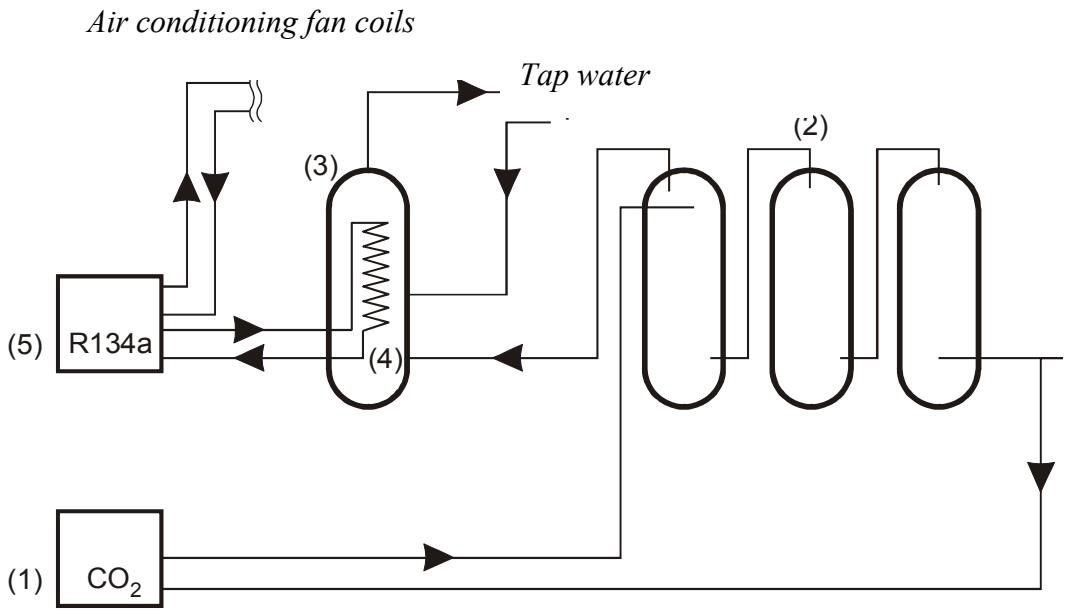

Figure 2.10 Hydraulic connections

In winter operation, the role of plate heat exchangers (4) and (5), and of the level sensors (6a and 6b), the switches (8a and 8b) and the valves (9a and 9b) is inverted, with the 4-way valve (3).

This unique and innovative system used for the laminating valve allows to feed the flooded evaporator directly, thereby increasing the performance. In addition, the liquid subcooling at the inlet throttling valve (7) reduces the title of the refrigerant that is sent to the evaporator, thus limiting the distribution problems that are typical of plate heat exchangers.

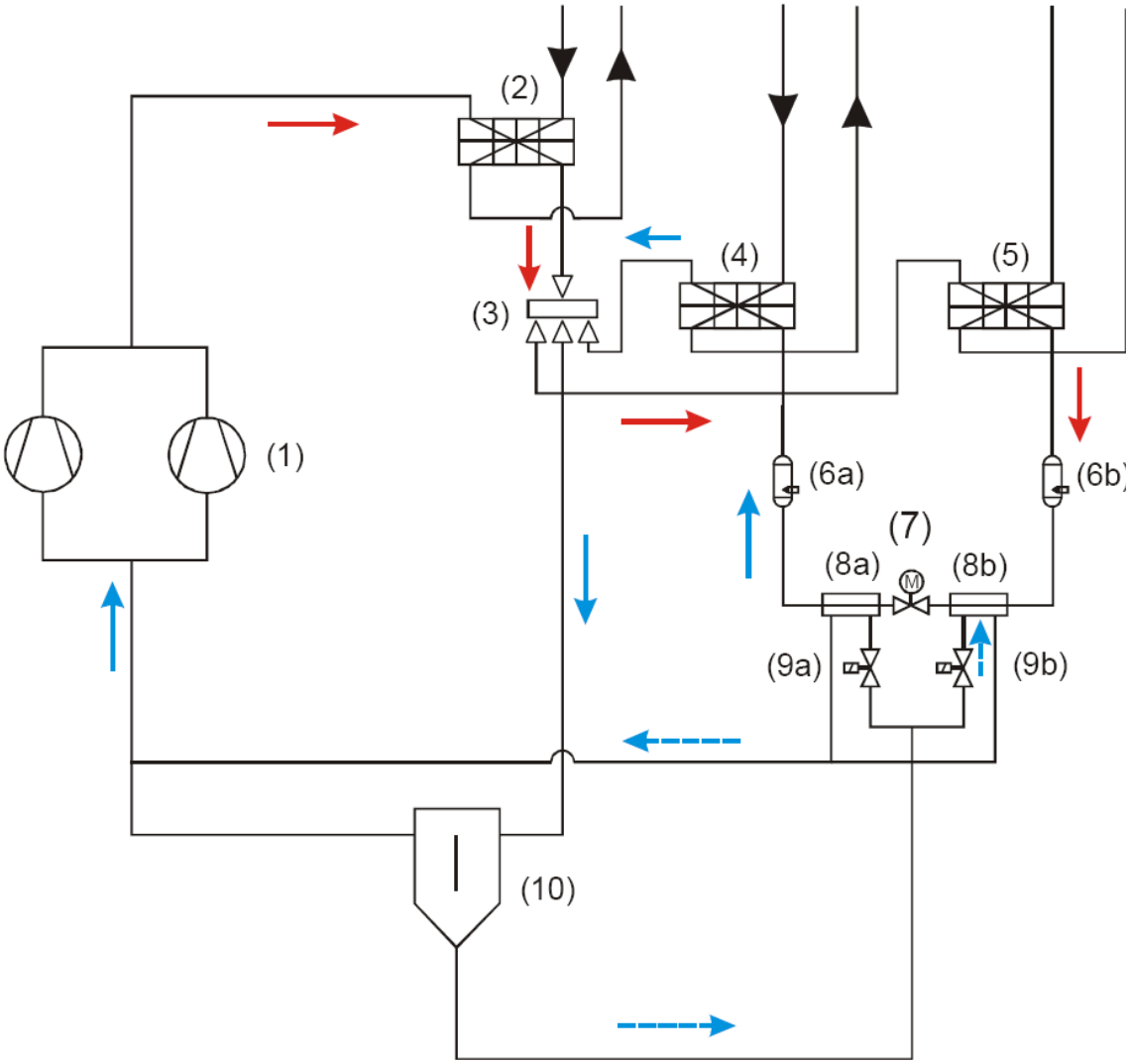

Figure 2.11 Air-conditioning system plant: Summer operative conditions

SUMMER

(1) Semihermetic reciprocating compressor. Swept volume 71 $[m^3 \cdot h^{-1}]$

(2) Superheating heat exchanger

(3) Four ways valve

(4) Plate heat exchanger: Condenser

(5) Plate heat exchanger: Evaporator

(6a) Level sensor

(7) Reversible expansion valve

(8a) Regenerative heat exchanger

(9a)On/off valve: Open

(9b) On/off valve: Closed

(10) Liquid separator

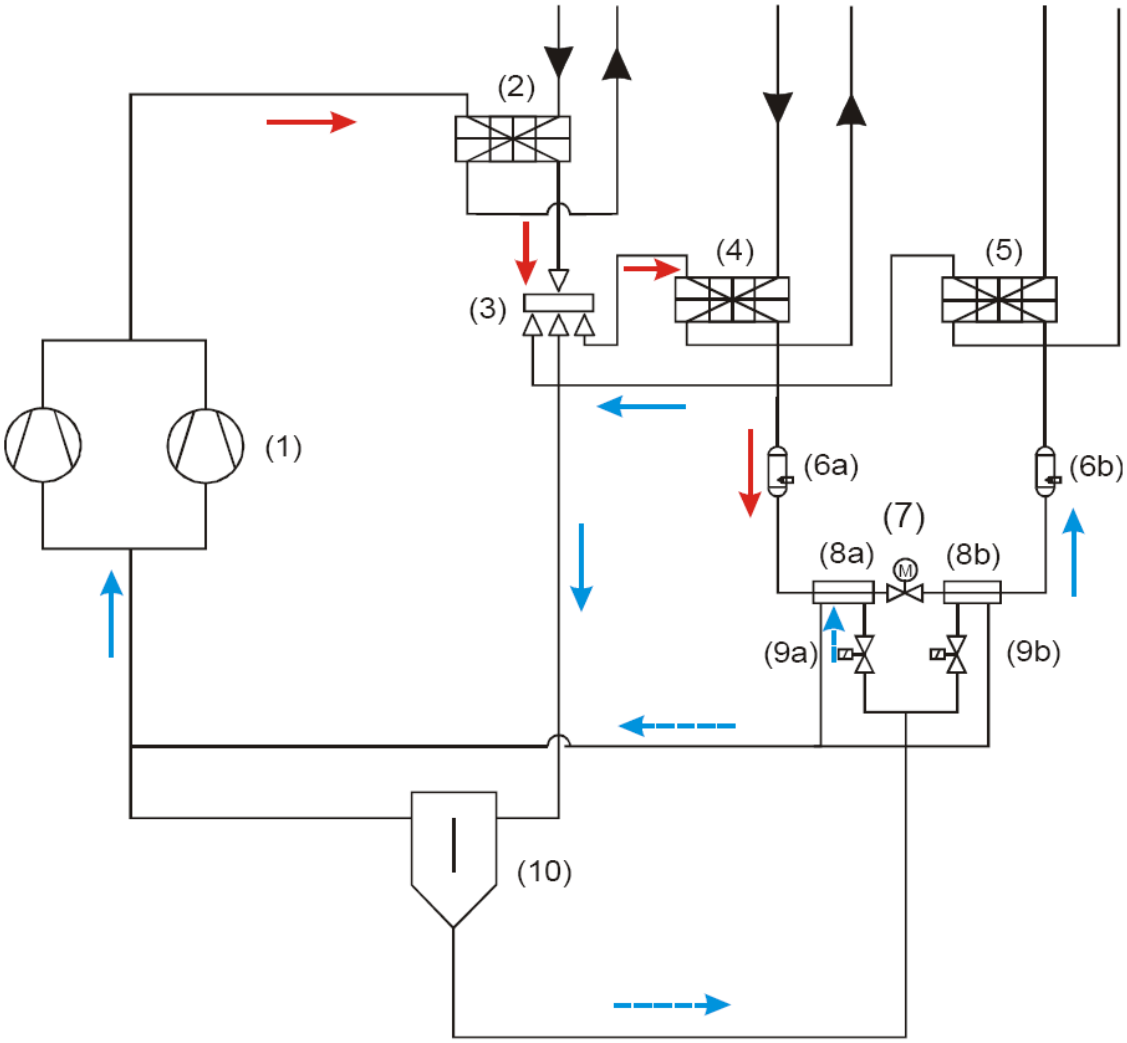

Figure 2.12 Air-conditioning system plant: Winter operative conditions

WINTER

(1) Semihermetic reciprocating compressor. swept volume 71 $[m^3 \cdot h^{-1}]$

(2) Superheating heat exchanger

(3) Four ways valve

(4) Plate heat exchanger: Evaporator

(5) Plate heat exchanger: Condenser

(6b) Level sensor

(7) Reversible expansion valve

(8b) Regenerative heat exchanger

(9a)On/off valve: Closed

(9b) On/off valve: Open

(10) Liquid separator

2.6 References

[1] Lorentzen G., 1994, Revival of carbon dioxide as a refrigerant, Int. J. of Refrigeration, vol. 17(5): 292-301.

[2] Nekså P., Rekstad H., Zakeri G R, Schiefloe P. A., 1998, CO_2 – heat pump water heater: characteristics, system design and experimental results, Int. J. of Refrigeration, vol. 21(3): 172-179.

[3] Nekså P., 2002, CO2 heat pump systems, Int. J. of Refrigeration., vol. 25(4): 421-427.

[4] Fornasieri E., Girotto S., Minetto S., 2008. CO_2 Heat Pump for domestic hot water. 8th IIR Gustav Lorentzen Conference on Natural Working Fluids, Copenhagen, 7-10 September.

[5] Cecchinato L., Corradi M., Fornasieri E., Zamboni L., 2005, Carbon dioxide as refrigerant for tap water heat pumps: A comparison with the traditional solution, Int. J. of Refrigeration, vol. 28(8): 1250-1258.

[6] Rieberer R, Kasper G, Halozan J, 1997, *CO2–a chance for once through heat pump heaters*, CO2 technology in refrigeration, heat pumps and air conditioning systems, IEA Heat Pump Centre, Trondheim, Norway.

[7] Liao S.M., Zhao T.S., Jakobsen A., 2000. A correlation of optimal heat rejection pressure in transcritical carbon dioxide cycles, Applied Thermal Engineering. vol. 20: 831-841.

[8] Sarkar J., Bhattacharyya S., Ram Gopal M., 2004. Optimisation of a trancritical CO_2 heat pump cycle for simultaneous cooling and heating applications, Int. J. of Refrigeration, vol. 27: 830-838.

[9] Chen Y., Gu J., 2005. The optimum high pressure for transcritical refrigeration system with internal heat exchangers. Int. J. of Refrigeration., vol. 28: 1238-1249.

[10] Cecchinato L., Corradi M., Minetto S., 2010, A critical approach to the determination of optimal heat rejection pressure in transcritical systems, Int. J. of Applied thermal Engineering, vol. 30: 1812-1823.

[11] Hihara E., 2003, Country report of Japan, IEA HPP Annex 26 N.38.

[12] Hashimoto K., 2006, Technology and Market Development of CO2 Heat Pump Water Heaters (ECO CUTE) in Japan, IEA Heat Pump Centre Newsletter, Volume 24 No.3/2006, pagg. 12-16.

[13] Taira S., 2007, Trends in next-generation heat exchangers for heat pump systems, IEA Heat Pump Centre Newsletter, Volume 25 No.3/2007, pag. 25-28.

PART 3
ENERGY EFFICIENCY IMPROVEMENTS OF HOUSEHOLD REFRIGERATORS

Since refrigerators and freezers are largely present in houses, the efficiency improvement of these systems represents an appreciable potential for global energy saving.

The subject of energy saving in these systems operation, has been studied by different national and international institutions, industrial companies and research organisations. In recent years industrial manufacturers insisted to produce energy-efficient appliances, but of course further improvements can still be possible.

Typical options to improve the efficiency of household refrigerators can be summarized in four areas: decreasing the cabinet heat load; reducing the energy to defrost; improving the refrigeration cycle efficiency and reducing the cycling losses. There are several literature references and review papers discussing technological innovations and developments of household refrigerators (Radermacher and Kim. (1996))

Since there are several refrigerators models on the market (i.e single-door refrigerators, combi systems, side-by-side combination, under-counter refrigerators, etcetera), in this work there isn't a complete dissertation of this topic, but only a presentation of two specific energy-saving solutions.

In the following chapter it is studied the effect of the cycling frequency on the electric consumptions of domestic refrigerators. The analysis is based on experimental tests on a under-counter prototype.

This work also provides a dynamic simulation model for evaporators to investigate further this topic.

This section ends with the study of a side-by-side refrigerator, which works with a single refrigeration unit, endowed with one evaporator only, but with two separated air-loops which cool the compartments alternatively .

3.1 The effect of cyclic frequency on the energy consumption of household refrigerator

3.1.1 Summary

This chapter analyses the effect of the cycling frequency on the electric consumption of a domestic refrigerator. An experimental study was carried out on a under-counter domestic refrigerator, working with R600a. The effect of several temperature differences between the upper and lower threshold of the thermostat and of the inertia of the system was investigated. The experimental results show a reduction in energy consumption when increasing the frequency of the compressor start-up. A possible way to explain this phenomenon in line with the current state of technical knowledge, is related to the thermal inertia of the metallic mass of the evaporator. This behaviour is amplified at a higher cycling frequency. Another possible explanation, which hasn't yet proposed by scientific literature, is related to the liquid expansion inside the evaporator, which occurs at each compressor start up. This phenomenon can be assimilated to the well known 'batch expansion' process.

3.1.2 Related works

As it is well-known in the technical literature, the cyclical operating of household refrigerator systems entails some phenomena which cause efficiency losses of the thermodynamic cycle. The energy penalization is mainly related to the refrigerant charge migration during compressor off periods. This is due to the use of capillary tubes as throttling devices, which don't prevent the pressure equalization in the refrigeration circuit during pauses.

Some Authors [1-4] experimentally quantify the penalization of this phenomena and they agree on stating that they diminish the energy efficiency. In order to reduce the entity of these penalizations, it's possible to adopt some technical devices such as the use of solenoid valves to intercept the refrigerant during off periods [1,5]. Another possibility is to reduce the compressor on/off cycles, extending the on periods. An opportunity in this sense is to adjust the compressor cooling capacity, but this solution required a variable speed compressor to face the peak loads and to quickly reach the

operative working conditions. Another solution is given by increasing the evaporator thermal inertia, which is achievable by employing phase change materials (PCM). These can be applied on the external surface of the heat exchanger, assuring the thermal contact. In this way, PCM are used as thermal tank.

The aim of this work is to evaluate the effect of the compressor cyclic frequency (CSF) on the energy consumption of an household refrigerator. In the following sections results of an experimental investigation of a single door refrigerator are proposed and discussed. The appliance was tested changing the temperature difference of the threshold set to the thermostatic control (ΔT-TC) and increasing the thermal inertia of the evaporator, using PCM. The electrical consumptions were recorded in a wide range of compressor starting frequency (CSF). This method has some consequence on the evaluation of the energy performance, because several technical papers state that the increase of the thermal inertia of the evaporator reduces the energy consumption [6]. The energy benefit is related to a slower decrease of the evaporating temperature, which allows for more favourable working conditions. That is to say that the cooling power is supplied with a higher average evaporating average temperature, as happen when the heat exchanger has a greater thermal transmittance. It can be stated that during pause periods the heat transfer increases due to the effect of the thermal inertia of the evaporator. This happens because the heat exchanger supplies cooling power even if the compressor is off. According to this effect, the average difference between the refrigerant temperature and the air temperature decreases due to more time available for cooling the compartment and not because of a greater thermal transmittance.

Azzuz *et al.* [6] quantified the potential benefit related to the increase of the evaporator thermal inertia. They present a dynamic model and its validation. They state that the use of PCM leads to increase the COP from 5% to 15%, depending on the thermal load. The energy benefit is relevant mainly at a the low thermal load, while the use of PCM seems to be less advantageous at high thermal load. In their work Azzuz *et al.* found approximately the same energy benefit potential founded by Cerri *et al.* [7]. Through the use of a dynamic model, these authors state that the COP could increase by about 12% even with small PCM quantities.

In a recent work, Wang *et al.* [8] present the dynamic simulation results of a refrigeration system endowed with a thermostatic expansion valve. This study shows

that by applying the thermal inertia before or after the compressor, it is possible to reduce the vapour superheating or the condensation pressure, respectively. If the thermal inertia is applied before the throttling valve, the COP increase of about 8%, due to the higher subcooling.

Figure 3.1.1 Household refrigerator – Re116A Whirlpool

In this work, the additional thermal inertia was applied only to extend the range of the compressor starting frequency.

To reduce the PCM effect on the energy consumption, the eutectic solution has been chosen in order to almost prevent PCM liquefaction. This choice reduces the effect of the thermal inertia on the evaporating temperature and, as a consequence, on the COP.

Experimental results show an increase of the COP when the compressor starting frequency gets higher. This result is at variance with the current opinion and it will be discussed in the following sections.

3.1.3 The experimental equipment

In this work a single-door refrigerator was experimentally investigated. The system was a Re116A Whirlpool model (137 litre net volume) (fig.3.1.1), available on the market. The system layout consists of:

- A reciprocating hermetic compressor, ACC HVY44AA model, R600a, with mineral oil lubricant;
- A wire-on-tube condenser (48 cm^3 internal volume) directly connected to the dryer before the capillary tube
- A capillary tube (3.25 m length and 0.63 mm internal diameter)
- A static evaporator embedded in the back wall of the cabinet. The refrigerant line is 7.5m long, with an internal volume of 214 cm^3.
- A Suction line heat exchanger. The evaporator outlet line ends on a tube with the capillary tube soldered on it.

The nominal refrigerant charge is 22 g of Isobutene (R600a). The thermostatic control of the original appliance is driven by a bulb placed in contact with the evaporator wall.

In this work an electronic thermostatic control was used instead of the traditional appliance control. This choice was made due to the necessity of great stability of the compartment temperature (which was set to +5°C). The instrument used is the Eliwell IC902, with accuracy of 0.5% FS (measurement range -50°C +140°C, resolution 0.1°C). The sensor was positioned according to the UNI/EN/ISO 15502 [9].

Table 3.1.1 reports the physical properties of the PCM material used to fill the inertial packs. These packs are used to increase the evaporator thermal inertia. The main ingredients of the substance are: sodium sulphate, water and additives.

The experimental equipment was instrumented with an acquisition system, in order to determine the energy consumption accurately. Temperature measures of the refrigerant line and of the heat exchangers have been recorded. The temperature sensors was T-type thermocouples (constantan-copper) positioned on the top of tube, assuring a good thermal contact with it.

The accuracy of the acquisition measurement system was estimated of ± 0,36°C. To determine the refrigerant temperature profile in the condenser, six thermocouples have been placed on the heat exchanger inlet and outlet, as well as on intermediate positions, corresponding to 25%, 50%, 75% and 100% of the condenser length.

The compressor temperature was monitored with four thermocouples, which were positioned on the suction, on the discharge line, on the basement and on the top of the compressor shell.

The room and the compartment temperatures have been measured in accordance to the UNI/EN/ISO 15502 [9]. Pressure transducers were placed at compressor inlet and outlet. The accuracy of the transducer is ±0,04% FS. The two sensors have a full scale of 10 barA and 20 barA for the low and high pressure, respectively.

The experimental tests were performed in a climatic room, which is built in accordance to the UNI/EN/ISO 15502 [9].

The electrical parameters such as power consumption, electric currency and supplied voltage, have been record using a power-meter. The measurement chain has an estimated accuracy of ±0,7 W, ±3 mA e ±0,3 V. The measure of power consumption have been carried out in accordance to the UNI/EN 153 [10]. Experimental power consumption data are shown in kWh/d, with an accuracy of ±0,02 kWh/d. Compressor start and stop period have been measured with an accuracy of ±0,013 s.

Table 3.1.1 Physical Data for ClimSel C7

Phase Change Temperature:	7	°C
Maximum temperature:	60	°C
Storage capacity 0-15 deg C	54	$Wh \cdot kg^{-1}$
Latent Heat of Fusion:	39	$Wh \cdot kg^{-1}$
Specific gravity:	1,42	$kg \cdot l^{-1}$
Thermal conductivity:	0,5-0,7	$W \cdot m^{-1} \cdot K^{-1}$
Packs weight	0,2	$kg \cdot pack^{-1}$

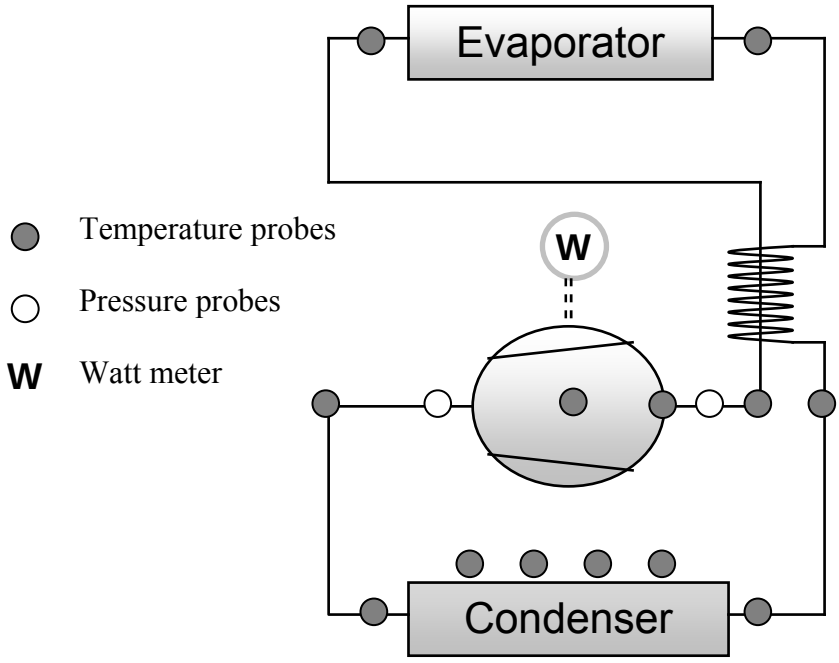

Figure 3.1.2 Refrigeration circuit layout and measurement

3.1.4 The experimental procedure

The refrigerator was studied with a wide range of compressor starting frequencies. To change this parameter, the prototype was tested with different ΔT of threshold set on the thermostatic control. It the evaporator thermal inertia was also modified by applying PCM packs on the back wall of the compartment. The additional thermal inertia was changed from zero to ten PCM packs.

Figures 3.1.3 and 3.1.4 show the appliance in the test configuration with seven packs. The two layouts differ for the position of the packs. The experimental data covers a wide range of compressor cyclic frequencies, from 8 to 50 [cicles·day^{-1}]. The investigated range has a lower limit because the need to contain the amplitude of the compartment temperature variations, while it has an upper limit due to the minimum ΔT threshold settable on the thermostatic control. In this work, the additional thermal inertia was applied with the sole aim of broadening the range of compressor starting frequency. This allows to exceed the limit imposed by the thermostatic control. An eutectic solution has been chosen conveniently, in order to minimize its effect on the energy consumption.

Experimental tests were performed with the temperature of the climatic room set to 25°C (±0,2°C).

The average temperature of the compartment was set at +5°C in accordance to UNI/EN 153 [10]. According to this norm, the compressor must work cyclically, for more than 24h, driven by the thermostatic control. The performance data started to be recorded, every 20s, when the system reached steady-state working conditions, or rather when the temperatures don't differ by more than 0.5°C from the average values.

3.1.5 Tests results

Table 3.1.2 summarises experimental test results. Figures 3.1.5 and 3.1.6 show the energy consumption versus the on-period and the [cicles·day^{-1}], respectively. Experimental results show that in all the test configurations, which differ for the PCM packs number, the reduction of the ΔT threshold always leads to a decrease of the on-time and of the energy consumption.

.

Figure 3.1.3 The prototype with 70% of the total PCM. Two configurations

Figure 3.1.4 The prototype with 70% of the total PCM. Two configurations

In particular, in the configuration with two additional PCM packs, it was recorded a reduction of the energy consumption of about 8.9%, by changing the ΔT threshold from 5°C to 0.8°C

In Figure 3.1.6 the energy consumption is plotted as a function of the on-off frequency. Experimental data demonstrates that the energy consumption decreases univocally when the cyclic frequency increases. On the contrary to the current opinion, it was recorded that an high number of compressor start-ups is not penalizing for the energy efficiency.

The penalization due to the start-up transient is usually attributed to several effects:

- The pressure equalization during pause periods, which leads to the refrigerant charge migration from the condenser to the evaporator, causing an increase of the internal energy of the evaporator system.
- The liquid suction at the following the compressor start. The liquid refrigerant goes into the compressor shell, wasting cooling effect.
- Vapour lamination through the capillary tube at the first steps of the compressor start-up, due to the absence of liquid at the capillary tube inlet.

These phenomena surely decrease the energy efficiency, but there are also other factors which lead to a positive effect.

At the compressor start-up the suction pressure decreases gradually, leading the system to work with the an higher mean then that of a longer run. This effect is shown clearly in figure 3.1.7. This is to say that with high cyclic frequencies the compressor runs on average with lower pressure ratios and with higher evaporating pressure. The COP is consequently higher. So, as discussed in the introduction, the effect is almost the same as that induced by the evaporator thermal inertia.

Another positive factor could be related to the decrease of the exergy losses which take place in the capillary tubes during the expansion process. This is related to the refrigerant liquid inside the evaporator at the compressor start, which expands according to the "batch expansion principle" [11,12].

As shown in figure 3.1.8 In a "batch expansion" refrigeration system, an auxiliary compressor is employed to reduce the pressure of the refrigerant stored inside a closed vessel. The compressor sucks the flash vapour, which is in thermodynamic equilibrium with the liquid, discharging it directly to the condenser.

This process produces some thermodynamic irreversibilities where the expansion take place due to the heat transfer with the receiver wall, but it is almost reversible from the fluid-dynamic point of view. In an isenthalpic expansion, the exergy losses are mainly consequent of the vapour lamination: when the process starts the vapour quality is zero and the isenthalpic transformation is almost equal to an isentropic transformation.

So, it is efficient to remove the flash vapour progressively, in order to avoid these thermodynamic irreversibilities

The "batch expansion" principle was never applied to refrigeration plants. This is probably due to practical issues related increased complexity of this solution. A similar process is realized in a household refrigerator at the compressor start-up. In this case the liquid expands on a small pressure difference with respect to condensing pressure.

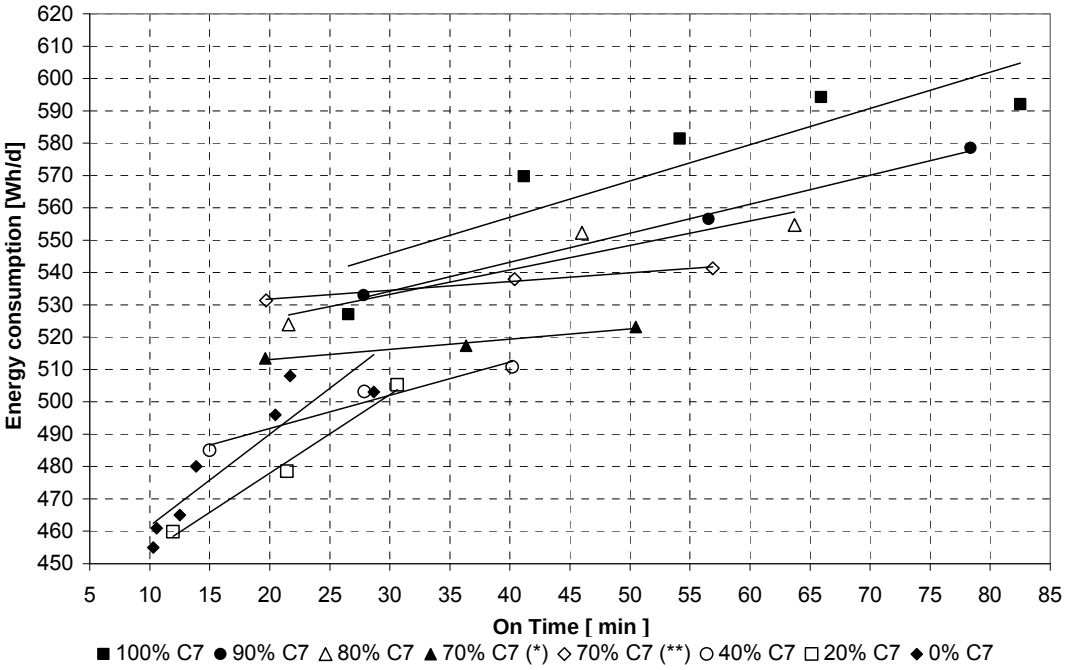

Figure 3.1.5 Energy consumption trends Vs. On time

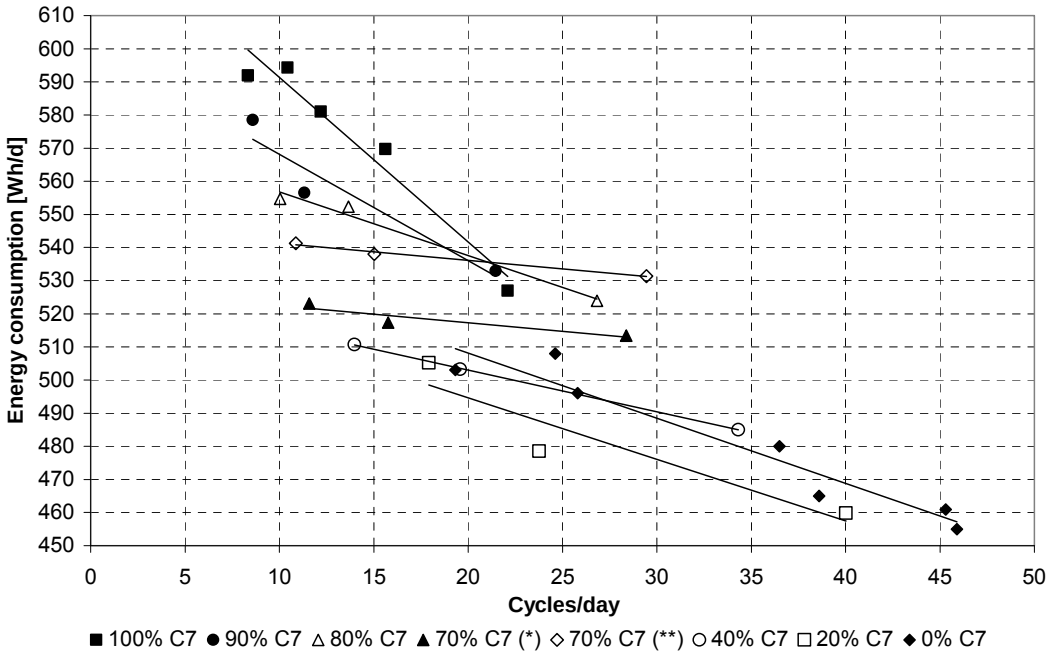

Figure 3.1.6 Energy consumption trends Vs. Cycles/day

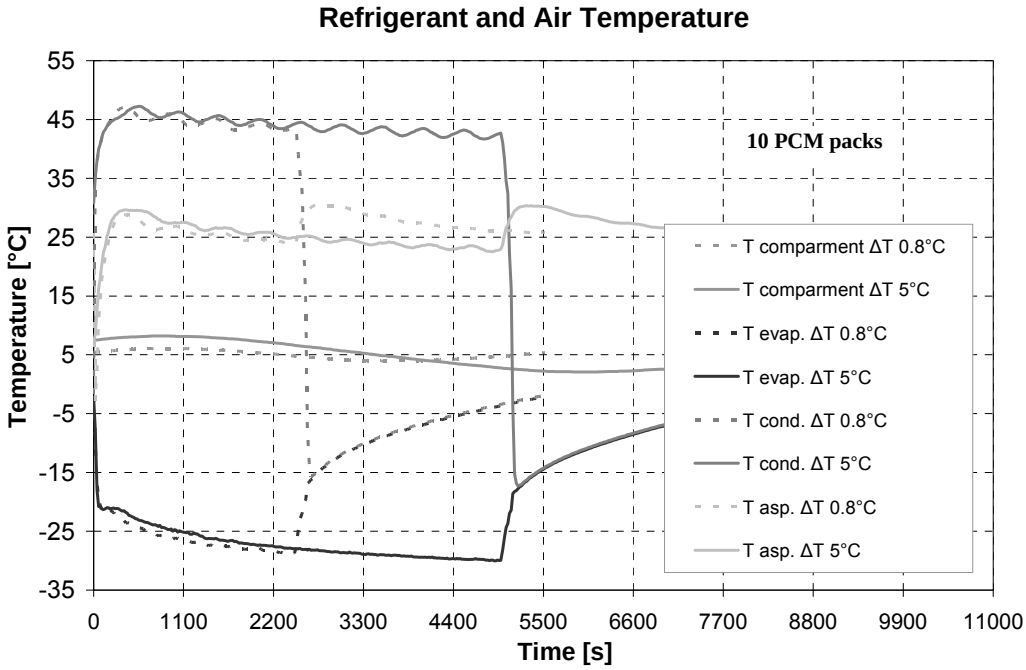

Figure 3.1.7 Prototype tested with ΔT threshold set to 0.8°C and 5°C. The refrigerant temperature

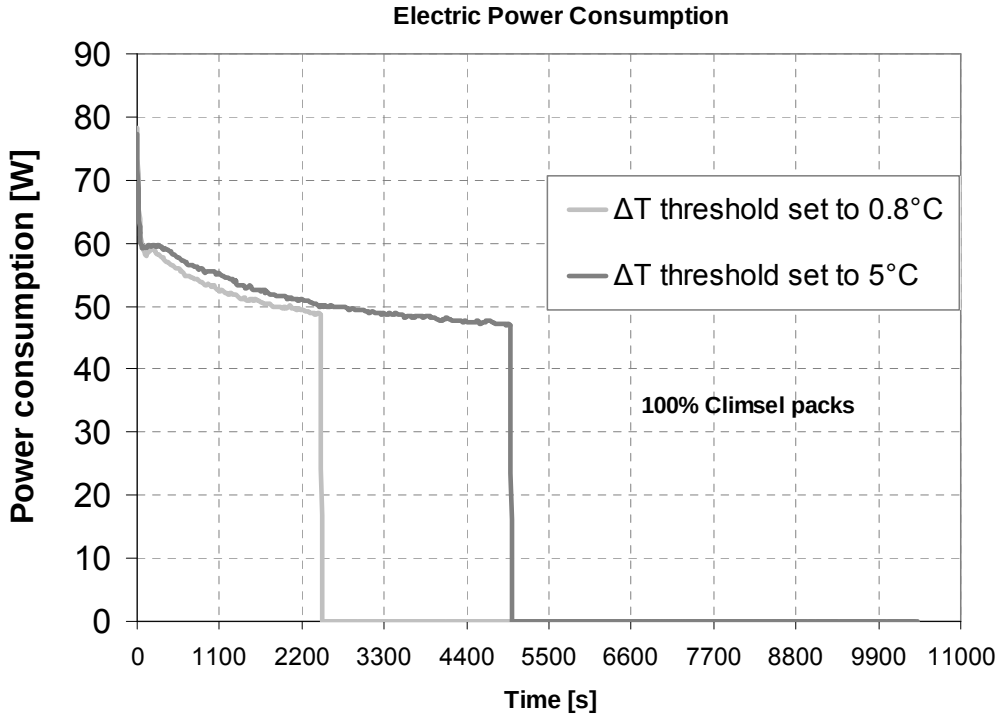

Figure 3.1.8 Prototype tested with ΔT threshold set to 0.8°C and 5°C. The electrical power consumption

Table 3.1.2 Experimental results

DT Termostatic Control [°C]	*On period* [min]	*Off period* [min]	*On frequency* [cycles/d]	*Energy Consumption* [Wh/d]	*Active Power (average)* [W]	*On / (On+Off)* [%]
Tests without additional PCM packs						
0,4	10,3	21,1	45,9	455	57,8	32,8
0,5	10,6	21,2	45,3	461	57,7	33,3
0,8	12,5	24,9	38,6	465	58,0	33,4
1,0	13,9	25,6	36,5	480	56,9	35,2
2,0	20,5	35,2	25,8	496	56,2	36,8
3,0	21,7	36,8	24,6	508	57,1	37,1
4,0	28,6	45,9	19,3	503	54,5	38,5
Tests with 2 additional PCM packs						
0,8	11,9	24,0	40,0	460	57,8	33,2
3,0	21,4	39,2	23,8	478	56,4	35,4
5,0	30,6	39,2	17,9	505	55,2	38,1
Tests with 4 additional PCM packs						
0,8	15,0	27,0	34,3	485	56,6	35,7
3,0	27,9	45,7	19,6	503	55,3	37,9
5,0	40,2	62,8	14,0	511	54,5	39,0
Tests with 7 additional PCM packs (first configuration)						
0,8	19,6	31,1	28,4	513	55,3	38,7
3,0	36,3	55,0	15,8	517	54,2	39,8
5,0	50,5	73,9	11,6	523	53,7	40,6
Tests with 7 additional PCM packs (second configuration)						
0,8	19,7	29,2	29,4	531	55,0	40,3
3,0	40,4	55,4	15,0	538	53,2	42,2
5,0	56,9	75,5	10,9	541	52,5	43,0
Tests with 8 additional PCM packs						
0,8	21,6	32,1	26,8	524	54,3	40,2
3,0	46,0	59,4	13,7	552	52,7	43,7
5,0	63,7	79,8	10,0	555	52,1	44,4
Tests with 9 additional PCM packs						
0,8	27,8	39,3	21,5	533	53,6	41,5
3,0	56,5	70,6	11,3	557	52,2	44,5
5,0	78,4	89,3	8,6	578	51,6	46,7
Tests with 10 additional PCM packs						
0,2	26,5	38,7	22,1	527	54,0	40,7
0,8	41,2	51,0	15,6	570	53,2	44,7
2,0	54,2	63,5	12,2	581	52,6	46,0
3,0	65,9	72,1	10,4	594	51,8	47,8
5,0	82,5	90,3	8,3	592	51,7	47,7

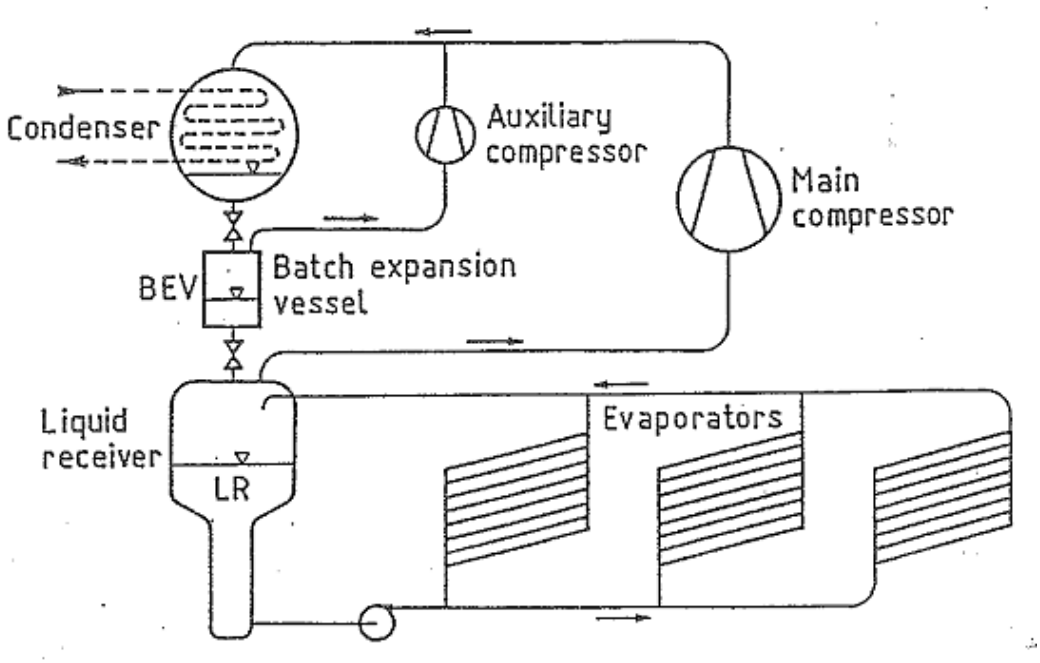

Figure 3.1.8 The plant layout of a "Batch expansion" refrigeration system

The effect of the additional thermal inertia on the energy consumption was not univocal. Figure 3.1.5 and 3.1.6 show that, at constant values of the compressor cyclic frequency, the minimum energy consumption was achieved with 2 additional PCM packs. With 4 packs, the effect of the additional thermal inertia is almost null. This results could be related to two opposed factors.

A negative effect due to less expansion and a positive effect due to high average evaporating temperature. This phenomenon could be further investigated by testing the system trying to find the optimal quantity of additional thermal inertia and its correct position. In the test configurations indeed, the PCM packs are applied on the internal wall of the refrigerator, thermally linked to the evaporator, but this layout increases the thermal resistance of the heat exchanger. A more efficient solution could be achieved adding the thermal mass between the evaporator and the insulation layer.

3.1.6 Conclusions

Experimental results demonstrate that the compressor cyclic on/off frequency of a household refrigerator has a significant influence on energy consumption. Contrary to

the current opinion, this investigation shows that energy-savings can be achieved at high frequency.
This result was explained with the presence of two concurrent factors:

- The average evaporating temperature rises due to the system thermal inertia and to frequent start-up transients periods;
- The exergy losses of the liquid expansion inside the evaporator decreases, due to the almost isentropic "batch expansion" instead of the isenthalpic lamination.

This investigation seeks to take into account the possibility of optimizing the compressor cyclic frequency, achieving energy efficiency improvements without increasing costs. Obviously the maximal increasing of the start frequency is limited by the compressor integrity and by considerations of the length of its cycle life.

3.1.7 References

[1] W.H. Coulter, C.W. Bullard, An Experimental analysis of cycling losses in domestic refrigerator-freezers, ASHRAE transactions vol. 103, n 1, pp 587-596, 1997.

[2] P.E. Krause, C.W. Bullard, Cycling and quasi-steady behaviour of a refrigerator, ASHRAE Transaction vol 102, n 1 pp 1061-1070, 1996.

[3] P.J. Rubas, C.W. Bullard, Factors contributing to refrigerator cycling losses, Int. J. Refrigeration, vol.18, n 3, pp 168-176, 1995.

[4] E. Bjőrk, B. Palm, Refrigerant mass charge distribution in a domestic refrigerator, Part I: Transient conditions, Applied Thermal Engineering, vol 26, pp 876-871, 2006.

[5] J. Wang, Y. Wu, Start up and shut-down operation in a reciprocating compressor refrigeration system with capillary tubes, Int. J. Refrigeration, vol 13 n 3, pp 187-190, 1989.

[6] K. Azzouz, D. Leducq, D. Gobin, Performance enhancement of household refrigerator by addition of latent heat storage, Int. J. Refrigeration, 2007. In press: available on line.

[7] G. Cerri, A. Palmieri, E. Monticelli, D. Pezzoli, Identification of domestic

refrigerator models including cool storage, Proc. 20th International Congress of Refrigeration, Washington D.C. 2003.

[8] F.Wang, G. Maidment, J. Missendem, R. Tozen, The novel use of change materials in refrigeration plant. Part 3: PCM for control and energy savings. Applied Thermal Engineering vol 27, pp 2902-2910, 2007

[9] UNI/EN/ISO 15502, 2006. Apparecchi di refrigerazione per uso domestico – caratteristiche e metodi di prova.

[10] EN 153, 2006. Metodi di misurazione del consumo di energia elettrica e delle caratteristiche associate dei frigoriferi, conservatori e congelatori di utilizzo domestico e loro combinazioni.

[11] E.Fornasieri, L.Mattarolo, Theoretical analysis of batch expansion process, Proc. 17th Int. Congress of Refrigeration, vol. b, pp. 825-832, Wien, 1987.

[12] G. Eric, U. Granryd. Method of improving refrigerant capacity and coefficient of performance in a refrigerating system, and a refrigerating system for carrying out said method. US_Pat 4014182, 1977

[13] R. Radermacher and K. Kim. Domestic refrigerators: recent developments, Int. J Refrig Vol.19 pp 61-69 1996

[14] Energy Efficiency in Household Refrigerators Freezers and Commercial refrigerating Equipment (1991) International Institute of refrigeration.

3.2. Simulation of Household refrigerators

3.2.1 Introduction

The energy efficiency of vapour compression refrigeration systems is closely related to thermodynamic states of the refrigerant at the different components. Forecast of the dynamic behaviour of the heat exchangers is the key issue to face refrigeration units advanced simulations. An essential consideration before getting into of development of vapor compression models is the intended use for the model. Dynamic models that capture slow dynamics are useful for analyzing issues of energy use and thermo-hygrometric conditions of the cooled compartment. From this perspective, the refrigerant circuit dynamics are virtually instantaneous, and refrigerant mass and energy accumulations can be negletable. Indeed, the bulk of the modelling task lies in modelling the refrigerated compartment, and not the refrigeration unit. On the contrary, the dynamic models that capture the fast dynamics are generally used to design and evaluate system control strategies (e.g. superheat regulation, pressure regulation, etc.). In this case, the conditions of the chilled compartment are generally viewed as static or steady-state.

Several methods of dynamic modelling heat exchangers are present in literature (Bendapoudy 2002, [1]) The research interest is on the development of models that are mathematically simple but without losing relevant detail. The modelling approach should be sufficiently accurate to capture the essential dynamic behavior, while remaining simple enough to provide insight into the dynamics and adequately tractable to be useful as a control design tool.

The largest task in modelling a refrigeration system is, usually, the modeling of the heat exchangers [1]. In terms of approaches, the most important differences are in the ways in which the refrigerant in the heat exchanger is treated. The heat exchangers models can be generally classified into three groups: discretized models, lumped parameter models, and moving boundary models.

The discretized volumes or finite difference approach results in models that are very accurate. These models are appropriate mainly for dynamic simulations and not for developing control algorithm. The appeal of this approach is the ability to predict the refrigerant behavior in a detailed manner. With these approaches, each heat exchanger is

divided into a number of fixed and equal-sized control volumes. The conservation equations are discretized and solved over the volumes and result in a system of ordinary differential equations.

A lumped parameter approach results in less complex sets of equations but it is not accurate in the superheat detection. It very often ignores important dynamics due to the complex heat exchanger behaviour associated with the moving boundary between the two-phase zone and the single-phase flow regions. For these reasons the use of this models is not reccomended in advance controls development.

Therefore, a lumped parameter model with a moving interface boundary is seen as the solution to capturing these important dynamics, while preserving the simplicity of lumped parameter models. Central to the modelling approach is the ability to predict the effective position of phase change in a heat exchanger. The moving boundary approach seeks to capture the dynamics of multiple fluid phase heat exchangers while preserving the simplicity of lumped parameter models.

It is quite important to get the tradeoffs between the finite-volume and moving-boundary model formulations. The moving-boundary model should require significantly less computation than the finite-volume approach because it utilizes fewer control volumes. However, this approach utilizes lumped characteristics for each of the control volumes, as a mean void fraction for the two-phase zone, which could lead to lower accuracy.

3.2.2 Modelling domestic refrigeration units

There are several literature references in dynamic modelling household refrigerator systems. Murphy and Goldschmidt (1984, 1985) [2] [3] developed a simplified system models to study start-up and shutdown transients for an air-to-air system. The start-up model handles the dynamics of the capillary tube and the phenomenon of liquid backing up into the condenser. The compressor was modelled from steady-state measurements and test data were used in place of an evaporator model. The refrigerant pressure and the tube material dynamics in the condenser were modelled. In the shutdown study, both the heat exchangers were modelled as tanks containing two-phase refrigerant at different initial pressures, naturally convected by air on the outside.

Ploug-Sorensen *et al.* [4] (1997) constructed a model of a domestic refrigerator, using the software package SINDA/ FLUINT which is used extensively in the aerospace industry. The analysis made is based on ine-dimentional fluid-dynamic equations for mass, momentum and energy and a carefull treatment of the heat-transfer mechanisms from fluid-to-wall an wall-to-ambient. The proposed model is in good agreement with experiments on an on/off compressor controlled domestic refrigerator for the pressures as well as the cabinet temperature.

S. Porkhial, *et al.*[5,6] (2004) (2005) presented distributed parameter models for the prediction of the transient performance of round bound evaporator and finned-coiled condenser. The heat exchangers are applied in a 12 ft^3 refrigerator with R12 as working fluid. The models are capable of predicting the refrigerant temperature distribution, tube wall temperature, quality of refrigerant, inventory mass of refrigerant as a function of position and time. An efficient two-level iteration method is proposed by the Authors to obtain the numerical solution of the models without solving a large set of non-linear equations simultaneously. Results indicate that the theoretical models provides a reasonable prediction of dynamic response compared with the experimental data.. The same authors (2002) [7] presented the dynamic model of a reciprocating compressor which was compared to experimental data.

Hermes *et al.* [8,9] (2008) (2009) presented a dynamic model of a household refrigerator based on the first-principles. The model was employed to simulate a typical frost-free 440-l top-mount refrigerator, in which the compressor is on–off controlled by the freezer temperature, while a thermo-mechanical damper is used to set the fresh-food compartment temperature. The authors presents the modeling approaches for each of the refrigerator components: heat exchangers, non-adiabatic capillary tube, reciprocating compressor, and refrigerated compartments. Numerical predictions were compared to experimental data showing a reasonable level of agreement for the whole range of operating conditions, including the start-up and cycling regimes.

One year later Borges *et al.* [10] (2010) presents a simulation model for the cycling behaviour of household refrigerators and, therefore, for predicting their energy consumption. The modelling methodology follows a quasi-steady approach, where the refrigeration system and also the refrigerated compartments are modelled following steady-state and transient approaches, respectively. The model is based on the set of

equations derived from the mass, energy and momentum conservation, whereas experimental data was collected and used to reduce the model closing parameters such as the thermal conductances and capacities. The experiments were carried out using a controlled temperature and humidity environmental chamber. The model predictions were compared to experimental data, when it was found that the energy consumption is well predicted by the model with a maximum deviation of ± 2%.

3.2.3 Models to predict the capillary tubes performance

The capillary tube is the most used expansion device in household refrigeration systems. Numerical simulation of the whole refrigeration unit have today a great diffusion due to numerical models for the capillary tubes performance prediction.

Zhang and Ding [11] (2003) presented an Approximate analytic solutions of adiabatic capillary tubes. The authors showed that the correlation is in good agreement with the experimental data in open literature.

Yang *et al.*[12] (2004) presented a generalized correlation for predicting the refrigerant mass flow rate through the adiabatic capillary tube. The correlation was developed with approximate analytic solutions based on the extensive data for several refrigerants, in which a homogeneous equilibrium model for two-phase flow is employed, and there is a subcooled liquid or saturated two-phase mixture at the inlet of the capillary tubes. The correlation shows an average deviation of ±0.83% and a standard deviation of 9% from the database.

Recently, Hermes *et al.*[13] (2010) presents a modelled of a capillary tube suction line heat exchanger with the same level of accuracy as found with more sophisticated first-principles models. The methodology treats the refrigerant flow and the heat transfer as independent phenomena, thus allowing the derivation of explicit algebraic expressions for the refrigerant mass flow rate and the heat exchanger effectiveness. Comparisons between the model predictions and the experimental data revealed that more than 90% and nearly 100% of all data can be predicted within ±10% and ±15% error bands, respectively.

3.2.4. A mass conservative evaporator model adopting the moving-boundary method

This section presents a generalised evaporator model based on the moving-boundary approach. The heat exchanger model is based on a numerical scheme which can switch between the dry-expansion and the fully-flooded model representations.

Temporal integration is applied to core variables leading the mean void fraction within the two phase-zone to be time-variant. The use of this kind of variables improves the model accuracy and speed with respect to boundary variables when the compressor start-up is simulated. This features makes the model suitable to face simulation of household refrigerators.

The switching algorithms introduce *pseudo-state* equations in order to track the un-active variables and ensure reasonable initial conditions when rezoning, keeping the robustness whenever superheated region appears or disappears.

Numerical results show that the model's mathematical basis are consistent with integral forms of energy and continuity equations. This work presents a qualitative case study showing that the model transient behaviour can well predict a finned coil evaporator performance.

3.2.4.1 .Related works

The energy consumption of refrigeration and air conditioning installations contributes to CO_2 emissions and reduces global energy resources. Efforts implemented by refrigeration stakeholders focus on the reduction of energy consumption thanks to increasing energy efficiency of vapour compression cycles.

This can be accomplished by designing advanced refrigeration equipment control systems (Beghi and Cecchinato, [14 ,15]).

It is generally agreed that, in spite of the advancements made in computer technology and its impact on the development of new control methodologies for Heating, Ventilation, and Air Conditioning and refrigeration systems (HVAC&R), the process of operating HVAC&R equipment in dwellings and in commercial and industrial buildings is still a low efficient and high-energy consumption process (Yaqub and Zubair, [16] 2001).

Nomenclature

A flow area [m^2]

L length [m]

d Tube diameter [m]

F Surface efficiency

h enthalpy [kJ kg^{-1}]

$\dot{m}$ mass flow rate [kg s^{-1}]

NTU Number of transport unit

p pressure [Pa]

x quality [-]

s thickness [m]

t time [s]

T temperature [°C]

X states vector

Y solution vector

z spatial coordinate [m]

c_p specific heat [J kg^{-1} K^{-1}]

U global transmittance [W m^{-2} K^{-1}]

Greek letters

α Heat transfer coefficient [W m^{-2} K^{-1}]

γ void fraction [-]

$\bar{\gamma}$ void fraction mean [-]

η fin efficiency [-]

ρ density [kg m^{-3}]

Ω fin efficiency [-]

φ Air relative humidity [-]

Subscripts

a air	o outlet
e evaporator	g vapour
i inlet	w wall
int interface	1 TP zone
l liquid	2 V zone

Classical control techniques such as ON/OFF controllers (thermostats) and proportional-integral-derivative (PID) controllers are still very popular, due to their low cost and ease of tuning and operation (Astrom and Hagglund [17], 1995;). However, more advanced control systems that are able to efficiently track the actual cooling/heating power requests from the plant, such as predictive or adaptive controllers, are best suited to meet the challenge of reducing the overall energy consumption for building heating and cooling. Dynamic modelling is an efficient and useful approach to the control oriented design of HVAC&R equipment and of vapour compressor machines in particular. This approach can be valuable for hardware-in-the-loop/software-in-the-loop simulation and embedded control and diagnostic applications (Rasmussen *et al.*[18], 2005).

Bendapudi and Braun [1] (2002) pointed out that two different modelling schemes are commonly adopted for vapour compression cycles dynamic simulation: finite-volume/difference distributed parameter and moving-boundary lumped parameter schemes. Bendapudi *et al.*[19] (2008) presented a study of a centrifugal chiller system. The authors compared a finite-volume and moving boundary flooded shell-and-tube heat exchanger model in the analysis of the unit start-up and load-change transients. Bendapudi *et al.* [19] (2008) found that the moving-boundary system model executed about three times faster than the finite-volume while maintaining nearly identical accuracy in the predictions of system steady-state and transient-performance. This confirmed what already stated by Grald and MacArthur [20] (1992). The velocity of the moving-boundary method makes it the most suitable simulation technique for control oriented applications and studies (He *et al.*[21], 1998; Jensen and Tummescheit [22], 2002; Lei and Zaheeruddin [23], 2005; Cheng and Asada [24], 2006; Rasmussen [25], 2006, Qi and Deng [26], 2008; Schurt *et al.* [27], 2009).

Different authors developed heat exchanger or vapour compression cycle simulation models adopting the moving-boundary method (Dhar and Soedel [28], 1979; Grald and MacArthur [20], 1992; He at el. [21], 1995; Willatzen *et al.* [29], 1998; Jensen and Tummescheit [22], 2002; Zhang and Zhang [30], 2006; Rasmussen [25], 2006; McKinley and Alleyne [31], 2008; Bendapudi *et al.* [19], 2008; Kumar *et al.* [32], 2008; Li and Alleyne [33], 2010). This approach consists in dividing the heat exchanger into control volumes (or zones), each volume corresponds to a refrigerant phase and model parameters are lumped for each of these volumes. The length of each zone, thus the boundary position between refrigerant phase, is dynamically determined and its correctness is mandatory to actually predict refrigerant mass, pressure and heat transfer. One of the main drawbacks of this technique is that, being constant the number of zones, if the length of a zone tends to zero, the corresponding set of mass and energy conservation equations becomes singular. This is the case of a unit start-up and shut-down operations both for the evaporator and the condenser. In order to avoid simulation fails, some authors (Dhar and Soedel [28], 1979; Willatzen *et al.* [29], 1998; Zhang and Zhang [30], 2006, McKinley and Alleyne [31], 2008, Bendapudi *et al.* [19], 2008; Li and Alleyne [33], 2010) adopted multiple modelling frameworks in the same simulation, introducing switching criteria between the models. Dhar and Soedel [28]

(1979) adopted three model representations or modes for condenser and one for the evaporator to correctly simulate evaporator start-ups. The proposed model switching approach potentially introduces discontinuities and numerical instability. Willatzen *et al.* [29] (1998) developed an evaporator model introducing auxiliary equations (Pettit *et al.* [34], 1998) to ensure that state derivatives remained relatively smooth during large transients resulting in destruction or creation of dynamic states. These equations ensure that the model structure remain unchanged, in fact when a state becomes redundant it is still integrated as a *pseudo-state* tracking an active state. Zhang and Zhang [30] (2006) showed that Willatzen *et al.* [29] (1998) model main weakness is associated to the constant time-invariant mean void fraction hypothesis. Zhang and Zhang [30] (2006) introduced an evaporator model characterized by a time-dependent mean void fraction in the two-phase region showing an improved robustness and smoother state parameters curves during large transients with respect to Pettit *et al.* [34] (1998) model. Bendapudi *et al.* [19] (2008) adopted three models for condenser and two for the evaporator for the simulation of load-change transients in centrifugal chillers. The proposed model switching approach is based on the initialisation of newly created dynamic states, the authors claim that smooth transitions are ensured without introducing large energy imbalances at the transition. McKinley and Alleyne [31] (2008) presented a two modes condenser model based on the switching approach adopting a different model structure with the two-phase mean void fraction in the system state vector and introducing a novel switching criteria based on void fraction. *Pseudo-state* variables were introduced to accommodate the transient dynamic states and the authors demonstrated the consistency of results with integral forms of the mass and energy conservation equations through several test cases. The authors also addressed accuracy concerns of previous models by including finned surfaces, nonlinear air temperature distributions, and non-circular passages. Li and Alleyne [33] (2010) extended McKinley and Alleyne [31] (2008) condenser model to five modes and developed a switched evaporator model with two modes. The authors also presented an experimental validation of the model considering two case studies.

In this section a new switched modelling approach is proposed; the model is specially oriented to the simulation of household vapour compression units with capillary tube as the throttling device and low charge amount, such as household

refrigerators and heat pump dryers. An evaporator model is developed accommodating two modes in a constant structure, the main difference between this model and the previous works is in the choice of the state variables and of the switching criteria. Rasmussen and Alleyne [35] (2004) underlined that the redundant nature of thermodynamic properties result in the possibility of expanding mass and energy equations with freedom in choosing the state variables. The authors also found that for model reduction purposes the best state representation of an heat exchanger is one containing a pure integrator associated with the accumulation of refrigerant mass. In the published approaches for the evaporator (Pettit *et al.* [34], 1998; Zhang and Zhang [30], 2006, Bendapudi *et al.* [19], 2008; Li and Alleyne [33], 2010), two different groups of state variables were adopted. In their two-phase and superheated two-zone representations Pettit et al [34]. (1998), Zhang and Zhang [30] (2006) and Bendapudi *et al.*[18] (2008) selected two-phase zone length, refrigerant pressure and evaporator outlet enthalpy as state variables. Instead, Li and Alleyne [33] (2010) adopted two-phase zone length, refrigerant pressure, superheated zone enthalpy and mean void fraction, adding an auxiliary equation for this last variable. Both the choices are not intrinsically mass conservative, this could be critical when simulating low mean void fraction start-ups; in fact for low evaporator outlet quality the approximation error associated to the expansion of the two-phase zone mass and energy conservation equations is acceptable only within limited variations of the state variables given the strong dependence of void fraction from quality. This would reduce considerably the minimum acceptable integration step size. The present approach introduces evaporator mean density as a state variable together with refrigerant pressure and superheated zone density, thus intrinsically ensuring refrigerant mass conservation during mode switching and low mean void fraction evaporator start-up. *Pseudo-state* variables are introduced following Pettit *et al.* [34] (2008) and Li and Alleyne [33] (2010) suggestions and suitable switching schemes are applied; this approach also ensures refrigerant energy conservation.

In Section 3.2.4.2 the modelling approach is described and the governing equations are reported. In Section 3.2.4.3 switching criteria are discussed and the solution procedure is outlined. In Section 3.2.4.4, model integrity and stability check results are reported. Different choices of state variables are compared considering a low mean void

fraction evaporator start-up. The proposed moving boundary model results are validated against Beghi and Cecchinato [14] (2009) finite-volume dynamic simulation model in Section 3.2.4.4.3. Concluding remarks are given in Section 3.2.4.5. In Appendix, more information on the derivation of the governing equations for the refrigerant and definition of the evaporator outlet enthalpy is provided.

3.2.4.2 .Modelling approach

The mathematical representation of the proposed evaporator model is represented in Figure 3.2.1. Air mass flow rate and inlet temperature and specific humidity together with refrigerant inlet enthalpy and inlet and outlet mass flow rate are considered as time dependent boundary conditions. The heat exchanger is divided into two zones or control volumes (see Figure 3.2.2a) each corresponding to a different state of the refrigerant. For the evaporator the two-phase and superheated states are considered and the time dependent interface position between the volumes is tracked by the model – hence the *moving bondary method*. As discussed by Rasmussen and Alleyne [35] (2004) a conceptually simple and straightforward way to derive the problem state equations is using the unsteady-state equations for conservation of mass and energy, assuming control volumes associated with each region of refrigerant and wall.

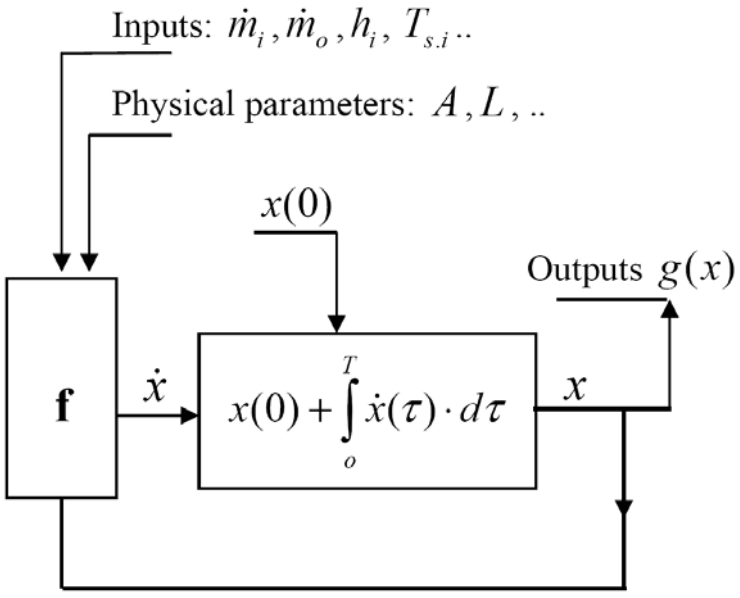

Figure 3.2.1 Mathematical solution procedure

The resulting equations can be expanded into the desired form with freedom in choosing the state variables given the redundant nature of thermodynamic properties.
As will be discussed in Section 3.2.4.4.2, the choice of the states is arbitrary but each solution leads to important consequences in the switching criteria and in the integrity conservation of the model. Here refrigerant pressure, p, average evaporator density, ρ_e, and superheated zone density, ρ_2, together with two-phase, T_{w1}, and superheated zone, T_{w2}, wall temperatures are selected. Thus at each time step the evaporator conditions can be represented by the following state vector:

$$x = \left[p,\ \rho_e,\ \rho_2,\ T_{w1},\ T_{w2} \right] \tag{1}$$

The time derivative of the state vector is a function (f) of the state vector (x), the model boundary conditions and different physical parameters as represented in fig. 3.2.1. Physical parameters occur to determinate the performance of the heat exchanger and they are constant inputs of the mathematical model. The state vector must be initialized to a known value, $x(0)$, to allow the problem integration. Model outputs can be obtained through a function (g) of the state vector.

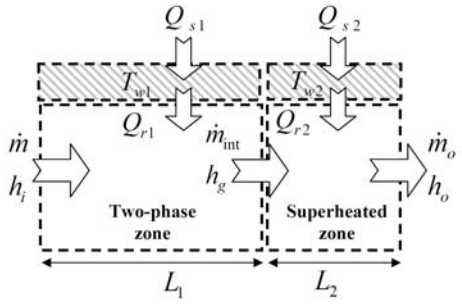

Figure 3.2.2 (a) Two zones scheme

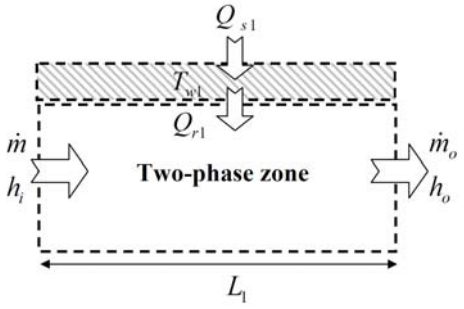

Figure 3.2.2 (b) One zone scheme

The following simplifying assumption must be made to reduce the complexity of conservation equations:

•the fluid flow is one-dimensional;

•there is no axial thermal heat conduction in the fluid flow;

•there is no axial thermal heat conduction in the structure;

•refrigerant pressure drop is negligible;

•the internal energy of the structure can be adequately represented using a constant specific heat and a single temperature value for the structure for each of the zones;

•the air flow is quasi-steady and incompressible;

•the air entering the heat exchanger has uniform temperature, pressure and velocity;

In the following sections the governing equations for an evaporator handling refrigerant and moist air are proposed. The evaporator is fed with two-phase refrigerant (or with saturated liquid in the case of flooded systems), according to these operative conditions the proposed model may have two regions (the two-phase region and the superheated one) or a single-zone representation with only the two-phase zone. According to Zhang and Zhang [30] (2006) the first representation is called TP-V model and the second one TP model. The simulation is switched is switched between the two models according to the existence of the superheated region. In case of no refrigerant superheating, the superheated zone implodes and one of the states variables is tracked to a suitable value adopting a *pseudo-state* equation as suggested by Pettit *et al.* [34] (2008) and Li and Alleyne [33] (2010).

3.2.4.2.1 Governing equations: refrigerant (TP-V model)

Here the state equations for the refrigerant in the two-zone model (TP-V) are reported in their final form, details about their derivation process can be found in Appendix. For the two-phase zone, the mass and energy equations can be written as follows:

$$\begin{aligned} &AL_1\left[\frac{\partial\rho_g}{\partial p}\overline{\gamma}+\frac{\partial\rho_l}{\partial p}\left(1-\overline{\gamma}\right)+\left(\rho_g-\rho_l\right)\left.\frac{\partial\overline{\gamma}}{\partial p}\right|_{h_i}\right]\frac{dp}{dt}+A\left(\rho_g-\rho_l\right)\left(\overline{\gamma}-1\right)\frac{dL_1}{dt}=\ldots \\ &=\dot{m}_i-\dot{m}_{\text{int}}-AL_1\left(\rho_g-\rho_l\right)\left.\frac{\partial\overline{\gamma}}{\partial h_i}\right|_p\frac{dh_i}{dt} \end{aligned} \tag{2}$$

$$AL_1\left[\frac{\partial\rho_g h_g}{\partial p}\overline{\gamma}+\frac{\partial\rho_l h_l}{\partial p}\left(1-\overline{\gamma}\right)+\left(\rho_g h_g-\rho_l h_l\right)\left.\frac{\partial\overline{\gamma}}{\partial p}\right|_{h_i}-1\right]\frac{dp}{dt}+A\left(\rho_g h_g-\rho_l h_l\right)\cdot\ldots$$
$$\ldots\cdot\left(\overline{\gamma}-1\right)\frac{dL_1}{dt}+\dot{m}_{\text{int}}h_g=\dot{m}_i h_i-AL_1\left(\rho_g h_g-\rho_l h_l\right)\left.\frac{\partial\overline{\gamma}}{\partial h_i}\right|_p\frac{dh_i}{dt}+\dot{Q}_{r1} \tag{3}$$

where the two-phase zone length is calculated from the actual value of the state variables, p, ρ_e and ρ_2, through the following equation:

$$L_1=L\frac{\rho_e-\rho_2}{\left[\rho_g\overline{\gamma}+\rho_l\left(1-\overline{\gamma}\right)\right]-\rho_2}, \tag{4}$$

and the mean void fraction of the two-phase zone is given by:

$$\overline{\gamma}=\frac{1}{x_o-x_i}\int_{x_i}^{1}\gamma(p,x)\cdot dx, \tag{5}$$

Beck and Wedekind *et al.* [36] (1981) assumed the existence of a generalized similarity relationship which implies the time invariance of the mean void fraction for constant inlet and outlet qualities. Considering constant two-phase zone inlet enthalpy and outlet quality equal to unity, this would imply that mean void fraction pressure partial derivative is negligible. Rasmussen [25] (2006) neglects the time derivative of the mean void fraction because the change in mean void fraction tends to be small during transients and because its time dependence is related to dynamic modes that are much faster than the dominant system dynamics. In their two-phase and superheated two-zone model, Li and Alleyne [33] (2008) introduce a sort of *pseudo-state* equation (Eq. (45)) defining the time derivative of the mean void fraction as a function of mean void fraction pressure partial derivative. This equation would not be necessary since in the two-zone representation the mean void fraction at each time step can be calculated given the refrigerant pressure value, being known the inlet enthalpy and outlet quality. Its time derivative present in Li and Alleyne [33] (2010) Eqs. (43) and (44) could also be differentiated over pressure (and eventually inlet enthalpy) at each time step and

calculated depending on the actual values of the state variables. These authors were forced to introduce the mean void fraction time derivative auxiliary Eq. (45) for switching purposes (McKinley and Alleyne [31] (2008)); in fact in their model mean void fraction is a state variable. In proposed model the pressure partial derivative term was included in Eqs. (2) and (3) even though it could be omitted if negligible. In fact, this would not cause any trouble to the model switching procedure since mean void fraction is not integrated.

For the superheated zone, the mass and energy conservation equations can be written as:

$$AL_2 \frac{d\rho_2}{dt} + A\left(\rho_g - \rho_2\right)\frac{dL_1}{dt} - \dot{m}_{\text{int}} = -\dot{m}_o \,, \tag{6}$$

$$\begin{aligned} &AL_2\left(\rho_2 \left.\frac{\partial h_2}{\partial p}\right|_{\rho_2} - 1\right)\frac{dp}{dt} + AL_2\left(\rho_2 \left.\frac{\partial h_2}{\partial \rho_2}\right|_{p} + h_2\right)\frac{d\rho_2}{dt} + A\left(\rho_g h_g - \rho_2 h_2\right)\frac{dL_1}{dt} = \ldots \\ &\ldots = \dot{m}_{\text{int}} h_g - \dot{m}_o h_o + \dot{Q}_{r2} \end{aligned} \tag{7}$$

where the superheated zone enthalpy, h_2, is determined from pressure, p, and superheated zone density, ρ_2, and the evaporator outlet refrigerant enthalpy, h_o, is calculated assuming a linear distribution of the enthalpy in the superheated zone:

$$h_o = 2h_2 - h_g \,. \tag{8}$$

Solving the algebraic system of Eqs. (2), (3), (6) and (7), the interface mass flow rate, $\dot{m}_{\text{int}}$, and the time derivatives of the state variables p and ρ_2 together with the time derivative of the two-phase zone length, L_1, can be obtained. The derivative of the evaporator average density, ρ_e, can be finally calculated from these values differentiating Eq. (4) or in a straightforward way from the following:

$$\frac{d\rho_e}{dt} = \frac{\dot{m}_i - \dot{m}_o}{AL} \,. \tag{9}$$

3.2.4.2.2 Governing equations: refrigerant (TP model)

If the refrigerant evaporation is not sufficient for complete phase change, the superheated zone disappears and the TP model is used instead of the TP-V model. The two-phase zone refrigerant mass and energy state Eqs. (2) and (3) become:

$$\frac{d\rho_e}{dt} = \frac{1}{AL}\left(m_i - m_o\right) \tag{10}$$

$$AL\left[\left(\rho_g\overline{\gamma} + \rho_l\left(1-\overline{\gamma}\right)\right)\frac{\partial h_1}{\partial p}\bigg|_{\rho_e} - 1\right]\frac{dp}{d\tau} + AL\left[\left(\rho_g\overline{\gamma} + \rho_l\left(1-\overline{\gamma}\right)\right)\frac{\partial h_1}{\partial \rho_1}\bigg|_{p} + h_1\right]\frac{d\rho_e}{d\tau} = \tag{11}$$
$$\ldots = m_i h_i - m_o h_o + \dot{Q}_{r1}$$

where the two-phase zone enthalpy, h_1, is defined by the equation:

$$h_1 = \frac{\rho_g h_g \overline{\gamma} + \rho_l h_l \left(1-\overline{\gamma}\right)}{\rho_e}. \tag{12}$$

As better detailed in Appendix, at each simulation time step, the two-phase zone outlet enthalpy, h_o, and density, ρ_o, are obtained algebraically considering the mean void fraction value calculated from the state variables:

$$\overline{\gamma} = \frac{\rho_e - \rho_l}{\rho_g - \rho_l}. \tag{13}$$

Since the superheated zone is inactive, Eqs. (6) and (7) are replaced with a *pseudo-state* equation (14) that makes the superheated zone refrigerant density tracking the outlet vapour density:

$$\frac{d\rho_2}{d\tau} = K(\rho_o - \rho_2). \tag{14}$$

3.2.4.2.3 Governing equations: wall structure

According with the assumption made, heat transfer to the wall structure occurs through refrigerant and air convection as well as conduction along fins. In the two-zone representation, the energy state equation for the average wall temperature of each zone can be written as:

$$\frac{dT_{w1}}{d\tau} = \frac{-\dot{Q}_{r1} + \dot{Q}_{s1}}{m_{w1} c_w} + \frac{T_{w2} - T_{w1}}{L} \frac{dL_1}{d\tau}, \tag{15}$$

$$\frac{dT_{w2}}{d\tau} = \frac{-Q_{r2} + \dot{Q}_{s2}}{m_{w2} c_w} + \frac{T_{w2} - T_{w1}}{L} \frac{dL_1}{d\tau}. \tag{16}$$

The second terms in the right-hand side of Eqs. (15) and (16) represent energy transport associated to zone interface movement or wall rezoning. These equations were derived according to the model proposed by Zhang and Zhang [30] (2006) assuming a weighted mean approximation for the interface wall temperature between the two zones. These authors underlined the critical aspects of the other two approximations reported in the open literature in order to obtain reasonable trends of the superheated zone wall temperature, $T_{w,2}$, and robust switching between the TP and TP-V models. In particular Grald and MacArthur [20] (1992), He at al.[21] (1995) and Willatzen *et al.*[29] (1998) regarded the interface as part of the two phase zone while McKinley and Alleyne [31] (2008) and Li and Alleyne [33] (2010) adopted a sort of *upwind* approximation basing the value of the interface temperature on the sign of the two-zone length derivative.

For a one zone representation, the superheated zone is inactive. In this case the interface velocity, $dL_1/d\tau$, term on the right-hand side of Eq. (15) disappears. Further, a *pseudo*-state equation replaces Eq. (16) causing the inactive superheated zone wall temperature to track the two-phase zone wall temperature:

$$\frac{dT_{w2}}{d\tau} = K_3 (T_{w1} - T_{w2}) \tag{17}$$

This equation should guarantee a smooth transition and provide a reasonable initial condition when the model switches from TP to TP-V.

The wall-to-refrigerant heat transfer rate for each zone is computed with the following expression:

$$\dot{Q}_{rj} = U_{rj} A_{wr} \frac{L_j}{L} (T_{wj} - T_{rj}) \tag{18}$$

where the overall heat transfer coefficient is calculated taking into account wall and fins thermal resistances and uniform refrigerant-side heat transfer coefficient along the heat exchanger with the equation:

$$U_{rj} = \left\{ \frac{s_w}{\lambda_w \left(1 - F_{fin-r}\right)} + \frac{1}{\alpha_{rj} \left[1 - F_{fin-r} \left(1 - \eta_{fr}\right)\right]} \right\}^{-1} . \tag{19}$$

3.2.4.2.4 Governing equations: air side

As previously stated in the modelling assumption, the air entering the heat exchanger has uniform temperature, pressure and velocity. The air flow is assumed to be incompressible and unmixed. The air thermal inertia is negligible if compared to structure and the refrigerant ones, and it was neglected. The air temperature profile can be derived analytically from the equations of one-dimensional steady state flow. Considering unmixed flow and uniform air-side heat transfer coefficient along the evaporator, the air temperature difference from the inlet to the outlet is obtained applying *P*-NTU solution (Shah and Sekulić [37] (2003)) obtaining the following expression:

$$T_{sj,o} = T_{wj} + \left(T_{sj,i} - T_{wj}\right) e^{\text{-NTU}} , \tag{20}$$

where

$$NTU = \frac{\alpha_s A_{ws} \left[1 - F_{fin-s} \left(1 - \eta_{fs}\right)\right]}{\dot{m}_s c_s} . \tag{21}$$

The heat transfer rate from the air to the wall structure for each zone is calculated with:

$$\dot{Q}_{sj} = \dot{m}_s c_s \frac{L_j}{L}\left(T_{sj,i} - T_{sj,o}\right), \tag{22}$$

In presence of mass transfer phenomena on the fin surface, assuming the humid air enthalpy as the driving potential for total heat transfer (for the lower value of the potential, the enthalpy is that of the saturated air at the temperature of the cold surface, $h_{sat,w}$), Eqs. (21) and (22) are replaced with the following:

$$h_{sj,o} = h_{sat,wj} + \left(h_{sj,i} - h_{sat,wj}\right)e^{-NTU}, \tag{23}$$

$$\dot{Q}_{sj} = \dot{m}_s \frac{L_j}{L}\left(h_{sj,i} - h_{sj,o}\right), \tag{24}$$

and the outlet air specific humidity is calculated as:

$$x_{sj,o} = x_{sj,i} - \left(h_{sj,i} - h_{sj,o}\right)\frac{x_{sj,i} - x_{sat,wj}}{h_{sj,i} - h_{sat,wj}} \tag{25}$$

3.2.4.3 Solution procedure

The solution flow-chart is plotted in fig.3.2.3. Switching between the one zone and two zone models is clearly pointed out. As suggested by Pettit *et al.* [34] (2008) and Li and Alleyne [33] (2010), *pseudo-state* Eqs. (14) and (17) have been introduced since this allows to switch between the one and two zone representations sharing the same vector of states (Eq. (1)). In particular, a switch from two to one zone representation is triggered by the following conditions:

$$\begin{cases} \rho_2 \geq \rho_g \\ L_2 \leq 0 \end{cases} \tag{26}$$

where L_2 is calculated from (4). This condition can be thus described "The superheated zone density is higher than the vapour density and the superheated zone length is negative". In the same condition Li and Alleyne [33] (2010) adopted as switching criteria two equations based on a minimum positive length of the superheated zone and on the sign of its derivative (Eqs. (50) and (51) in Li and Alleyne [33] (2010)). With the proposed state equations formulation any condition on the time derivative of the superheated zone density sign was introduced since matrix singularities were not observed during simulations as it will be detailed in section 3.2.4.4. Switching from one to two-zone representation occurs when:

$$\begin{cases} \rho_2 < \rho_g \\ L_2 > 0 \end{cases} \tag{27}$$

Considering condition (27) on the superheated zone density, *pseudo-state* equation (14) appears well fitted since it tracks the superheated zone density to the outlet density. In fact the switching occurs when the calculated refrigerant outlet enthalpy, h_o, is higher then the saturated vapour enthalpy, h_g, and consequently Eq. (14) tracks the superheated zone density to a value lower than the saturated vapour density one. This switching technique implies that, for a limited amount of time, the one zone representation is adopted when the value of the states ρ_e and p would imply the presence of superheated vapour. This time amount can be negligible if a suitable constant K is chosen in equation (28).

McKinley and Alleyne [31] (2008) underlined the importance of a suitable definition of the switching criteria for assuring mass conservation. Considering the refrigerant associated state variables, and in particular the presence of a pure integrator, ρ_e, associated with the accumulation of refrigerant mass, the definition of the switching criteria doesn't influences mass conservation in the proposed model.

The solution flow-chart shown in Fig. 3 was implemented in Matlab/Simulink but it can be implemented (McKinley and Alleyne [31], 2008) in any software package or language which is capable of solving linear equation sets and ordinary differential equations. The state independent intensive thermodynamic properties are pressure and

density for the superheated zone and pressure for the two-phase zone (pressure and density for the one zone TP model). Thermophysical properties and their partial derivatives are calculated at each time step in dependence of state variables actual values. All required thermophysical properties are evaluated by spline interpolation of REFPROP 7.0 data (Lemmon *et al.* [38], 2002). Phenomenological correlations are applied for the determination of heat transfer coefficients and void fraction. Zivi [39] (1964) model is employed in this work to take into account the non-homogeneous flows of the liquid and vapour in the two-phase evaporating flow region. A slip ratio void fraction model was preferred to mass flux dependent models because of its simplicity and possibility of obtaining the analytic correlation of the mean value over the two-phase region as it is discussed in Appendix. For the superheated zone Gnielinski [40] (1976) correlation is used assuming as mass flow rate the outlet mass flow rate. The average heat transfer coefficient in the two-phase zone is obtained integrating over quality Gungor and Winterton [41] (1987) correlation. Dry-out phenomena are accounted for with Mori *et al.* [42] (2000) dry-out quality correlation. The inlet mass flow rate is assumed as mass flow rate of the two-phase zone. The air-side heat transfer coefficients are as in Wang *et al.* [43] (2000). Fin efficiencies are determined from classical fin theory equations (Incropera *et al.* [44], 2007). In presence of mass transfer phenomena on the fin surface, the air mass transfer coefficient is calculated in the hypothesis of unitary Lewis number and Kuehn *et al.* [45] (1998) theory is adopted to calculate the fin efficiency.

Eqs. (2), (3), (6), (7) and (9) form a set of five linear equation ($Ay = b$) for the two zone representation where the vector is:

$$y = \left[\frac{dp}{dt},\ \frac{d\rho_e}{dt},\ \frac{d\rho_2}{dt},\ \frac{dL_1}{dt},\ \dot{m}_{\text{int}} \right] \tag{28}$$

It is worth noticing that with the proposed set of state variables as the value of the superheated zone density, ρ_2, approaches the saturated vapour density value, the system matrix, A, doesn't become singular contrarily to Li and Alleyne [33] (2010) model. In fact the calculated superheat zone length, obtained from Eq. (4), is by definition greater than zero. This why in (25) and (26) the switching occurs when the

difference between the superheated zone density and the equilibrium density equals zero and not a minimum threshold difference. The vector y includes the derivative of three states and of the interface velocity rate allowing the solution of (15) and (16) for the determination of the wall structure temperature time derivatives. Thus, all state derivatives are defined and the solution can be integrated over time.

Now considering the one zone representation, Eqs. (10) and (11) form a set of two linear equation ($Ay = b$) where the vector is:

$$y = \left[\frac{dp}{dt}, \frac{d\rho_e}{dt} \right] \tag{29}$$

his vector includes the derivative of two states. *Pseudo*-state Eq. (14) sets the third refrigerant state derivative. Eq. (15) and *pseudo*-state Eq. (17) are finally solved for the determination of the wall structure temperature time derivatives considering null the interface velocity, $dL_1/d\tau$, term on Eq. (15) right hand side. Therefore, all state derivatives are defined and the solution can be integrated over time.

3.2.4.4. Model checks

3.2.4.4.1. Model integrity check

The integrity is the consistency of the computer simulation and the governing equations. The model error is non-zero for several reasons:

- Integration errors;
- Linearity assumption, second order terms are usually neglected;
- Discretization of the partial differential correlation with finite differences.
- Round-off.

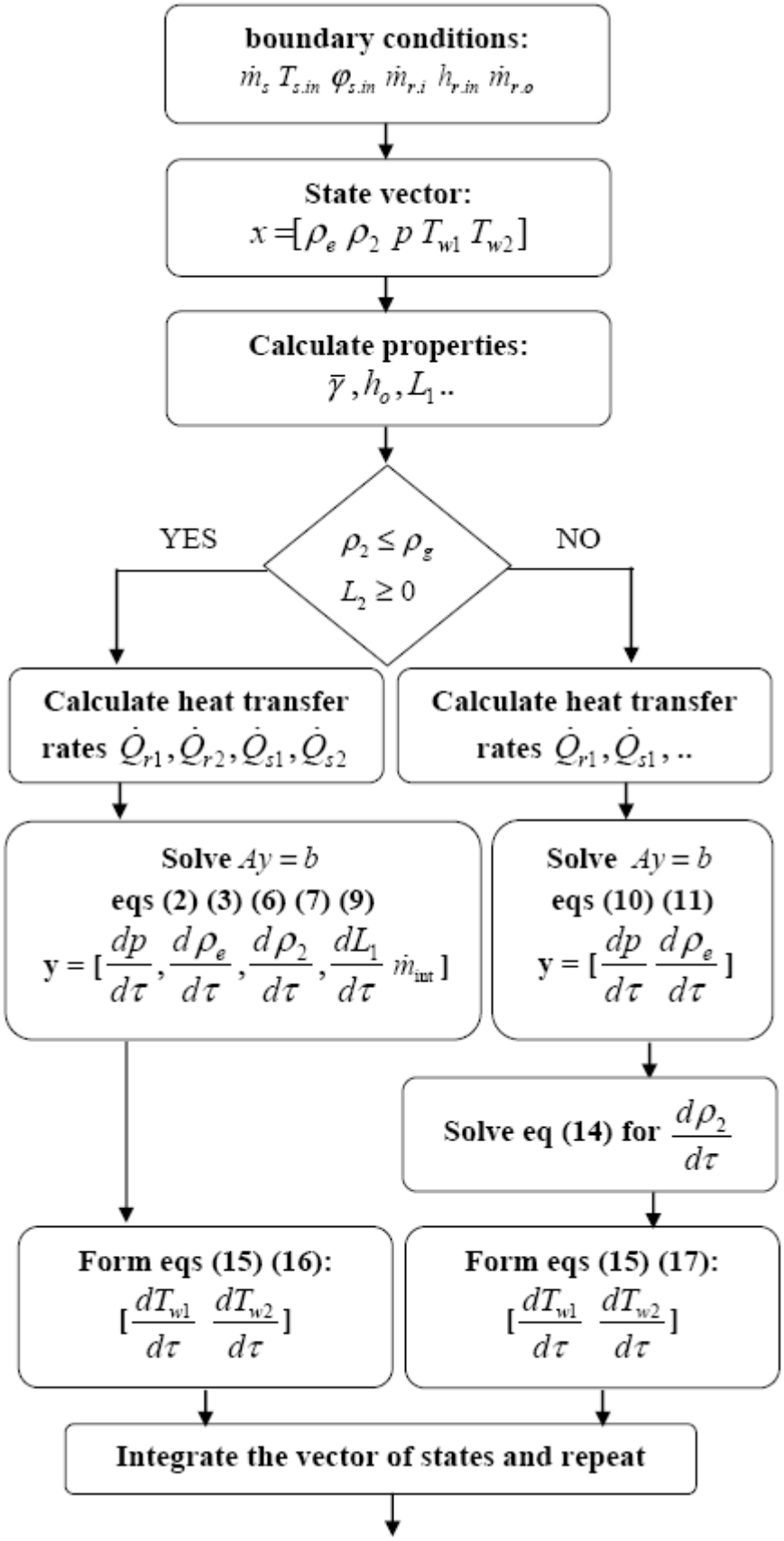

Figure 3.2.3 Solution procedure flow chart

The model integrity was checked looking at the consistency of the simulation results with the integral forms of the continuity and energy equation. Several test cases are presented in the following.

Table 3.2.1 Model integrity check

	Test case 1	**Test case 2**	**Test case 3**	**test case 4**	**Test case 5**	**Test case 6**	**Test case 7**	**Test case 8**
Number of zones	Two	Two	Two	Two	One	One	One	One
Waveform								
Air mass flow rate	Costant	Square	Costant	Costant	Costant	Square	Costant	Costant
Inlet air temperature	Square	Costant	Costant	Costant	Square	Costant	Costant	Costant
Outlet ref mass flow rate	Costant	Costant	square	Costant	Costant	Costant	square	Costant
Inlet ref enthalpy	Costant	Costant	Costant	Sawtooth	Costant	Costant	Costant	Sawtooth
Refrigerant mass (kg)								
Initial condition	0.4	0.4	0.4	0.4	2.96	2.96	2.96	2.96
Amplitude model	0	0	-0.17	0	0	0	-0.17	0
Amplitude integral	0	0	-0.17	0	0	0	-0.17	0
Relative amplitude (%)	0	0	-43.21	0	0	0	-5.91	0
Relative Error (%)	0.0E+00	0.0E+00	-6.2E-14	0.0E+00	0.0E+00	0.0E+00	2.0E-14	0.0E+00
Ref. Int energy (kJ)								
Initial condition	107.6	107.6	107.6	107.6	673.2	673.2	673.2	673.2
Amplitude model	10.1	-4.9	-43.1	13.1	26.2	-23.8	-39.6	66.0
Amplitude integral	10.1	-4.9	-43.1	13.1	26.2	-23.8	-39.6	66.0
Relative amplitude (%)	9.36	-4.53	-40.05	12.13	3.89	-3.54	-5.89	9.81
Relative Error (%)	-1.9E-03	2.8E-03	-5.7E-03	-2.2E-03	-2.0E-04	7.0E-06	9.0E-05	1.7E-03
Wall Int. Energy (kJ)								
Initial condition	512.0	512.0	512.0	512.0	519.4	519.4	519.4	519.4
Amplitude model	29.2	-8.3	6.4	3.2	10.2	-9.5	-1.0	20.9
Amplitude integral	29.2	-8.3	6.4	3.2	10.2	-9.5	-1.0	20.9
Relative amplitude (%)	5.71	-1.62	1.25	0.62	1.96	-1.83	-0.19	4.01
Relative Error (%)	6.2E-05	2.0E-04	-9.1E-03	-1.0E-03	-1.1E-12	1.3E-13	-9.9E-14	1.9E-13
Wall+Ref. Int. Energy (kJ)								
Initial condition	619.7	619.7	619.7	619.7	1192.6	1192.6	1192.6	1192.6
Amplitude model	39.3	-13.2	-36.7	16.2	36.4	-33.3	-40.6	86.9
Amplitude integral	39.3	-13.2	-36.7	16.2	36.4	-33.3	-40.6	86.9
Relative amplitude (%)	6.34	-2.13	-5.93	2.62	3.05	-2.79	-3.41	7.28
Relative Error (%)	-2.7E-04	6.5E-04	-8.5E-03	-1.2E-03	-1.2E-04	3.9E-06	5.1E-05	9.5E-04

The model was excited with different waveforms, comparing the mass and internal energy of the model to the values calculated with the integral forms. Analytic

development the integrity check method is presented in Appendix. Table 3.2.1 summarize tests results, which includes both TP and TP-V model simulations. Peak-to-peak amplitudes and errors were expressed as percentage of the initial values. Recorded errors were always less then 0.0085% .

3.2.2.4.2. State variable choice

Rasmussen and Alleyne [35] (2004) underlined that the redundant nature of thermodynamic properties results in the possibility of expanding mass and energy equation with freedom in choosing the state variables. The complete derivation for the gas cooler for three different choices of refrigerant state variables was presented, namely 1) pressure and outlet enthalpy, 2) pressure and mass, 3) zone enthalpy and mass. The second and the third state representations are intrinsically mass conservative since they contain a pure integrator associated with the accumulation of refrigerant mass. The authors also found that for model reduction purposes these are the best choices. In this paper model the second state representation was adopted and fitted to the multiple modelling framework considering evaporator pressure, p, and mean density, ρ_e, as the refrigerant state variables together with average density, ρ_2, for the superheated zone characterization. A fully (mass and energy) conservative derivation is also possible if refrigerant pressure is replaced with the evaporator internal energy, u, in Eq. (1). In this case the two-phase zone length can not be determined straightforwardly by Eq. (4) and algebraic manipulation is required.

In the published approaches for the evaporator, two different groups of state variables were adopted, namely 1) pressure, outlet enthalpy and two-phase zone length (Pettit *et al.* [3]; 1998, Zhang and Zhang [30], 2006; Bendapudi *et al.* [19], 2008) and 2) pressure, mean void fraction and superheated zone enthalpy and two-phase zone length (Li and Alleyne [33], 2010). As discussed in Section 3.2.4.2.2, Li and Alleyne [33] (2010) added an auxiliary equation determining mean void fraction time derivative. The resulting mass and energy state equation for one-zone model for the these two approaches are reported in Appendix. Both the approaches are not intrinsically mass and energy conservative if the approximation errors associated to the expansion of the governing equations are considered. This could be critical when simulating evaporators

start-up from low mean void fraction considering the strong dependence of void fraction from quality. This would force to considerably reduce the minimum acceptable integration time step size. Besides this consideration a proper choice should be done for the simulation of particular conditions, such as the evaporator dynamic behaviour with very low void fraction mean ($\overline{\gamma}$). This is a typical working condition of refrigeration systems such as domestic refrigerators which require pressure equalization before compressor start up. During off periods most of the refrigerant charge flows to the evaporator, resulting in a very low mean void fraction at compressor start-up.

Here a comparison between this model and the cited models is reported considering initial condition characterized by a very low mean void fraction (0.21), compressor start-up and no inlet mass flow rate. Table 3.2.3 summarises the considered system geometry. In the solution system $Ay = b$, the b vector was set to a fixed value b = [-0.25 ; -51500].

Figures 3.2.4 and 3.2.5 shows the mass and energy conservation errors (normalized to the mass and energy fluxes) after a single simulation time step as a function of the simulation time step length ranging from 0.01 to 10 s. In the Figure, the paper model is referred as "p-ρ_e", model 1) as "p-h_o" while model 2) as "p-γ". As it can be pointed out, for all the models considered, conservation errors correctly tend to zero as the time step approaches zero. Clearly the mass conservation error for "p-ρ_e" is zero being the model intrinsically mass conservative. However "p-γ" model shows good performance, the mass conservation error ranging from 2.36 10^{-7} to 0.228% for 0.01 and 10 s respectively. Instead model "p-h_o" appears strongly affected by expansion errors as the simulation time steps increases, the mass conservation error ranging from 4.39 10^{-5} to 12.1% for 0.01 and 10 s respectively.

Simulations of 20 s period were carried out for four different constant integration time steps (0.01-0.1-1-10 s) considering both Zivi [38] (1964) and the homogeneous void fraction models. Table 3.2.2 summarises the results at the end of the simulation in terms of mass and energy conservation errors (normalized to the initial values), pressure, mean void fraction and outlet enthalpy.

Table 3.2.2 Start up simulation results. Models comparison

Step-size	State variables / Void fraction model	p - ρe	p - γ Zivi	p - ho	p - ρe	p - γ homogeneous	p - ho
0.01	Mass integrity error [%]	-3.15E-12	-1.06E-03	5.95E-02	-3.15E-12	-1.06E-03	2.77E-01
	Energy integrity error [%]	6.27E-03	4.47E-04	5.88E-02	6.27E-03	4.47E-04	2.70E-01
	Gamma_mean	0.7154	0.7154	0.7149	0.7154	0.7154	0.7129
	Pressure [Bar]	5.53	5.52	5.52	5.53	5.52	5.53
	Outlet entalpy [kJ kg-1]	276.07	276.03	275.82	222.57	222.54	222.22
0.1	Mass integrity error [%]	-1.61E-13	-1.02E-02	3.46E-01	-1.61E-13	-1.02E-02	5.48E-01
	Energy integrity error [%]	1.84E-02	3.85E-03	3.44E-01	1.84E-02	3.85E-03	5.41E-01
	Gamma_mean	0.7154	0.7155	0.7123	0.7154	0.7155	0.7105
	Pressure [Bar]	5.53	5.53	5.54	5.53	5.53	5.54
	Outlet entalpy [kJ kg-1]	276.18	276.17	274.98	222.67	222.64	221.98
1	Mass integrity error [%]	1.15E-14	-9.71E-02	3.09E+00	1.15E-14	-9.71E-02	4.61E+00
	Energy integrity error [%]	1.32E-01	3.58E-02	3.08E+00	1.32E-01	3.58E-02	4.55E+00
	Gamma_mean	0.7153	0.7161	0.6878	0.7153	0.7161	0.6743
	Pressure [Bar]	5.61	5.61	5.65	5.61	5.61	5.69
	Outlet entalpy [kJ kg-1]	276.92	277.43	267.54	223.63	223.63	218.69
10	Mass integrity error [%]	0.00E+00	-6.40E-01	2.58E+01	0.00E+00	-6.40E-01	4.63E+01
	Energy integrity error [%]	8.35E-01	2.24E-01	2.54E+01	8.35E-01	2.24E-01	4.51E+01
	Gamma_mean	0.7143	0.7201	0.4836	0.7143	0.7201	0.2989
	Pressure [Bar]	6.09	6.09	6.17	6.09	6.09	6.21
	Outlet entalpy [kJ kg-1]	283.13	285.46	229.92	229.02	229.99	203.57

In Figure 3.2.6 dew-point temperature and outlet quality trend for 1 s time step and Zivi (1964) model are plotted. From Table 3.2.2 results it can be again pointed out that the paper model "p-ρ_e" and "p-γ" model show similar performance while "p-h_o" model appears strongly affected by expansion errors as the simulation time steps increases. Adopting Zivi (1964) void fraction model , the "p-γ" model mass conservation error ranges from -1.06 10^{-3} to -0.640%, while "p-h_o" from -5.95 10^{-2} to 25.8% for 0.01 and 10 s time step respectively.

It can be concluded that models adopting state variables positioned on the evaporator geometrical boundaries seem critical from the mass and energy conservation point of view. Intrinsically conservative models or representations adopting averaged core state variables (such as the "p-γ" with the mean void fraction) appears the best suited for simulating very low mean void fraction conditions at compressor start-up.

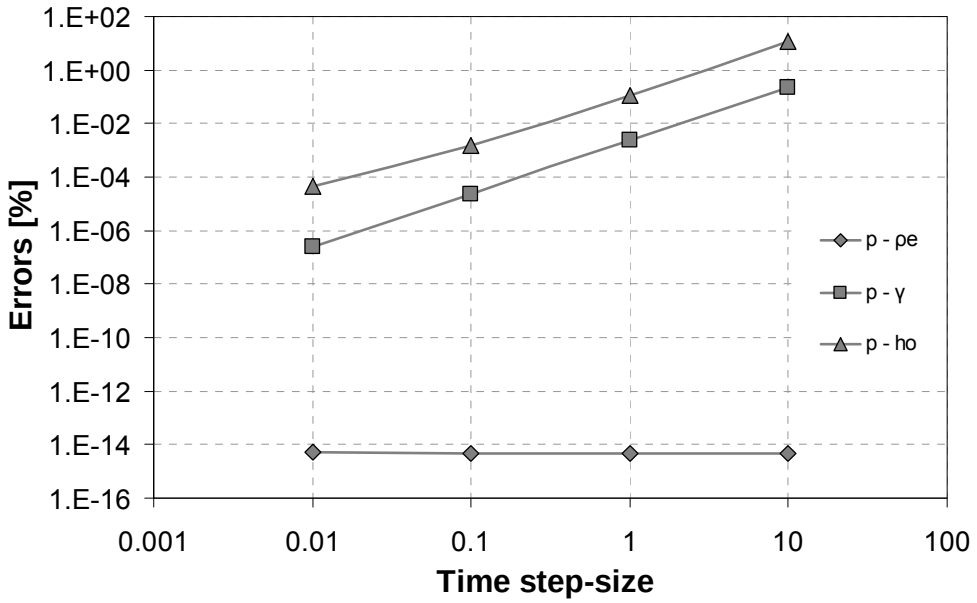

Figure 3.2.4 Mass errors vs step-size simulation

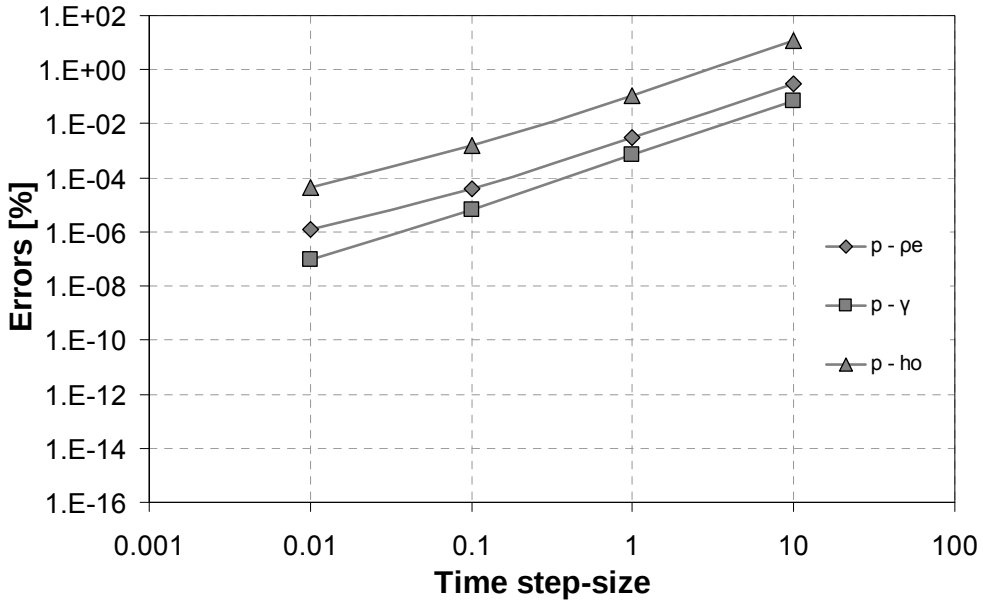

Figure 3.2.5 Internal energy errors vs step-size simulation

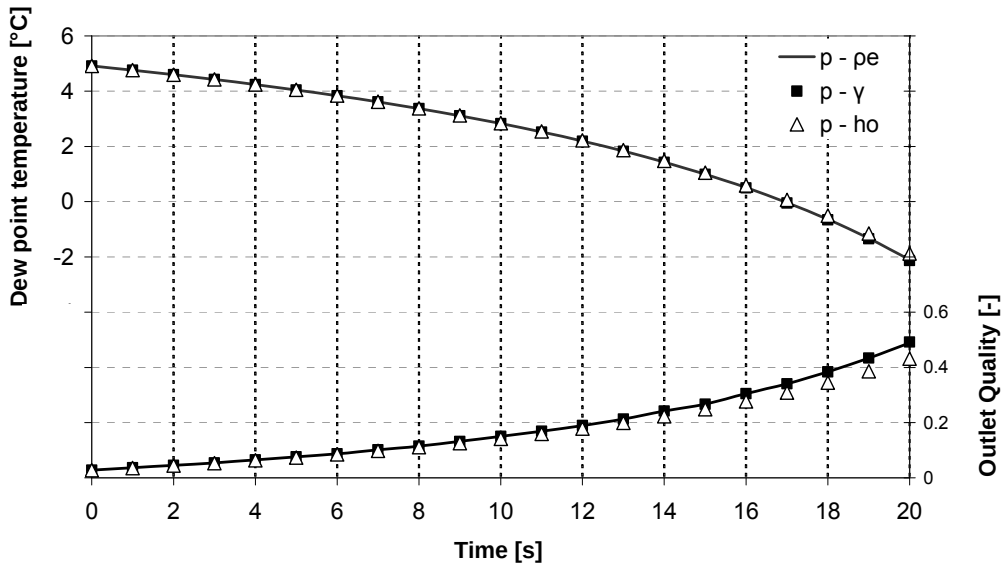

Figure 3.2.6 Dew point temperature and outlet quality trends in start-up simulations

2.4.4.3. Model stability check

The numerical stability of the model was checked with a test case simulation, holding constants the air and refrigerant inlet conditions and varying the refrigerant outlet mass flow rate with a sinusoidal shape trend. Thus leads to force repeated switching between representation schemes. Table 3.2.3 summarises the physical parameters, initial and boundary conditions for the test case. As is it possible to see from fig. 3.2.7, the model simulation presents stiff transitions and smooth shaped outputs. Figure 3.2.9 reports integrity errors of the mass and of the refrigerant and wall internal energy. After a thousand seconds of simulation, the errors results less than 0.13%. This results confirms the model integrity under repeated switching between schemes.

3.2.4.4.3. Model validation

The moving boundary model was compared to one-dimensional finite volume evaporator model, which was developed and presented by Beghi and Cecchinato [14] (2009).

Table 3.2.3 Stability check simulations. Conditions and Parameters

Flow arrangement			Counter-flow		
Boundary conditions					
Air			*Refrigerant*		
Inlet flow rate	[$m^3 \cdot s^{-1}$]	0.22	Inlet mass flow rate	[$kg \cdot s^{-1}$]	0.0372
Inlet temperature	[°C]	7	Inlet enthalpy	[$kJ \cdot kg^{-1}$]	210
Inlet pressure	[Pa]	10^5	Outlet mass flow rate	[$kg \cdot s^{-1}$]	$\dot{m}_i + 0.03\sin(\frac{2\pi}{0.03}\tau)$
Relative humidity	[%]	78.9			
Starting conditions			**Physical parameters**		
Total Refrigerant mass	[kg]	0.48	Wall specific heat	[$J \cdot kg^{-1} \cdot K^{-1}$]	390
Wall temperature two-phase zone	[°C]	-6.5	Wall thermal conductivity	[$J \cdot m^{-1} \cdot K^{-1}$]	380
Wall temperature single phase zone	[°C]	-1.5	Wall density	[$kg \cdot m^{-3}$]	8900
Pressure	[bar]	4.35			
Geometrical parameters			**Correlations**		
			Air		
Tubes length	[mm]	2.16	Air-side heat transfer coefficient	Wang *et al.* (2000)	
Tubes pitch	[mm]	27.5	Fin efficiencies	(Incropera *et al.*2007)	
Row pitch	[mm]	27.5			
Number of rows	[-]	6	*Refrigerant*		
Tubes each row	[-]	3	Single-phase heat transfer coefficient	Gnielinski (1976)	
Fin pitch	[mm]	7	Two-phase heat transfer coefficient	Gungor-Winterton (1987)	
Internal diameter	[mm]	16	Void fraction correlation	Zivi (1964)	
Total surface Area	[m^2]	7.72	dry-out quality correlation	Mori (2000)	

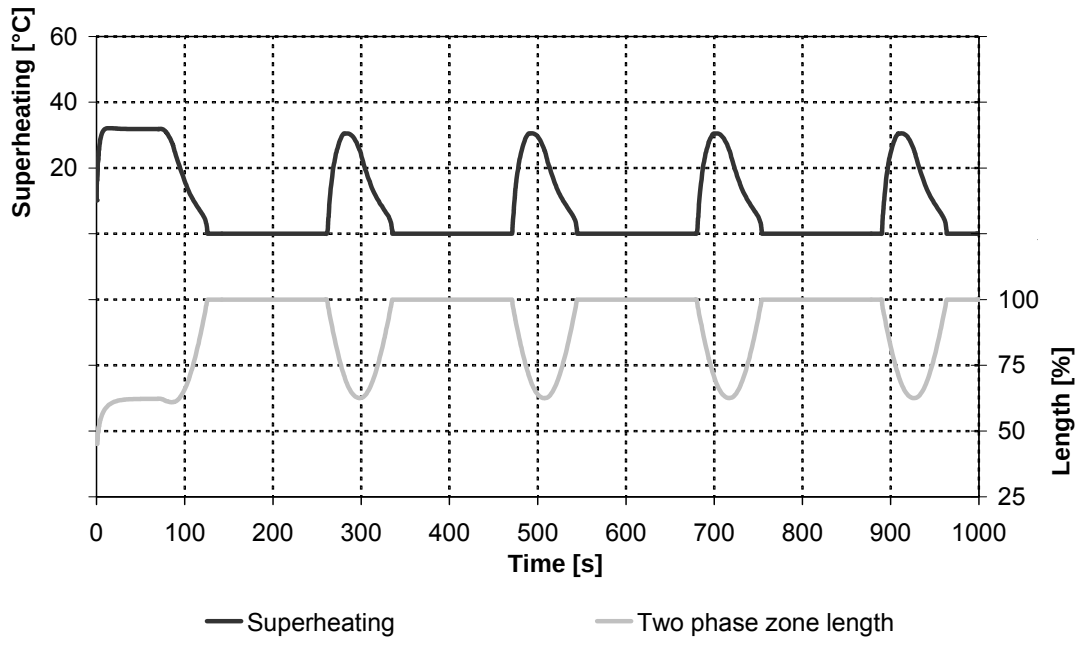

Figure 3.2.7 Refrigerant superheating and two-phase zone length in stability check simulations

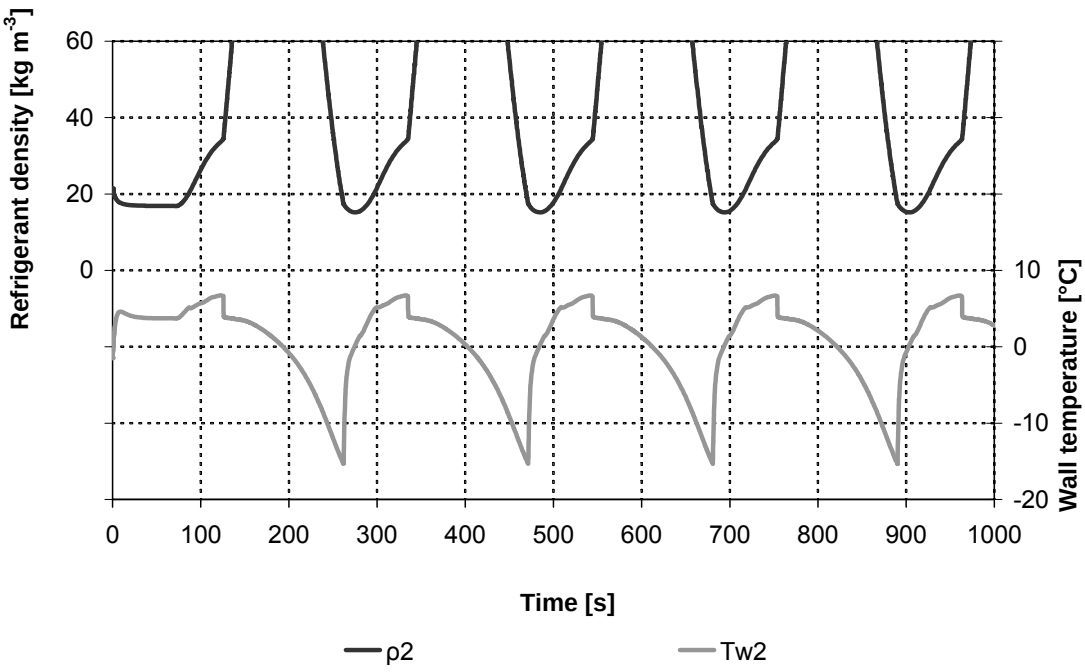

Figure 3.2.8a Refrigerant density ρ_2 and structure temperature T_{w2} in stability check simulation

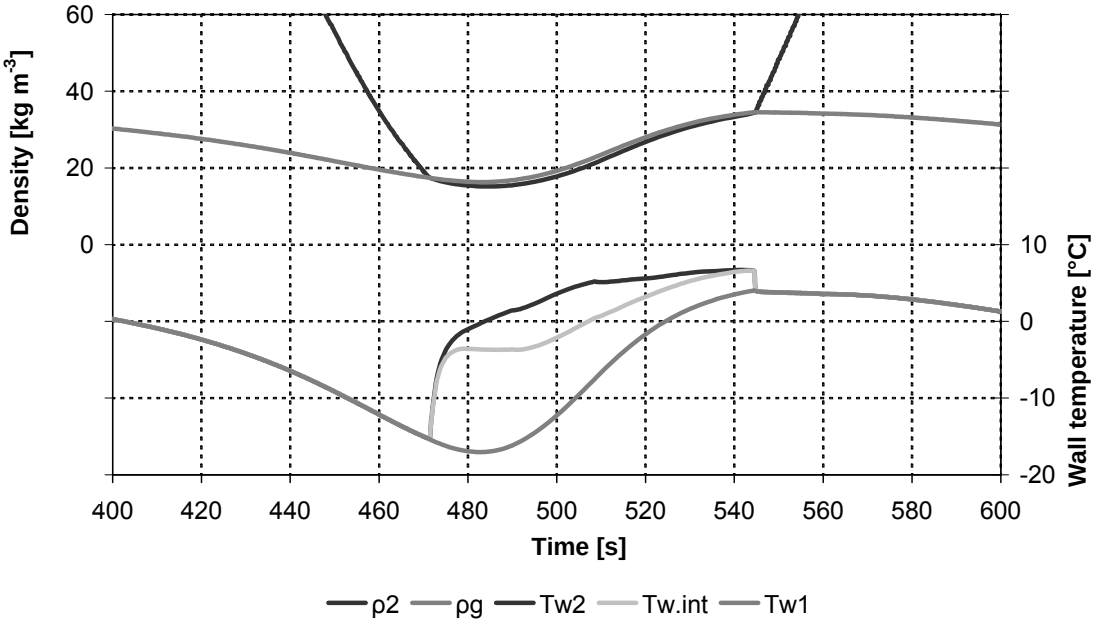

Figure 3.2.8b Properties trends in stability check simulation

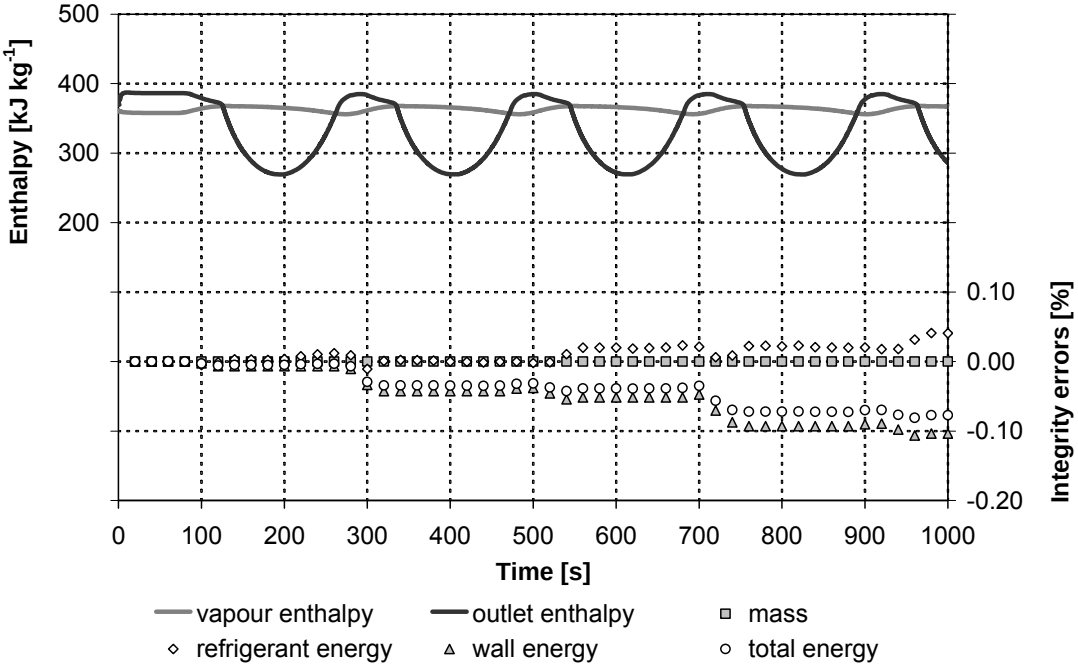

Figure 3.2.9 Validity check simulation. Switching procedure and model errors

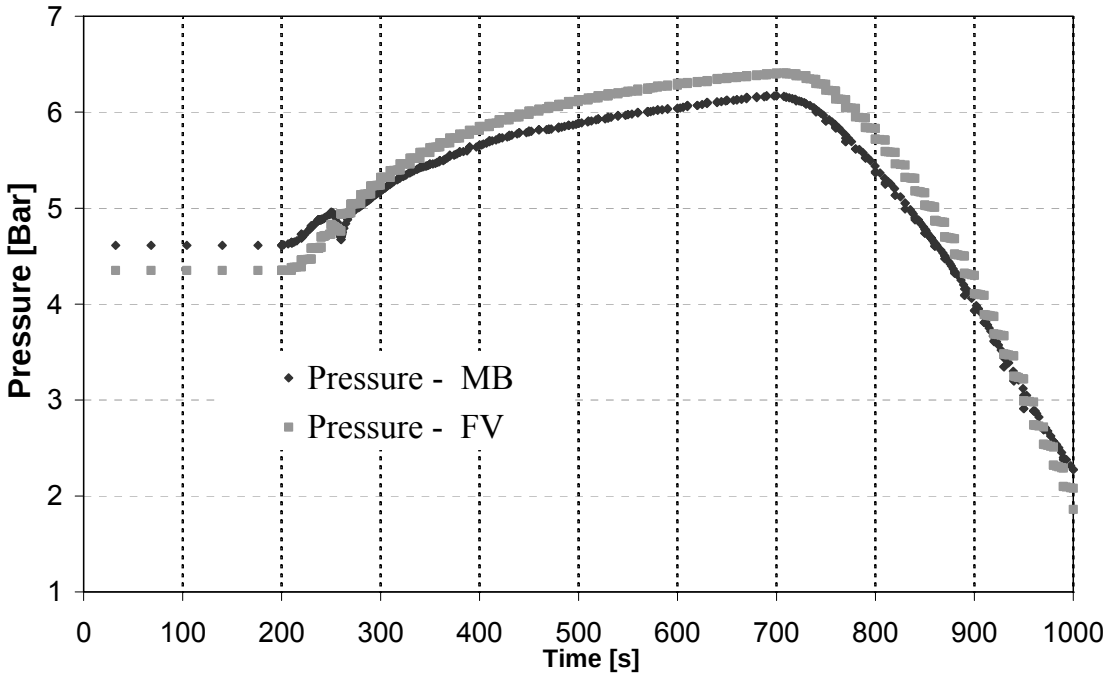

Figure 3.2.10. Model validation: Pressure trends

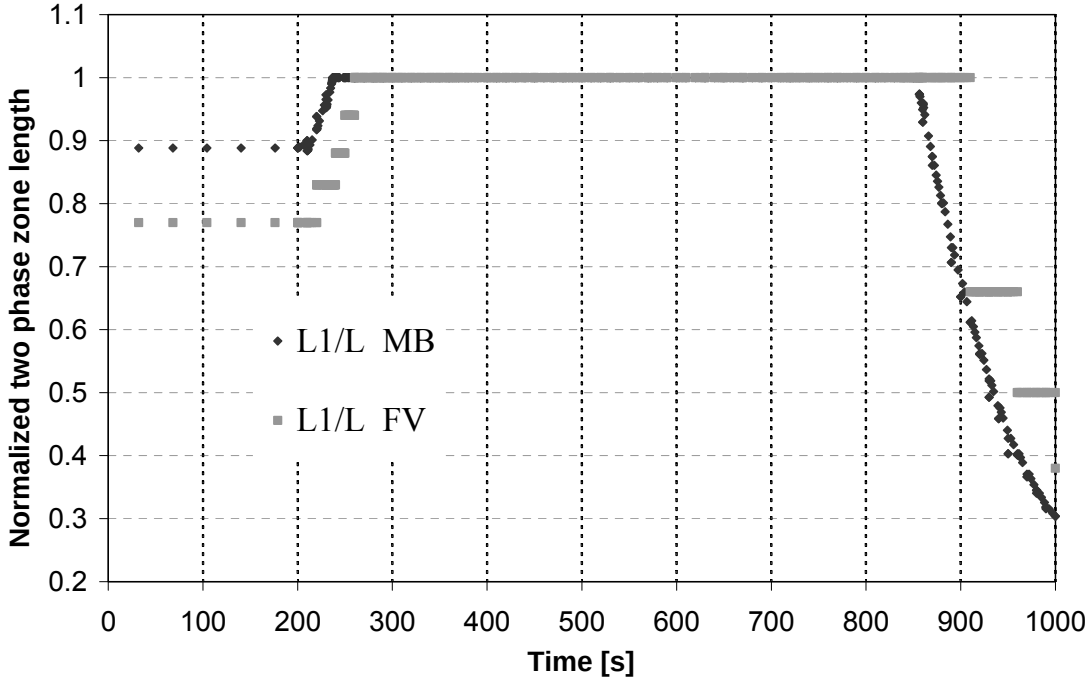

Figure 3.2.11. Model validation: Normalized zone length trends

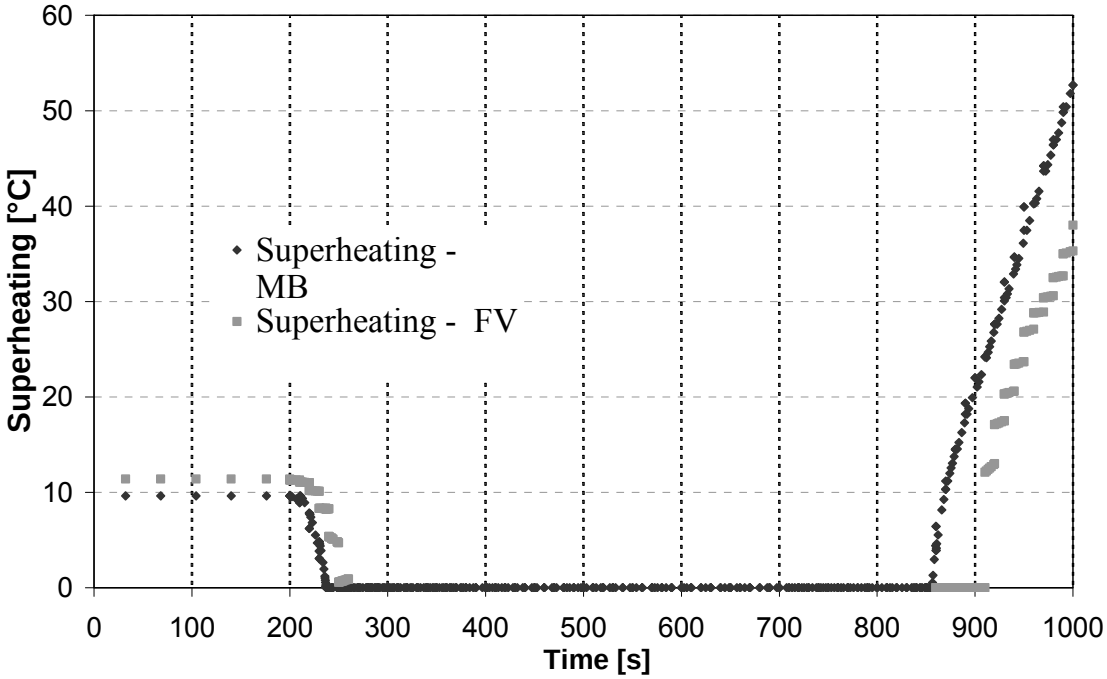

Figure 3.2.12 Model validation: superheating

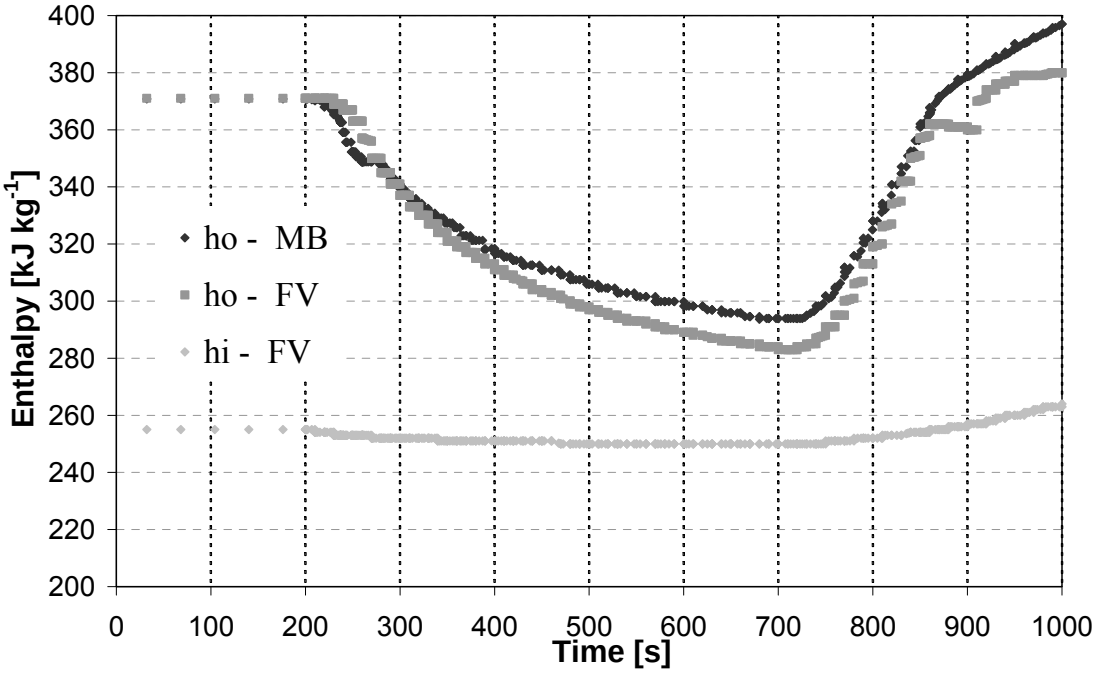

Figure 3.2.13 Model validation: refrigerant enthalpy trends

The Authors provided the model validation, comparing simulation results with experimental data. Geometrical features of the heat exchanger are reported in table (3.2.3). The heat-exchanger was modelled with eighteen finite volumes. Both the model where filled with the same initial refrigerant charge and exited with the same boundary inputs. Figure (3.2.10-13) compare the model performances. Simulation results let state that the two models are in good agreement, as it was already demonstrated by Bendapoudy et al (2008) [19].

3.2.4.5 Conclusions

This section presents a generalised evaporator model based on the moving-boundary approach. The heat exchanger model is based on a numerical scheme which can switch between the dry-expansion and the fully-flooded model representations.

An original technique for switching was presented. Numerical results show that the model's mathematical basis are consistent with integral forms of energy and continuity equations. Temporal integration is applied to core variables leading the mean void fraction within the two phase-zone to be time-variant. The use of this kind of variables improves the model accuracy and speed with respect to boundary variables when the compressor start-up is simulated. This work presents a qualitative case study showing that the model transient behaviour can well predict a finned coil evaporator performance simulated with one-dimensional finite volume code.

In its current form, the model is specific to evaporators. Future works will also include development of a corresponding condenser model and the extension to simulation of the complete refrigeration..

3.2.4.6 Appendix

This section provides more information about the derivation of the state equation from the mass and energy governing equation. The evaporator outlet enthalpy calculation method is discussed and the one-zone model equations for alternative state representations are supplied. Following Rasmussen and Alleyne [35] (2004) modelling approach, the unsteady-state equations for conservation of mass and energy were used

and expanded, assuming control volumes associated with each region of refrigerant. This is detailed for the two-zone model two-phase zone, and an analogous approach was taken for the superheated zone. The continuity equation is:

$$A\int_0^{L_1}\frac{\partial\rho}{\partial t}dz=\dot{m}_i-\dot{m}_{\text{int}}\,. \tag{29}$$

If the applying the Leibniz's rule is applied, the left hand side of Eq. (29) can be written as:

$$\begin{aligned}&A\int_0^{L_1}\frac{\partial\rho}{\partial t}dz=A\left(\frac{d}{dt}\int_0^{L_1}\rho dz-\rho\left(L_1\right)\frac{dz}{dt}\bigg|_{z=L_1}+\rho(0)\frac{dz}{dt}\bigg|_{z=0}\right)=\ldots\\&A\left(\frac{d\left(L_1\rho_1\right)}{dt}-\rho_g\frac{dL_1}{dt}\right)=A\left(L_1\frac{d\rho_1}{dt}+\left(\rho_1-\rho_g\right)\frac{dL_1}{dt}\right)\end{aligned}\,, \tag{30}$$

where the two phase zone density, $\rho_{1,}$ is defined as:

$$\rho_1=\frac{1}{L_1}\int_0^{L_1}\rho dz=\frac{1}{L_1}\int_0^{L_1}\left[\rho_g\gamma+\rho_l\left(1-\gamma\right)\right]dz=\rho_g\overline{\gamma}+\rho_l\left(1-\overline{\gamma}\right), \tag{31}$$

and the mean void fraction, $\overline{\gamma}$, can be calculated from the following equation assuming a linear quality distribution inside the evaporator:

$$\overline{\gamma}=\frac{1}{L_1}\int_0^{L_1}\gamma(p,z)dz=\frac{1}{1-x_i}\int_{x_i}^{1}\gamma(p,x)\cdot dx\,. \tag{32}$$

Considering Eqs. (30) and (31), Eq. (29) can be now rewritten as:

$$A\left[L_1\frac{d\rho_1}{dt}+\left(\rho_g-\rho_l\right)\left(\overline{\gamma}-1\right)\frac{dL_1}{dt}\right]=\dot{m}_i-\dot{m}_{\text{int}}\,. \tag{33}$$

Considering (31), the first term on the left hand side of Eq. (33) can be differentiated as:

$$\begin{aligned}\frac{d\rho_1}{dt} &= \left.\frac{\partial\rho_1}{\partial p}\right|_{h_i}\frac{dp}{dt} + \left.\frac{\partial\rho_1}{\partial h_i}\right|_{p}\frac{dh_i}{dt} = \ldots \\ &= \left[\frac{\partial\rho_g}{\partial p}\overline{\gamma} + \frac{\partial\rho_l}{\partial p}\left(1-\overline{\gamma}\right) + \left(\rho_g-\rho_l\right)\left.\frac{\partial\overline{\gamma}}{\partial p}\right|_{h_i}\right]\frac{dp}{dt} + \left(\rho_g-\rho_l\right)\left.\frac{\partial\overline{\gamma}}{\partial h_i}\right|_{p}\frac{dh_i}{dt}\end{aligned}, \tag{34}$$

being null the mean void fraction two-phase zone partial derivative, as it can be easily demonstrated applying the Leibniz's rule to Eq. (31). Substituting (34) in (33), the final form of the mass conservation equation (2) can be easily obtained.

Analogously, applying the Leibniz's rule is applied, the energy equation can be written as:

$$A\left[L_1\frac{d\left(\rho h\right)_1}{dt} + \left(\rho_g h_g - \rho_l h_l\right)\left(\overline{\gamma}-1\right)\frac{dL_1}{dt}\right] - AL_1\frac{dp}{dt} = \dot{m}_i h_i - \dot{m}_{\text{int}} h_g + Q_1, \tag{35}$$

where the zone volumetric enthalpy, $\left(\rho h\right)_1$, is defined by the following equation:

$$\left(\rho h\right)_1 = \frac{1}{L_1}\int_0^{L_1}\rho h dz = \frac{1}{L_1}\int_0^{L_1}\left[\rho_g h_g\gamma + \rho_l h_l\left(1-\gamma\right)\right]dz = \frac{1}{L_1}\left[\rho_g h_g\overline{\gamma} + \rho_l h_l\left(1-\overline{\gamma}\right)\right]. \tag{36}$$

Considering (36), the first term on the left hand side of Eq. (35) can be differentiated as:

$$\begin{aligned}\frac{d\left(\rho h\right)_1}{dt} &= \left.\frac{\partial\left(\rho h\right)_1}{\partial p}\right|_{h_i}\frac{dp}{dt} + \left.\frac{\partial\left(\rho h\right)_1}{\partial h_i}\right|_{p}\frac{dh_i}{dt} = \left[\frac{\partial\rho_g h_g}{\partial p}\overline{\gamma} + \frac{\partial\rho_l h_l}{\partial p}\left(1-\overline{\gamma}\right) + \ldots\right. \\ &\left.\ldots + \left(\rho_g h_g - \rho_l h_l\right)\left.\frac{\partial\overline{\gamma}}{\partial p}\right|_{h_i}\right]\frac{dp}{dt} + \left(\rho_g h_g - \rho_l h_l\right)\left.\frac{\partial\overline{\gamma}}{\partial h_i}\right|_{p}\frac{dh_i}{dt}\end{aligned}. \tag{37}$$

Substituting (37) in (35), the final form of the energy conservation equation (3) can be easily obtained. The energy equation for the two-phase zone is derived in an analogous manner while the one-zone model energy equation is:

$$AL_1\left(\frac{d(\rho h)_1}{dt}-\frac{dp}{dt}\right)=\dot{m}_i h_i - m_o h_o + Q_1, \tag{38}$$

and the following differentiation was adopted to expand the first term on the left hand side of Eq. (38):

$$\begin{aligned}&\frac{d(\rho h)_1}{dt}=\left.\frac{\partial(\rho h)_1}{\partial p}\right|_{h_i,\rho_e}\frac{dp}{dt}+\left.\frac{\partial(\rho h)_1}{\partial \rho_e}\right|_{h_i,p}\frac{d\rho_e}{dt}+\left.\frac{\partial(\rho h)_1}{\partial h_i}\right|_{p,\rho_e}\frac{dh_i}{dt}=\ldots\\&\ldots=\rho_e\left.\frac{\partial h_1}{\partial p}\right|_{h_i,\rho_e}\frac{dp}{dt}+\left(\rho_e\left.\frac{\partial h_1}{\partial \rho_e}\right|_{h_i,p}+h_1\right)\frac{d\rho_e}{dt}+\rho_e\left.\frac{\partial h_1}{\partial h_i}\right|_{p,\rho_e}\frac{dh_i}{dt}\end{aligned}, \tag{39}$$

where the two-phase zone enthalpy, h_1, is defined by Eq. (11) as

$$h_1=\frac{(\rho h)_1}{\rho_e}. \tag{40}$$

The two-phase zone enthalpy inlet enthalpy partial derivative, $\left.\frac{\partial h_1}{\partial h_i}\right|_{p,\rho_e}$ associated term in (39) is null. In fact, considering (31), at constant pressure and average evaporator density, mean void fraction has to be constant. With reference to (11), this implies that the two-phase zone enthalpy is constant and its partial derivative $\left.\frac{\partial h_1}{\partial h_i}\right|_{p,\rho_e}$ is null.

Next some details regarding the outlet refrigerant enthalpy from one-zone model TP are provided. Given the mean void fraction value calculated from the state variables with Eq. (12), the refrigerant outlet quality is calculated through a Newton-Raphson using the following analytical correlation of the integral of the void fraction model:

$$\bar{\gamma} = \frac{1}{x_o - x_i}\left(\frac{C}{(C-1)^2} \log\left(\frac{\left| x_i(C-1) - C \right|}{\left| x_o(C-1) - C \right|} \right) + \frac{x_o - x_i}{C-1} \right), \tag{41}$$

where $C = \left(\frac{\rho_g}{\rho_l} \right)$ for the homogeneous model and $C = \left(\frac{\rho_g}{\rho_l} \right)^{0.67}$ for the Zivi [39] (1964) model. The refrigerant outlet enthalpy is calculated from the resulting outlet quality.

Finally as it was anticipated in section 3.2.4.4, the resulting one-zone model mass and energy state equations for the two alternative refrigerant state variable groups are reported. Both the sets of equations were obtained neglecting the inlet enthalpy time derivative associated terms. Considering "p-h_o" model (Pettit *et al.*[34]; 1998, Zhang and Zhang [30], 2006; Bendapudi *et al.* [19], 2008) the following mass and energy equations can be obtained expanding the governing equations with pressure, outlet enthalpy as state variables:

$$\begin{aligned} & AL\left[\bar{\gamma} \left. \frac{\partial \rho_g}{\partial p} \right|_{h_o} + (1-\bar{\gamma}) \left. \frac{\partial \rho_l}{\partial p} \right|_{h_o} + AL(\rho_g - \rho_l) \left. \frac{\partial \bar{\gamma}}{\partial p} \right|_{h_o} \right] \frac{dp}{d\tau} + \ldots \\ & \ldots + AL(\rho_g - \rho_l) \left. \frac{\partial \bar{\gamma}}{\partial h_o} \right| \frac{dh_o}{d\tau} = \dot{m}_i - \dot{m}_o \end{aligned}, \tag{42}$$

$$\begin{aligned} & AL\left[\bar{\gamma} \frac{\partial \rho_g h_g}{\partial p} + (1-\bar{\gamma}) \frac{\partial \rho_l h_l}{\partial p} + (\rho_g h_g - \rho_l h_l) \left. \frac{\partial \bar{\gamma}}{\partial p} \right|_p - 1 \right] \frac{dp}{d\tau} + \ldots \\ & AL(\rho_g h_g - \rho_l h_l) \left. \frac{d\bar{\gamma}}{dh_o} \right|_p \frac{dh_o}{d\tau} = \dot{m}_i h_i - \dot{m}_o h_o \end{aligned}, \tag{43}$$

which are, for example, the same equations proposed by Zhang and Zhang [30] (2006) (Eqs. (17) and (18)) with $dh_o = (h_g - h_l)dx_o$.

Considering "p-γ" model (Li and Alleyne [33], 2010), the following mass and energy equations can be obtained expanding the governing equations with pressure, mean void fraction as state variables:

$$AL\left(\overline{\gamma}\left.\frac{\partial\rho_g}{\partial p}\right|_{\overline{\gamma}}+(1-\overline{\gamma})\left.\frac{\partial\rho_l}{\partial p}\right|_{\overline{\gamma}}\right)\frac{dp}{d\tau}+AL(\rho_g-\rho_l)\frac{d\overline{\gamma}}{d\tau}=\dot{m}_i-\dot{m}_o, \tag{44}$$

$$AL\left(\overline{\gamma}\frac{\partial\rho_g h_g}{\partial p}+(1-\overline{\gamma})\frac{\partial\rho_l h_l}{\partial p}-1\right)\frac{dp}{d\tau}+AL(\rho_g h_g-\rho_l h_l)\frac{d\overline{\gamma}}{d\tau}=\dot{m}_i h_i-\dot{m}_o h_o, \tag{45}$$

which, with some manipulation, can be written in the form of the Eqs. (48) and (49) proposed by Li and Alleyne [33] (2010).

3.2.5 References

[1] Bendapudi, S., Braun, J.E., 2002. A Review of Literature on Dynamic Models of Vapor Compression Equipment. ASHRAE Report, No. 4036–5.

[2] Murphy, W., Goldschmidt, V., 1984. Transient response of airconditioners – a qualitative interpretation through a sample case. ASHRAE Transactions 90 (Part 1).

[3] Murphy, W., Goldschmidt, V., 1985. Cyclic characteristics of a typical residential air-conditioner – modeling of start-up transients. ASHRAE Transactions 91 (Part 2).

[4] Ploug-Sorensen, L., Fredsted, J.P., Willatzen, M., 1997. Improvements in modeling and simulation of refrigerant systems: aerospace tools applied to a domestic refrigerator. International Journal of HVAC&R Research 3 (4).

[5] S. Porkhial a,*, B. Khastoo b, M.R. Modarres Razavi Transient response of finned-tube condenser in household refrigerators Applied Thermal Engineering 26 (2006) 1725–1729

[6] S. Porkhial, B. Khastoo *, M. Saffar-Avval Transient response of dry expansion evaporator in household refrigerators. Applied Thermal Engineering 24 (2004) 1465–1480

[7] S. Porkhial a, B. Khastoo a,*, M.R. Modarres Razavi Transient characteristic of reciprocating compressors in household refrigerators Applied Thermal Engineering 22 (2002) 1391–1402

[8] Christian J.L. Hermes*, Claudio Melo, Assessment of the energy performance of household refrigerators via dynamic simulation Applied Thermal Engineering 29 (2009)

1153–1165

[9] Christian J.L. Hermes, Claudio Melo, A first-principles simulation model for the start-up and cycling transients of household refrigerators (2008) International Journal of Refrigeration 31 (2008) 1341 – 1357

[10] Bruno N. Borges a, Christian J.L. Hermes b, Joaquim M. Gonçalves c, Cláudio Melo a Transient simulation of household refrigerators: A semi-empirical quasi-steady approach Applied Energy 88 (2011) 748–754

[11] Chunlu Zhang, Guoliang Ding, Approximate analytic solutions of adiabatic capillary tube, International Journal of Refrigeration 27 (2004) 17–24

[12] Li Yang, Wen Wang, A generalized correlation for the characteristics of adiabatic capillary tubes, International journal of refrigeration 31 (2008) 197 – 203.

[13] Christian J.L. Hermes , Cláudio Melo, Fernando T. Knabben, Algebraic solution of capillary tube flows. Part II: Capillary tube suction line heat exchangers, Applied Thermal Engineering 30 (2010) 770–775.

[14] Beghi, A., Cecchinato, L., 2009. A simulation environment for dry expansion evaporators with application to the design of autotuning control algorithms for electronic expansion valves. Int. J. Refrigeration 32, 1765-1775

[15] Beghi, A., Cecchinato, L., 2011. Modelling and Adaptive Control of Small Capacity Chillers for HVAC. App. Therm. Eng., In Press, http://dx.doi.org/10.1016/j.applthermaleng.2010.12.007.

[16] Yaqub, M., Zubair, S.M., 2001. Capacity control for refrigeration and air conditioning systems: a comparative study. Int. J. Energy Res. Tech 123, 92-99.

[17] Astrom, K.J., Hagglund, T., 1995. PID Controllers: Theory, Design, and Tuning, second ed.. Instrument Society of America, Research Triangle Park, NC 27709, USA.

[18] Rasmussen, B.P., Musser, A., Alleyne, A.G., 2005. Model-driven system identification of transcritical vapor compression systems. IEEE Trans. Control Syst. Technol. 13, 444–451.

[19] Bendapudi, S., Braun, J.E., Groll, E.A., 2008. A comparison of moving-boundary and finite-volume formulations for transients in centrifugal chillers. Int. J. Refrigeration 31, 1437–1452.

[20] Grald, E.W., MacArthur, J.W., 1992. A moving-boundary formulation for modeling time-dependent two-phase flows. Int. J. Heat Fluid Flow 13 (3), 266–272.

[21] He, X.D., Liu, S., Asada, H., 1995. Modeling of vapor compression cycles for advanced controls in HVAC systems. In: Proceedings of the ACC, vol. 5. IEEE, Seattle, WA USA, pp. 3664–3668.

[22] Jensen, J.M., Tummescheit, H., 2002. Moving boundary models for dynamic simulations of two-phase flows. In: Proceedings of the Second International Modelica Conference, March 18–19, Oberpfaffenhofen, Germany, pp. 235–244.

[23] Lei, Z., Zaheeruddin, M., 2005. Dynamic simulation and analysis of a water chiller refrigeration system. App. Thermal Eng 25, 2258-2271.

[24] Cheng, T., Asada, H. H., 2006. Nonlinear observer design for a varying-order switched system with application to heat exchangers. In: Proceedings of the ACC. IEEE, Minneapolis, MN, USA, pp. 2898–2903.

[25] Rasmussen, B.P., 2006. Dynamic modeling and advanced control of air conditioning and refrigeration systems. PhD thesis, University of Illinois at Urbana-Champaign.

[26] Qi Q, Deng S, 2008. Multivariable control-oriented modeling of a direct expansion (DX) air conditioning (A/C) system. Int. J. of Refrigeration, 31, 841-849.

[27] Schurt, L. C., Hermes, C. J. L., Neto Trofino, A., 2009. A model-driven multivariable controller for vapor compression refrigeration systems. . Int. J. of Refrigeration, 32, 1672-1682.

[28] Dhar, M., Soedel, W., 1979. Transient analysis of a vapor compression refrigeration system. In: Proceedings of the 15th International Congress of Refrigeration, Venice, vol. 2, pp. 1031–1067.

[29] Willatzen, M., Pettit, N.B.O.L., Ploug-Sorensen, L., 1998. A general dynamic simulation model for evaporators and condensers in refrigeration. Part I: moving-boundary formulation of two-phase flows with heat exchange. Int. J. Refrigeration 21 (5), 398–403.

[30] Zhang, W.-J., Zhang, C.-L., 2006. A generalized moving boundary model for transient simulation of dry-expansion evaporators under larger disturbances. Int. J. Refrigeration 29, 1119–1127.

[31] McKinley, T.L., Alleyne, A.G., 2008. An advanced nonlinear switched heat exchanger model for vapor compression cycles using the moving-boundary method. Int. J. Refrigeration 31, 1253–1264.

[32] Kumar, M., Kar, I.N., Ray, A., 2008. State space based modeling and performance evaluation of an air-conditioning system. HVAC&R Res. 14 (5), 797–816.

[33] Li, B., Alleyne, A.G., 2020. A dynamic model of a vapor compression cycle with shut-down and start-up operations. Int. J. Refrigeration 33, 538–552.

[34] Pettit, N.B.O.L., Willatzen, M., Ploug-Sorensen, L., 1998. A general dynamic simulation model for evaporators and condensers in refrigeration part II: simulation and control of an evaporator, Int. J. Refrigeration 21 (5), 404-414.

[35] Rasmussen, B.P., Alleyne, A.G., 2004. Control-oriented modeling of transcritical vapor compression systems. ASME J. Dyn. Syst. Meas. Control 126, 54–64.

[36] Beck, B.T., Wedekind, G.L., 1981. A generalization of the system mean void fraction model for transient two-phase evaporating flows. J. Heat Transfer 103, 81–85.

[37] Shah, R.K., D.P. Sekulić, 2003. Fundamentals of heat exchanger design, 1st edition, New York; Wiley.

[38]Lemmon, E.W., McLinden, M.O., Huber, M.L., 2002. NIST Reference Fluid Thermodynamic and Transport Properties Refprop 7.0, NIST Std. Database.

[39] Gnielinski V., 1976. New equations for heat and mass transfer in turbulent pipe and channel flow. Int. Chem. Eng. 16, 359-368.

[40] Zivi, S.M., 1964. Estimation of steady-state steam void-fraction by means of the principle of minimumentropy production. J Heat Transfer 86, 247–252.

[41] Gungor, K. E., Winterton, R. H. S., 1987. Simplified general correlation for saturated flow boiling and comparison of correlation with data. Chem. Eng. Res. Des. 65, 148-156.

[42] H. Mori, S. Yoshida, K. Ohishi, Y. Kakimoto, Dryout quality and post-dryout heat transfer coefficient in horizontal evaporator tubes, 3rd Europ. Thermal Sc. Conf., pp. 839-844, 2000.

[43] Wang, C., Chi, K., Chang, C., 2000. Heat transfer and friction characteristics of plain fin-and-tube heat exchangers. Int. J. Heat Mass Transf. 43, 2693–2700.

[44] Incropera, F.P., Dewitt, D.P., Bergman, T.L., Lavine, A.S., 2007. Fundamentals of Heat Transfer, sixth ed. John Wiley & Sons, New York, NY, USA, pp. 137–162.

[45] Kuehn, T.H., Ramsey, J.W., Threlkeld, J.L., 1998. Thermal Environmental Engineering, third ed. Prentice-Hall Inc., New Jersey.

3.3. Multi-Temperature Evaporator Refrigeration system

3.3.1. Summary

In traditional total no-frost combi refrigerators the fresh food compartment is cooled by air streams coming from the freezer and by the heat flux through the partition wall between the two compartments. A damper is used to control the fridge temperature. Therefore, the refrigeration unit produces its cooling effect at a temperature which is suitable for the freezer, but considerably colder than what is needed for the fresh food compartment. Consequently the system works with the thermodynamic disadvantage of supplying the cooling power at the lowest level of temperature.

This section presents the study of a combined household refrigerator (fridge/freezer), which works with a single refrigeration unit, but with two different air-loops. The unit consists of one compressor, one condenser and a single evaporator which is employed to cool the two compartments. The air flow involving the heat exchanger comes alternately from the fridge or from the freezer.

A damper is used to deflect the air stream and to control the temperature of the two cabinets. In this way the system works at two different evaporating temperatures, improving the thermodynamic efficiency when the fresh food compartment requires the cooling supply. The system was conventionally named Multi-Temperature Evaporator Refrigeration System (MTE).

In order to reduce the energy efficiency losses, two solenoid valves alternate two different capillary tubes, which are optimized for the two working conditions, respectively.

The MTE solution was tested on a 26” Side-by-Side refrigerator. Experimental results indicate the energy consumption decrease of about 4% respect to the original Total-No-Frost appliance. Theoretical simulations indicates that the energy efficiency improvements could be even greater employing a variable speed compressor.

3.3.2 System description

This section presents a description of the investigated system. Figure n.1a and 1b show the layout of a Side-by-Side Total-No-Frost refrigerator (TNF). The evaporator is

a finned coiled tube heat exchanger and it is placed inside an air channel behind the back wall of the freezer (fig. 3.3.1b). The fresh food compartment is cooled by the heat leakages through the divider and by frozen air streams coming from the freezer. The thermal insulation of the divider should be enough to prevent frost formation on the internal wall of the fridge cabinet. The energy performance of this equipment is not affected by the thermal insulation of the divider.

Figures 3.3.2a e 3.3.2b show the working principle of the Multi-Temperature Evaporator Refrigerator (MTE). The air flow involving the evaporator comes alternately from the fridge or from the freezer, making two independent air loops. A damper is placed after the evaporator fan in order to deflect the air flow toward the two compartments.

During pause periods, humidity migration from the fridge could cause frost formation on frozen products. A second air damper could be used to prevent this issue, closing all the gateways between the two compartments. In this analysis this practical drawback was not investigated. During tests trails, the prototype ran using one damper only.

The MTE system seems to be very promising for the improvement of the food preservation, due to less dry-out in the fresh food compartment and to the reduction of frozen air streams, which could damage the fresh products positioned near the gateways.

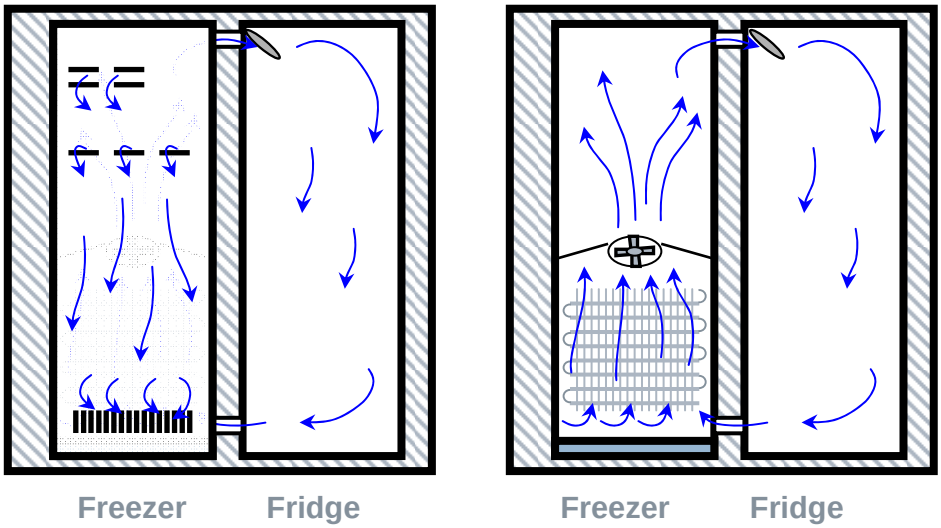

Figure (3.3.1a) (3.3.1b). Traditional Total no frost Side by Side refrigerator

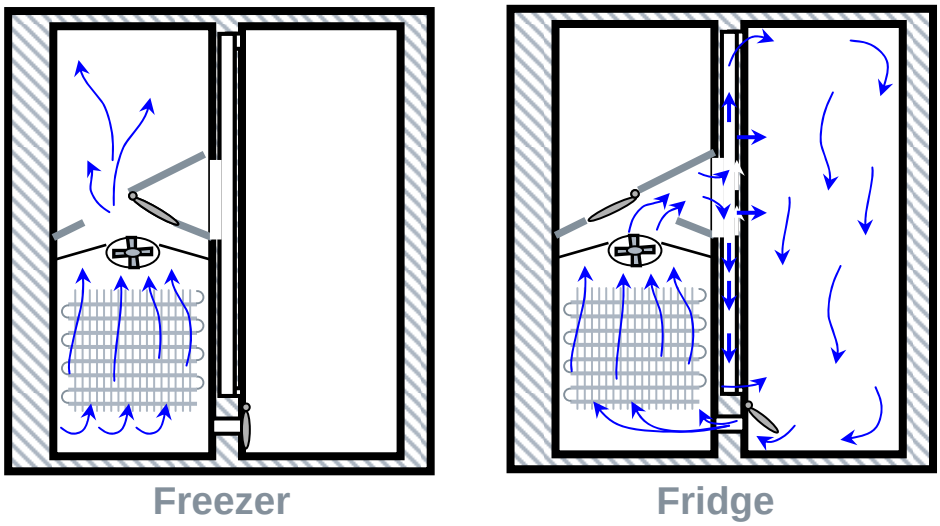

Figure (3.3.2a) (3.3.2b). Side by Side refrigerator with (MTE)

The investigated solution presents another energy-saving potential: from the theoretical point of view, it could be possible to perform a natural defrosting process [1,2]. When the compressor is off, the surface of the evaporator could be defrosted by blowing fresh air from the fridge. This cycle may produce both a cooling effect and humidity transfer to the fridge and it could allow to reduce the activation of the electrical heater. The efficiency of the natural defrosting process was not experimentally investigated in this work.

Whirlpool patented this solution in 1992 (US patent 5,231,847) [3]. The patent describes the general outline of the cooling system with multiple expansion devises (capillary tubes) and separated air flow between refrigerator and freezer.

A similar concept was studied by Park et al [4]. The authors tested a 510 litres top-mounted refrigerator with a single evaporator and two air fans. Each fan is dedicated to air recirculation for fridge and freezer respectively. Tests results reveals that compared to the conventional system, the energy consumption is reduced by about 9%. Nevertheless this solution was never on the market

Nomenclature

TNF – Total No Frost refrigeration system.

MTE – Multi Temperature Evaporator refrigeration system.

FF – Fresh food mode – Operating mode in which the system cools the fridge.

FZ – Freezer mode – Operating mode in which the system cools the freezer.

SLHE – Suction line heat exchanger.

3.3.3 Experimental apparatus and test procedure

The baseline test was conducted on a modified 26" Side-by-Side refrigerator which is marketed in the USA. The refrigerator had a net capacity of 590 litres (388 litres fridge, 202 litres freezer). The refrigeration unit was equipped with a R134a reciprocating compressor (Panasonic DHS66C10RBU) supplied at 110V 60Hz. The performance data in the ASHRAE32 test conditions are COP of 1.71 and 238 W of cooling capacity. The evaporator and the condenser are forced convection counter-flow heat exchangers. The original appliance was modified by adding a double air damper after the evaporator and making an additional gateway on the divider. The prototype was tested in the traditional total-no-frost operating mode (test 1) and in the MTE mode (test 2). During test 1 the double damper (figure 3.3.6) was always opened toward the freezer channel, and the refrigerator temperature was regulated using the original small damper on the top of cabinet (figure 3.3.7). During test 2 this damper was always closed.

The refrigerating unit has been modified to allow for the use of two capillary tubes (fig. 3.3.4 and 3.3.5). After the condenser two solenoid valves can open and close at the same time the liquid lines toward the expansion devices (fig 3.3.9). The two capillary tubes were rolled and soldered on the suction line tube (fig 3.3.8), which was rebuilt outside of the refrigerator cabinet. In order to have a better management of the refrigerant charge, an accumulator was positioned at the evaporator outlet.

The performance of the system was investigated with measurements of temperatures, pressures and electric power consumption.

The pressure transducers were placed at the compressor inlet and outlet. T-type thermocouples (copper-constantan) were used to measure temperatures.

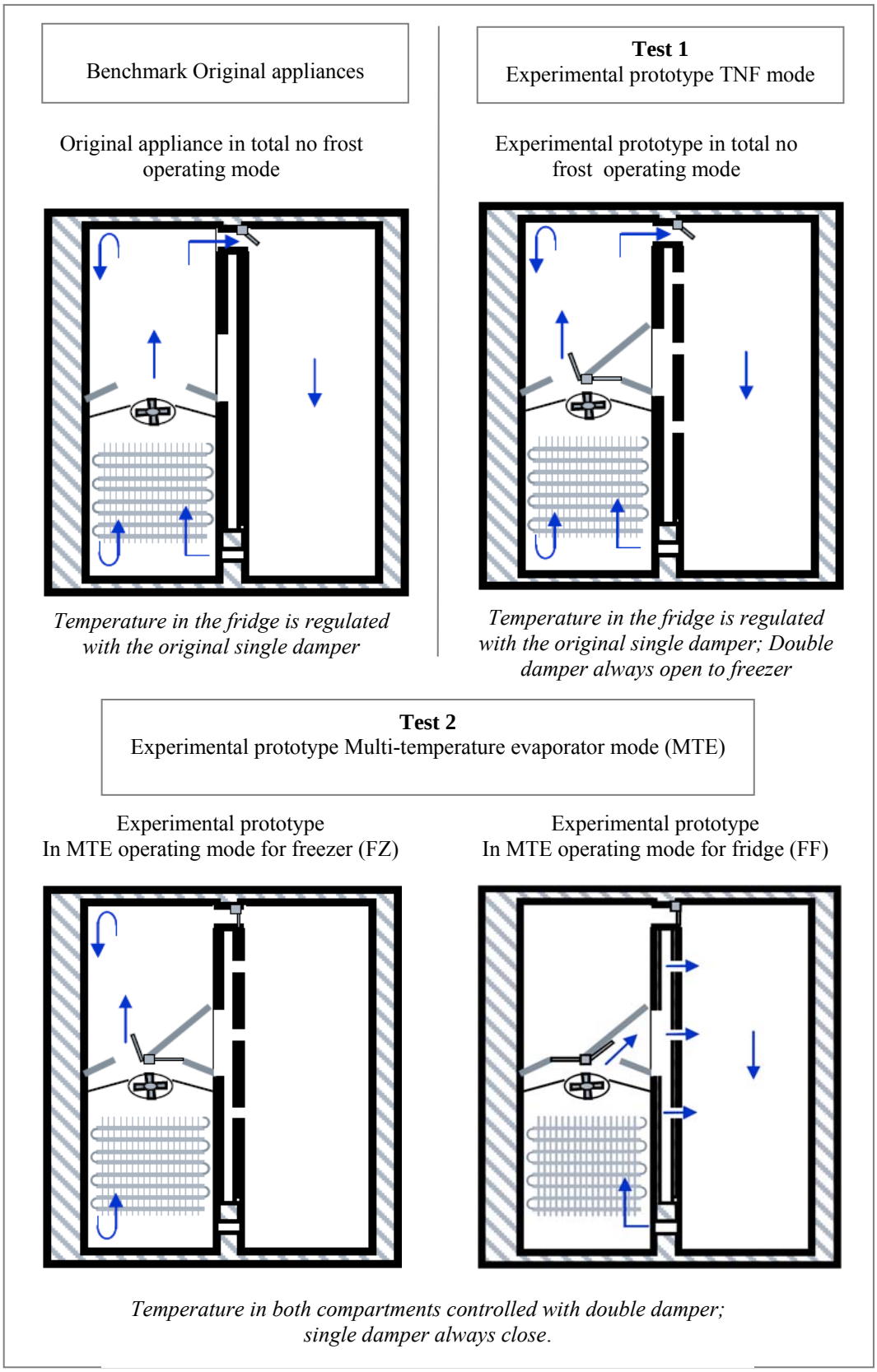

Figure 3.3.3 Original appliance and the experimental prototype

The baseline test was conducted on a modified 26” Side-by-Side refrigerator which is marketed in USA. The refrigerator had a net capacity of 590 litres (388 litres fridge, 202 litres freezer). The refrigeration unit was equipped with an R134a reciprocating compressor (Panasonic DHS66C10RBU) supplied at 110V 60Hz. The performance data in the ASHRAE32 test conditions are COP of 1.71 and 238 W of cooling capacity. The evaporator and the condenser are forced convection counter-flow heat exchangers.

The original appliance was modified adding a double air damper after the evaporator and making an additional gateway on the divider. The prototype was tested in the traditional total-no-frost operating mode (test 1) and in the MTE mode (test 2). During test 1 the double damper (figure 3.3.6) was always opened toward the freezer channel, and the refrigerator temperature was regulated using the original small damper on the top of cabinet (figure 3.3.7). During test 2 this damper was always closed.

The cabinet air temperatures were measured by thermocouples inserted in a copper mass according to the Association of Home Appliance Manufacturers (AHAM) standard [5]. The instantaneous active power consumption was measured every 0.1 seconds by a digital watt-meter.

The electronic controls of the refrigerator were disabled and all the devices such as the compressor, fans, dampers, electronic valves, were activated by relays controlled by software. The appliance was tested in accordance to AHAM test conditions [5]: Ambient temperature set to 32.2°C (90F), temperature set-point set to 7.2°C (45F) and -15°C (5F) for the refrigerator and freezer, respectively. The defrost heater was disconnected during tests. The defrost energy was not taken into account in the performance comparison. For the test results presented in this work, the refrigeration system is assumed to be optimized when there is no superheating of the refrigerant at evaporator outlet and when the refrigerant subcooling at the capillary tubes inlet was about 3 - 4°C. Such optimisation was obtained by manipulating the capillary tube length and the refrigerant charge.

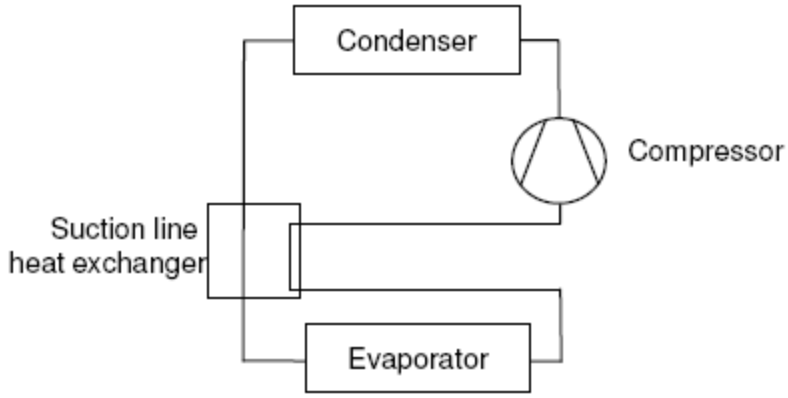

Fig.3.3.4 Layout of the original refrigeration unit

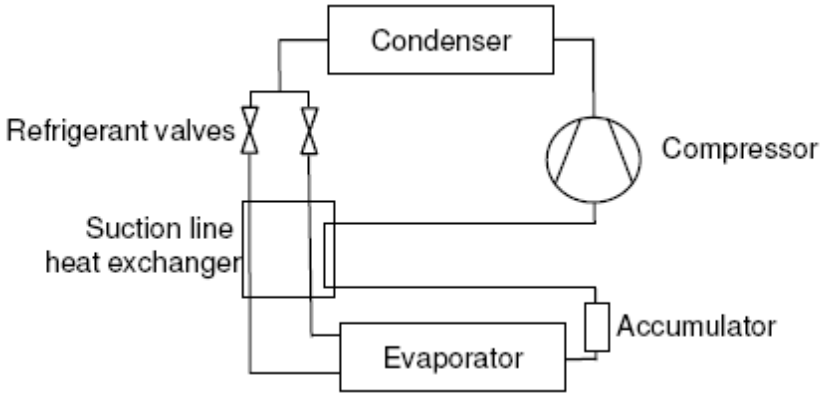

Fig.3.3.5 Layout of the prototype

Figure 3.3.6 Double door air damper

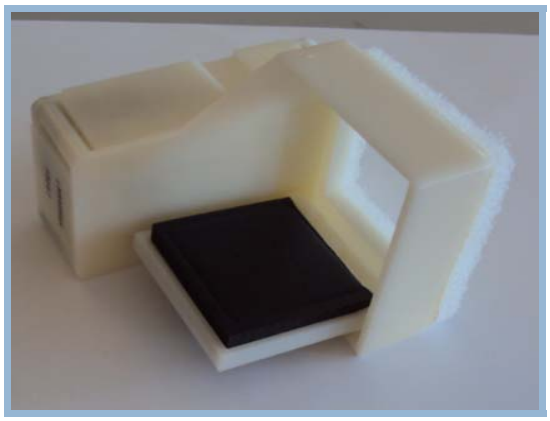

Figure 3.3.7 Original air damper

Figure 3.3.8 Suction line heat exchanger

Figure 3.3.9 Solenoid valves after the dryer

The energy consumption was calculated by integrating the active power measure. All the analogical inputs were recorded by NI acquisition modules and processed by a computer through a data-processing software. Data was recorded every 10 seconds.

3.3.4 Experimental results

Table 3.3.1 presents the experimental results recorded during test 1 and 2. Test 1 is the baseline test and it was preformed with the unit in TNF operating mode. Test 2 was performed with the unit in MTE operating mode. During tests the air temperature of the room and the average temperatures inside the two compartments were almost the same, respectively.

Table 3.3.1 Experimental results

	Test 1 TNF mode		Test 2 MTE mode	
	°C	°F	°C	°F
FF air	7.2	44.9	7.2	44.9
FZ air	-15.0	4.9	-15.1	4.8
Ambient	32.1	89.7	32.1	89.8
FZ mode				
Evaporation Temperature	-26.2	-15.2	-27.1	-16.8
Condensation Temperature	39.5	103.1	41.4	106.5
FF mode				
Evaporation Temperature	n/a	n/a	-19.3	-2.7
Condensation Temperature	n/a	n/a	39.7	99.9
Energy consumption [kWh/day]	1.77		1.70	
Energy saving[%]	-		4%	
Run time [%]	-		4%	

The table presents the average evaporation and condensation temperatures during the compressor run time. It is possible to see that with the MTE solution, the energy consumption decrease from 1.77 to 1.70 kWh/day, corresponding to a decrease of 4%. It is evident that the energy benefit comes from an increased evaporating temperature when the system operates in refrigerator mode.

The refrigerant mass flow rate and the cooling power have been calculated in the different working conditions, assuming constant volumetric efficiency (0.64). The COP was defined as the ratio between the cooling power and the Active Power consumption of the appliance (including compressor and fans).

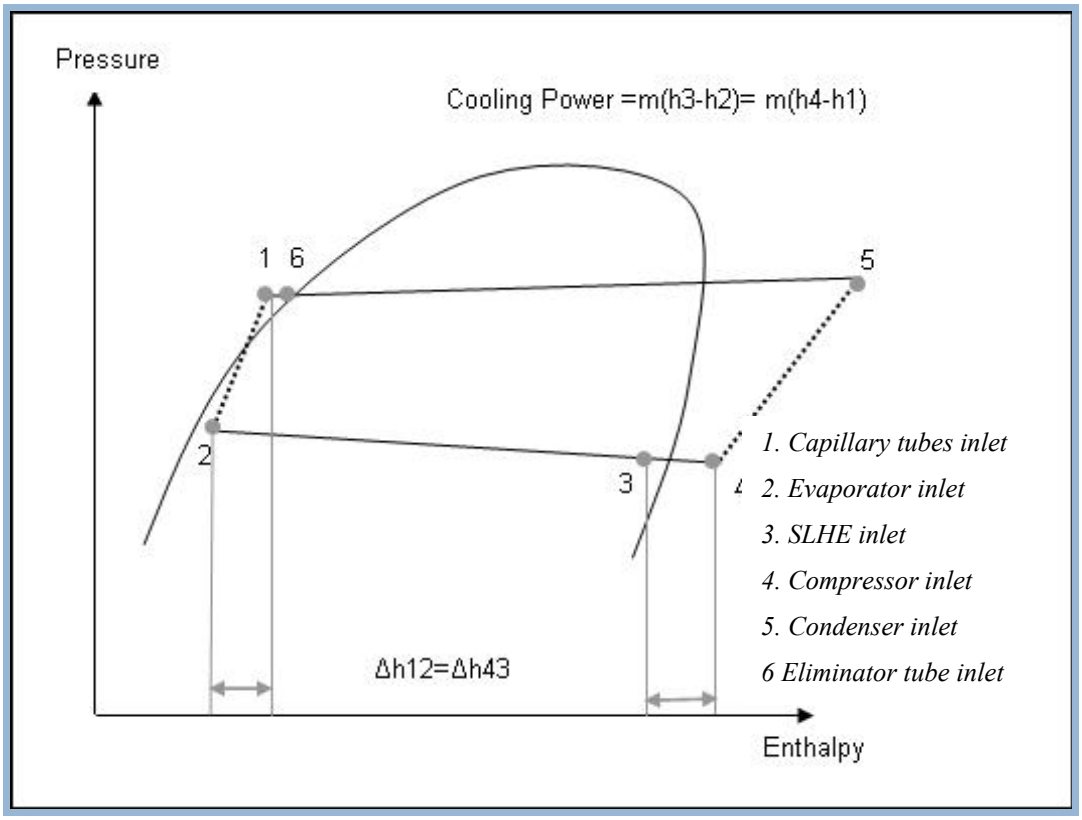

Figure 3.3.10 Pressure-Enthalpy diagram. The thermodynamic cycle

Assuming the SLHE to be adiabatic toward the ambient, it is possible calculate the cooling power with the following correlation (1); the COP was here defined as the ratio between the cooling power supplied and the total electric power consumption, taking into account the compressor and auxiliary motors.

Figures 11-16 present an overview of the prototype performance during tests.

$$Cooling\ \ power = \dot{m}_{ref}(h_4 - h_1) \qquad (1)$$

$$COP = \frac{Cooling\ \ power}{Total\ \ Active\ Power} \qquad (2)$$

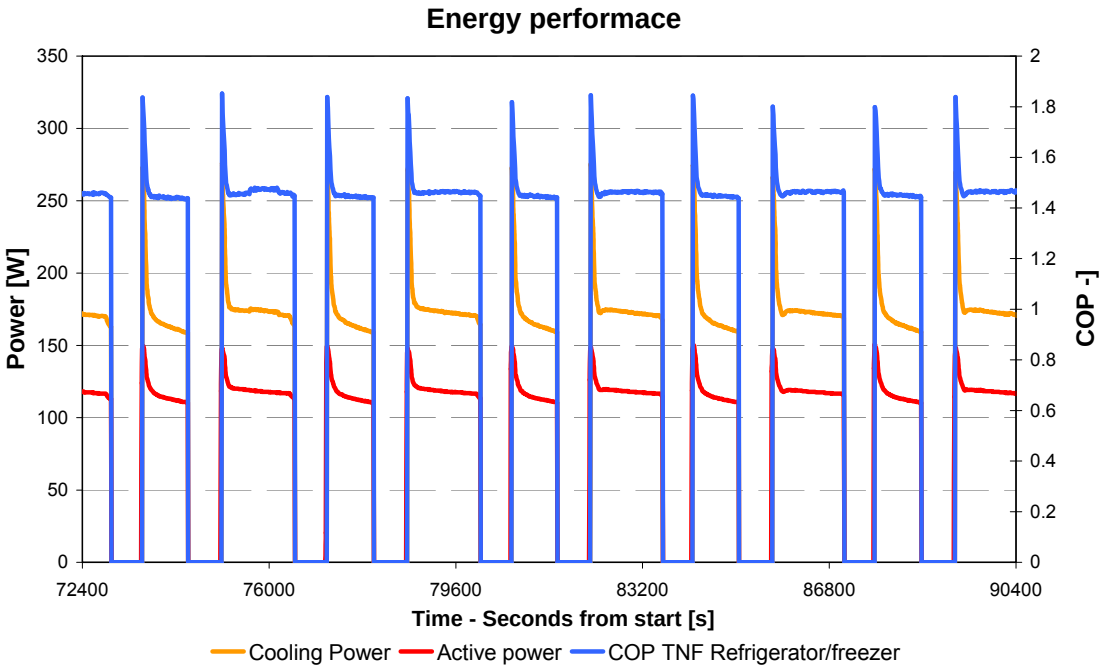

Figure 3.3.11 Energy test 1 – Prototype in TNF mode – Energy performance

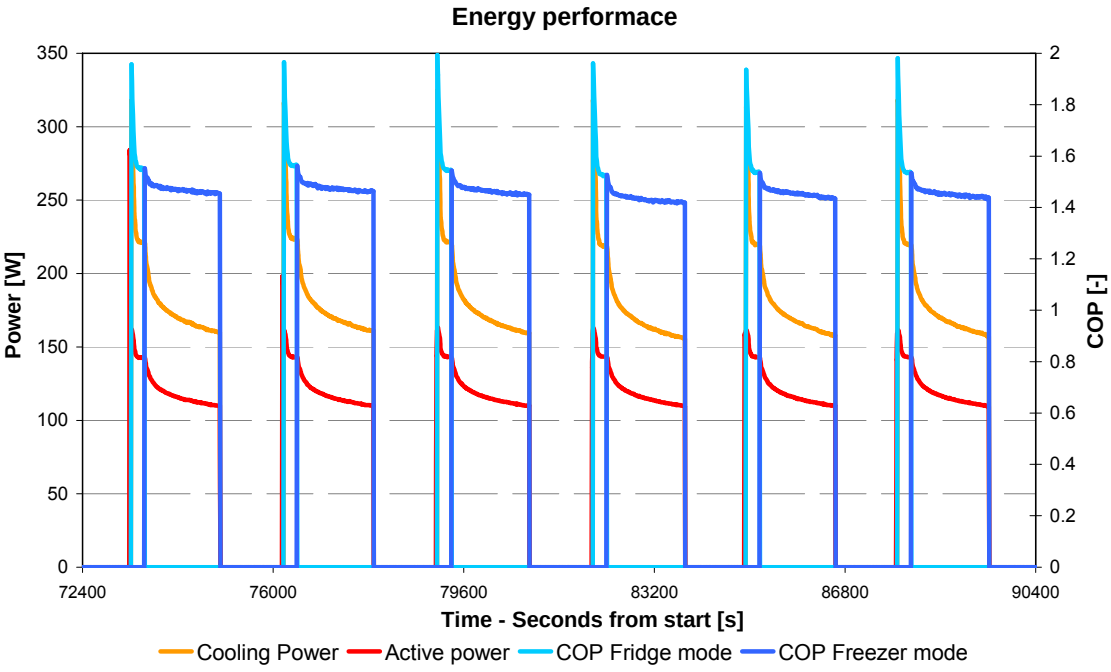

Figure 3.3.12 Energy test 2 – Prototype in MTE mode – Energy performance

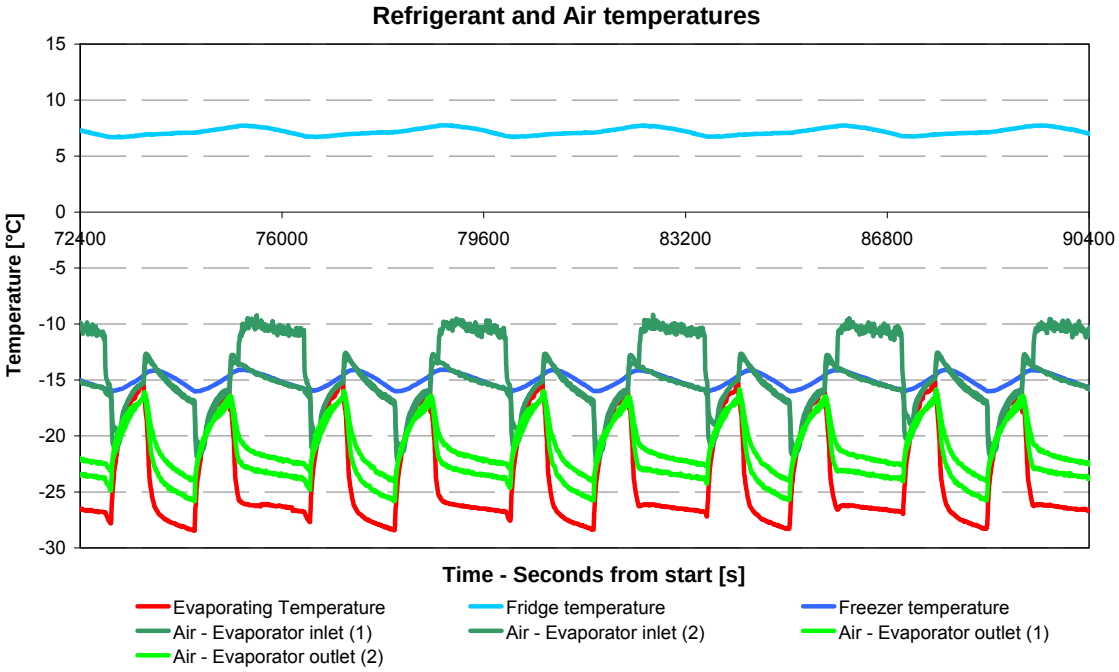

Figure 3.3.13 Energy test 1 – Prototype in TNF mode – Refrigerant and Air temperatures

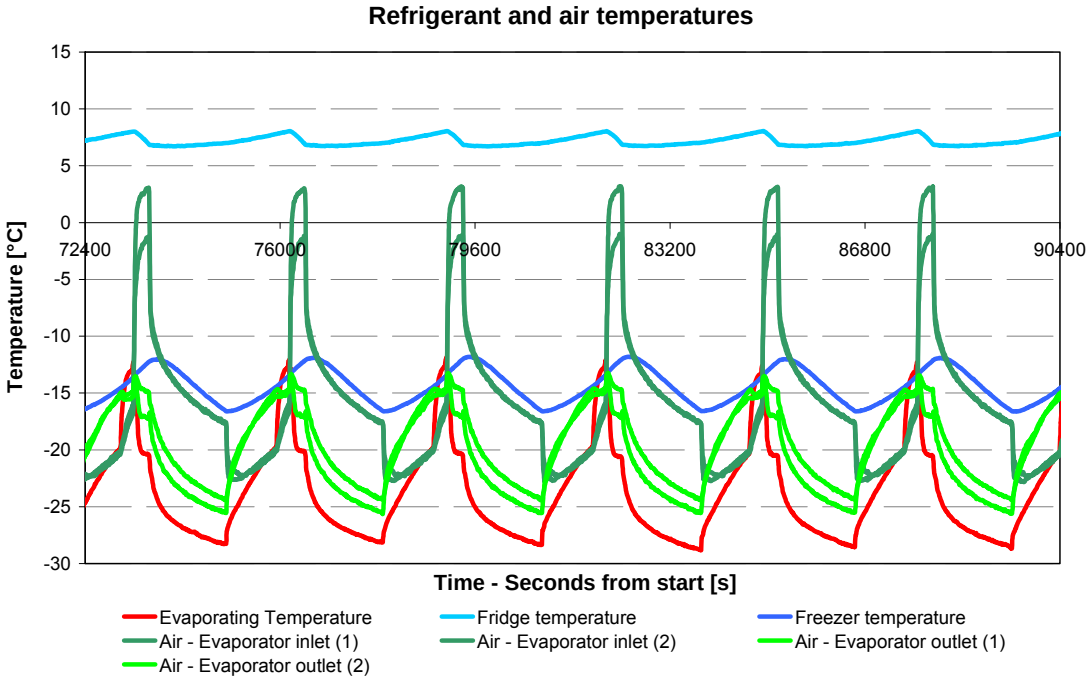

Figure 3.3.14 Energy test 2 – Prototype in MTE mode – Refrigerant and Air temperatures

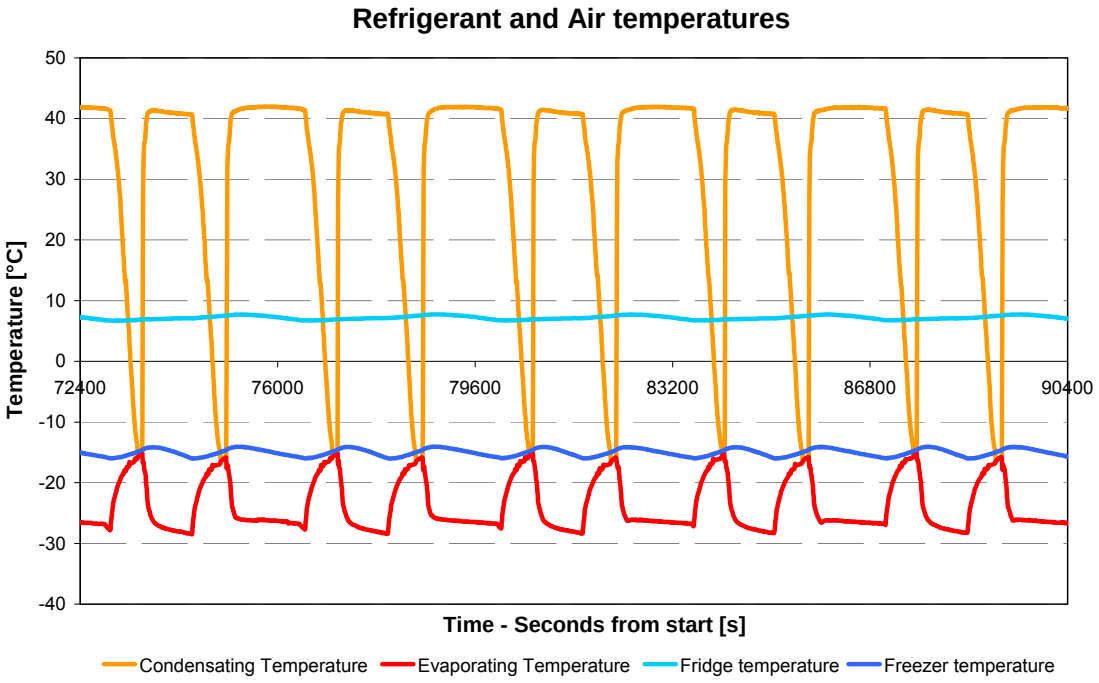

Figure 3.3.15 Energy test 1 – Prototype in TNF mode – Refrigerant and Air temperatures

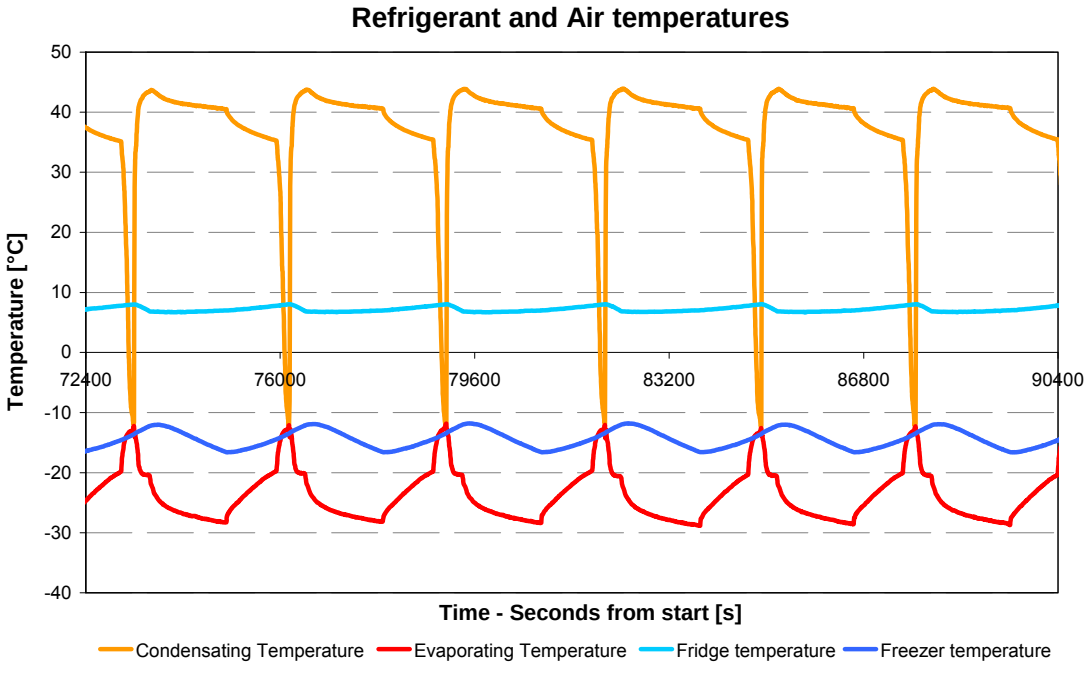

Figure 3.3.16 Energy test 2 – Prototype in MTE mode – Refrigerant and Air temperatures

In TNF test mode, figure 3.3.13, the starts and stops of the compressor are determined by the thermostatic control of the freezer temperature, while the opening and closing of the damper control the temperature of fresh food compartment. As shown in figure 3.3.14, in MTE mode the compressor starts when the fridge requires the cooling supply and the the freezer is cooled directly after the fridge has been cooled. During stops the evaporator fan was always switched off.

By heat leakage estimation the fridge cooling load is about 35% of the total load. With the same approach the thermal gain trough the divider was calculated in about 20% of the total fridge load. During test 2 the prototype worked on FF mode for about 16% of the compressor running time. During this period the fresh food compartment has been supplied with about 21% of the total cooling energy. These calculations have been done by energy balances, based on the compressor performance. Even if this is a low accuracy method, it can be seen that a considerable amount of cooling power is transferred through the partition wall between the compartments and due to possible air recirculation into the freezer during FF mode. This is difficult to be avoid entirely due to the specific layout of the Side-by-Side refrigerator, in which the evaporator air channel is positioned in the back wall of the freezer, with a non-tight divider used to separate it from the compartment. An additional air damper, placed at the evaporator inlet (freezer side), could significantly reduce air recirculation.

Figure 3.3.16 shows that both the valves closed the liquid line at the compressor stops. This device prevents the undesired refrigerant flow, coming from the capillary tubes [4,6,7]. The valves open some seconds before the compressor start, in order to allow pressures equalization.

3.3.5 Design devices

As previously stated, in a TNF refrigerator the thermal insulation of the divider should be enough to prevent frost formation on the internal wall of the fridge cabinet. There is no interest in increasing the insulation thickness more than necessary because this doesn’t affect the energy performance. On the contrary, the design target of a MTE architecture is the maximal decrease of the thermal heat transfer between the two compartments and the reduction of possible air leaks between them. These devices

should partially reduce the energy efficiency losses. They mainly depend to the position of the evaporator air channel. For instance, Fig. 3.3.17 presents a combi-top system architecture with the evaporator positioned in the partition wall between the two compartments.

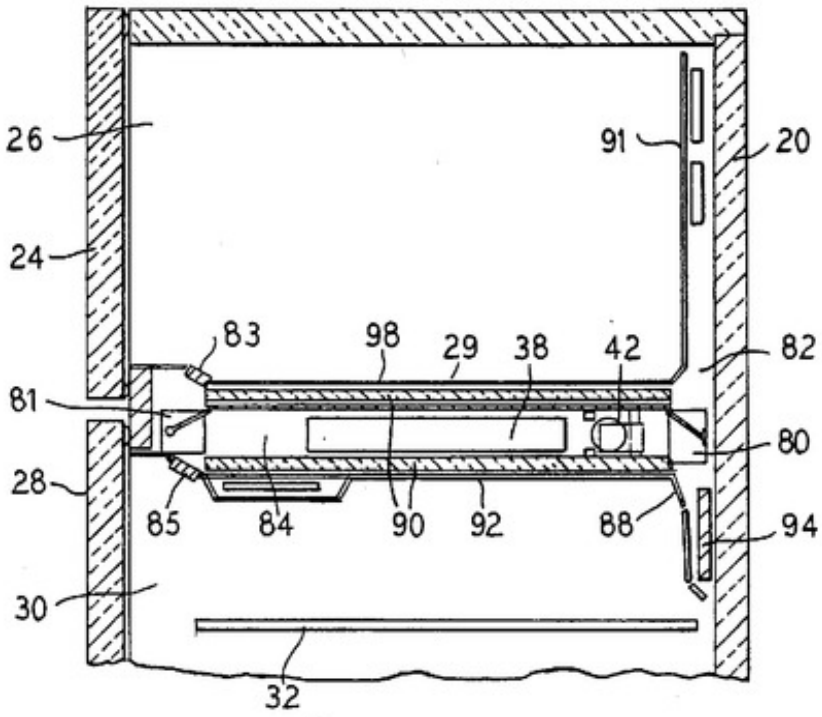

24 – first openable door
26 – First interior compartment
28 – Second openable door
29 – Mullion section
30 - Second interior compartment
38 - Evaporator
42 - Air moving device
80 – Air damper
81 – Air damper
82 – Opening
83 – Air inlet
84 - Plenum
85 – Air inlet
88 – Air outlet with diffusers
90 – Vacuum panels
91 – Air outlet with diffusers

Figure. 3.3.17 US patent 5,231,847 [3] *(Page 5 – fig 7)*

Compared to a Side-by-Side refrigerator, where the evaporator air channel is positioned in the back wall of the freezer, this architecture looks more suitable for a MTE system due to the small surface area between the compartments. Furthermore, the MTE solution well fits with systems which have a different proportion between the thermal loads of the two compartments. For this reason MTE seems to be very promising for combi-top or combi bottom refrigerators, where the fridge cooling load is usually greater than the freezer load.

3.3.6 Simulations and performance prediction

A simulation model was used to calculate the expected energy saving from a MTE system compared to the traditional TNF refrigerator. Simulations take into consideration different proportion between the compartment loads. The numerical model used is a first-principle steady-state model, which characterizes the condenser and the evaporator with constant values of the global heat transmittances.

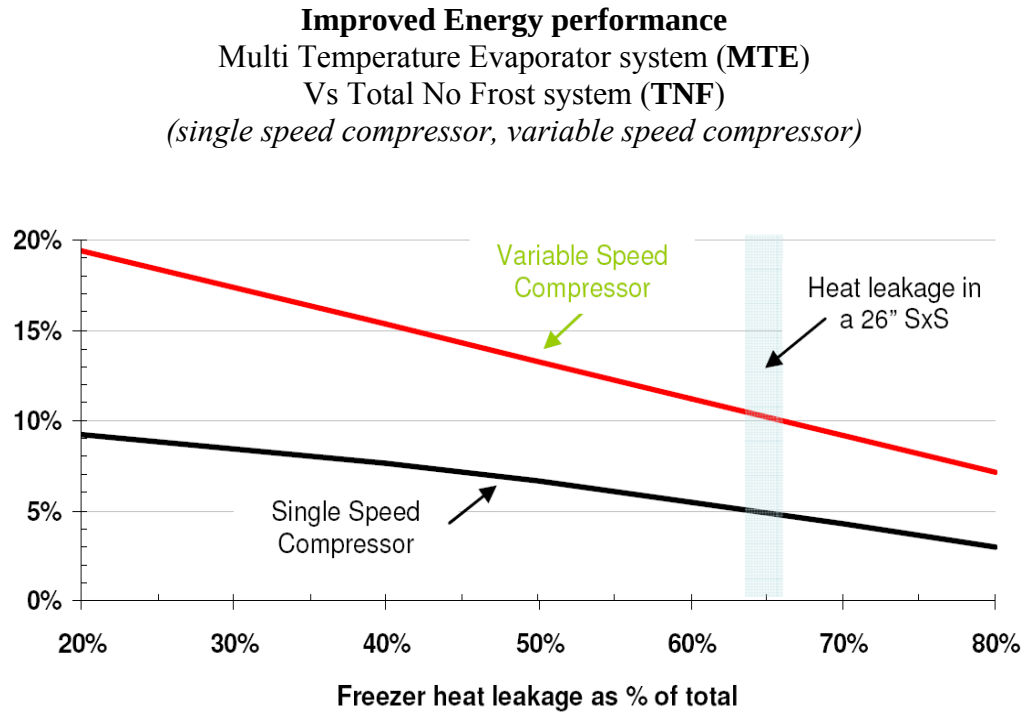

Fig.3.3.18 Energy saving potential as function of the freezer heat load as % of total

Figure 3.3.18 presents the simulation results. The expected energy saving is plotted versus the freezer load as percentage of the total heat leakages. The system is simulated with two different compressors: a single speed compressor, which is the same model used during experimental tests, and a variable speed compressor.

Since the freezer heat leakage as a percentage of the total heat leakage is calculated of about 65%, the simulated energy benefit of the MTE system is about 5% with a single speed compressor. This result is in good agreement with the experimental data.

The energy benefit could be about 10% with a variable speed compressor, compared to a traditional Side-by-side TNF system with a variable speed compressor. It can be seen that the MTE solution is very promising in systems where the fridge cooling load is greater than the freezer load, such as combi-top and combi-bottom refrigerators.

3.3.7 Conclusions

This work indicates that the Multi-Temperature-Evaporator Refrigerator is an interesting solution for new energy-efficient domestic refrigerators.

The solution was tested on a 26" Side-by-Side refrigerator. Experimental results indicate a decrease in the energy consumption of about 4% respect to the original Total-No-Frost unit. Theoretical simulations indicates that the energy efficiency improvements could be even greater (10%) employing a variable speed compressor.

3.3.8 References

[1] Lee J., Cho K. Y., Lee K. T., Daewoo Electronics Company, Ltd., Korea; "A New Control System of a Household Refrigerator-Freezer, Purdue International Refrigeration Conference, R-5, 1994.

[2] Ameen F.R., Coney J.E.R., Sheppard C.G.W., "Experimental study of warm-air defrost of heat pump evaporator".

[3] US patent 5,231,847 Multi-temperature evaporator refrigerator system with variable speed compressor

[4] Park J. K., Park, S. T., Kwak, T. H., Im K. S., LG Electronics, Korea; Dual-Controlled Indirect Cooling Refrigerator/Freezer Using Two Capillary Tubes and an Air Flow Switching System, Purdue International Refrigeration Conference, R-12, 1998.

[5] AHAM Standard: American Home appliances Manufacturer http://www.aham.org/industry/ht/d/sp/i/1731/pid/1731

[6] W.H. Coulter, C.W. Bullard, An Experimental analysis of cycling losses in domestic refrigerator-freezers, ASHRAE transactions vol. 103, n 1, pp 587-596, 1997.

[7] P.E. Krause, C.W. Bullard, Cycling and quasi-steady behaviour of a refrigerator, ASHRAE Transaction vol 102, n 1 pp 1061-1070, 1996.

[8] P.J. Rubas, C.W. Bullard, Factors contributing to refrigerator cycling losses, Int. J. Refrigeration, vol.18, n 3, pp 168-176, 1995.

4. Final remarks

This work treated the energy efficiency of household heat pump systems, analyzing different possibilities and technological innovations to improve the vapour compression unit performances. The dissertation makes its contribution to three distinct areas: heat pump dryers, tap water heat pumps and domestic refrigerators.

The transcritical CO_2 cycle was compared to the traditional R134a subcritical cycle in heat pump dryers. The theoretical analysis of the two cycles shows that CO_2, operating in transcritical conditions, is a possible alternative to the traditional technology. Tests performed on an experimental prototype have definitely returned a positive assessment for CO_2 as working fluid in this applications.

The second topic that has been faced is the efficiency optimisation of tap water heat pumps working with the CO_2 transcritical cycle. An upper cycle pressure control system, based on adaptive control logic, was developed and presented. An heat pump prototype was factory tested to verify its energy performance and to validate the control logic. The present work reports also an experimental investigation of the same appliance, using a double wall plate heat exchanger gas cooler. This solution was studied as a possible way to reduce the risk of tap water contamination with lubricant oil.

Finally, there were investigated innovative solutions to improve the energy efficiency of household refrigerators. The effect of the cycling frequency on the electric consumptions of domestic refrigerators has been analyzed. An experimental study was carried out on a under-counter refrigerator, working with R600a. The experimental results show a reduction of the energy consumption when the compressor on/off frequency increases. In agreement with the current state of technical knowledge, a possible way to explain this phenomenon is related to the thermal inertia of the metallic mass of the evaporator. This behaviour is amplified at higher cycling frequency. Another possible explanation, which has not been proposed so far by scientific literature, is related to the liquid expansion inside the evaporator, which occurs to each compressor start up. This phenomenon can be assimilated to the well known ‘batch expansion’ process.

This work also provided a simulation tool to investigate further this topic. The model is developed following the "moving boundary" scheme. The simulation model is accurate and fast when the compressor start-up is simulated, due to the choice of core variables. This choice was considered to be suitable to face the simulation of household refrigerators, which typically work with continues on/off cycles. In its current form, the model is specific for evaporators. Future works will also include development of a corresponding condenser model, and then the extension to the complete refrigeration unit simulation.

The present dissertation ended with the study of a combined household refrigerator (fridge/freezer), which works with a single refrigeration unit, but with two different air-loops. The solution was conventionally called MTE (Multi temperature evaporator system) and it was tested on a Side-by-Side refrigerator. Experimental results indicate the energy consumption decrease of about 4% respect to the original Total-No-Frost appliance. Theoretical simulations shows that the energy efficiency improvements could be even greater employing a variable speed compressor.

Tables list

Figures list